FURTHER DEVELOPMENT AND TESTING OF A BIMODAL AEROSOL DYNAMICS MODEL

Debra A. Youngblood and Sonia M. Kreidenweis

Department of Atmospheric Science
Colorado State University
Fort Collins, CO 80523

Funding Agencies:

Western Regional Center of the National Institute for Global Change #W/GEC 91-114

Colorado State University Graduate School

LIBRARIES
JUN 1 1994
COLORADO STATE UNIVERSITY

April, 1994

Colorado State University

DEPARTMENT OF ATMOSPHERIC SCIENCE

PAPER NO. 550

FURTHER DEVELOPMENT AND TESTING OF A BIMODAL AEROSOL DYNAMICS MODEL

Debra A. Youngblood and Sonia M. Kreidenweis

Department of Atmospheric Science
Colorado State University
Fort Collins, CO 80523

Funding Agencies:

Western Regional Center of the National Institute for Global Change #W/GEC 91-114

Colorado State University Graduate School

April, 1994

U18401 0242028

550

FURTHER DEVELOPMENT AND TESTING OF A BIMODAL AEROSOL DYNAMICS MODEL

Debra A. Youngblood
Sonia M. Kreidenweis
Department of Atmospheric Science
Colorado State University
Fort Collins, CO 80523

Research Supported by

Western Regional Center of the National Institute for Global Change
W/GEC 91-114
and
Colorado State University Graduate School

Spring, 1994

Atmospheric Science Paper No. 550

QC
852
.C6
no. 550
ATMOS

ABSTRACT

FURTHER DEVELOPMENT AND TESTING OF A BIMODAL AEROSOL DYNAMICS MODEL

A previously reported bimodal monodisperse aerosol model is further developed and tested. The starting point is the BImodal MOnoDisperse Aerosol Model (BIMODAM I) which was developed to model the formation of ammonium sulfate ($(NH_4)_2SO_4$) particles from sulfuric acid (H_2SO_4) vapor. The model follows the evolution of two monodisperse modes where each mode, *i*, is characterized by a unique mean diameter and the number of particles with that mean diameter.

The aerosol distribution is assumed to undergo typical atmospheric processes such as condensational growth, coagulation, nucleation, and deposition. In BIMODAM I, the effect of each process on the aerosol distribution is represented as a rate equation. The prognostic equations are coupled, so a variable time step differential equation solver is utilized to simultaneously solve the system of equations to predict the mass and number concentration in each mode. The diameter of each mode is diagnosed from the mass and number concentrations.

In the first part of this work, two new parameterizations were developed for BIMODAM I. First, a condensation rate factor was developed to account for the lack of polydispersity in the model. Second, a criterion was developed which dictates when the two modes may be merged without generating large errors.

In the second part of this work, a new version of the model (BIMODAM II) was developed to give the same accurate results as BIMODAM I without using the variable time step differential equation solver. A key development in BIMODAM II is a parameterization for the process of homogeneous nucleation. This parameterization is based on the approximation of the time-dependent nucleation rate with a triangular function; using this approach, only two parameters are needed to predict the total number of particles resulting from a nucleation event. The two parameters are

correlated to chemical source rate and relative humidity. Therefore, prediction of the number concentration of particles resulting from a nucleation burst depends on knowing the relative humidity and determining the chemical source rate. This development has been shown to perform well in the presence and absence of preexisting particles and over short and long time scale simulations.

Further developments in BIMODAM II include simple analytical solutions of the differential equations for coagulation and deposition. Using a mass balance equation, a simple solution was also derived to predict the amount of sulfuric acid in the vapor phase at any time during the simulation. From this calculation, the amount of mass in the aerosol phase is calculated by subtracting the amount in the vapor phase from the total amount of sulfuric acid produced during any given time step.

By using the simplifications and parameterizations mentioned above, computational time is saved by eliminating the variable time stepping differential equation solver. This model is shown to perform well when compared against a simulation which uses a more detailed description of the aerosol size distribution.

ACKNOWLEDGMENTS

This research was sponsored by the Western Regional Center of the National Institute for Global Environmental Change. The support of Dr. Marvin Goldman, Co-Director of WESTGEC is greatly appreciated. Debra Youngblood was partially supported by a fellowship from the Colorado State University Graduate School.

Debra Youngblood wishes to thank Dr. David Dandy, Dr. Bill Cotton, Dr. Dave Schimel, Tara Jensen-Leute, and Wendy Richardson for their help in preparing this work. Thanks also to Dr. R. N. Mower for getting me interested in atmospheric science at Central Michigan University and for encouraging me to continue my studies at Colorado State University. Special thanks goes to Jerry Harrington for his support above and beyond the call of duty.

TABLE OF CONTENTS

LIST OF SYMBOLS

A - area

α - condensation rate correction factor

β - correction factor to the continuum profile of air

χ - merging criterion

D_j - molecular diffusion coefficient

D_p - diameter

$\overline{D}_p$ - mass mean diameter

J - nucleation rate

k - Boltzman's constant

K_{11} - coagulation rate for 1-1 collisions

K_{12} - coagulation rate for 1-2 collisions

K_{22} - coagulation rate for 2-2 collisions

K_d - deposition rate

Kn - Knudsen number

λ - mean free path

$\overline{m}_p$ - mass per particle ratio

m_p - molecules of sulfate in per each new particle

μ - viscosity of air

M - aerosol mass concentration

N - aerosol number concentration

Q - mass concentration in a section

Qn - number concentration in a section

ρ - density

R - gas constant

R_g - total chemical source rate

$\hat{R}_g$ - effective chemical source rate

R_c - condensation rate

S - saturation ratio

ψ - sticking coefficient

σ_g - variance of the distribution

t - time

T - temperature

τ - optical depth

v - volume

V - vapor concentration

y1 - number fraction in mode 1

y2 - number fraction in mode 2

CHAPTER 1 INTRODUCTION

1.A. MOTIVATION

I. Aerosol effects

There has been increased recognition of the importance of aerosols in climate change and climate prediction. Aerosols affect the climate both directly, through scattering and absorption of incoming solar radiation, and indirectly, through their ability to act as cloud condensation nuclei (CCN). The CCN population represents a small fraction of the total aerosol population known as condensation nuclei (CN). The direct effect of aerosols is rather straightforward to quantify, while the effect of CCN on cloud properties is much less certain and difficult to quantify.

Direct effects

Whether the effect of aerosols on global average air temperature is one of net warming or net cooling depends upon the chemical and physical makeup of the particles. If the aerosol scatters more solar radiation back to space than it absorbs, the cooling effect will dominate. If the aerosol absorbs more than it scatters, and it acts as a blackbody so that the absorbed solar radiation is emitted from the aerosol, the effect will be to warm the atmosphere. Sulfur particles, however, do not absorb significantly in the visible wavelengths

Recent studies such as those by Charlson *et al.* (1991) suggest that the effects of aerosols may be similar in magnitude, but opposite in sign, to the projected global warming attributed to greenhouse gas accumulation. A three-dimensional meteorological-chemical model was used to estimate the effects of anthropogenic

sulfate aerosols on clear-sky optical depth. The resulting forcing due to sulfate aerosol is calculated as -1.1 W m^{-2} over the Northern Hemisphere, compared with a +1.5 W m^{-2} forcing attributed to anthropogenic CO_2. The aerosol forcing is, therefore, similar in magnitude, but opposite in sign to the current greenhouse forcing to date in the Northern Hemisphere.

Kiehl and Briegleb (1993) used a 3-D diagnostic model to estimate the direct radiative effect of sulfate aerosols in comparison with the radiative effect of greenhouse gases. The resulting globally-averaged annual forcing attributed to anthropogenic sulfate aerosols was calculated as -0.3 W m^{-2}; when natural sulfate forcing is included, the total forcing increases to -0.6 W m^{-2}. The conclusion is made that aerosol climate forcing from a number of regions in the Northern Hemisphere is large enough to reduce the greenhouse gas forcing.

Indirect effects

Aerosols may also indirectly affect climate through their impact on cloud microphysical properties (Twomey, 1977). Cloud microphysical properties determine the albedo, lifetime, and the precipitation efficiency of the cloud. The albedo of optically thin clouds is highly sensitive to droplet size and number concentration as seen in the following approximate relationship between optical depth, τ, number concentration, N, and drop radius, r (Twomey, 1991):

$$\tau = 2N\rho\bar{r}^{2}h, \quad (1.1)$$

where h is the depth of the cloud, $\bar{r}^{2}$ is the mean radius of the droplet distribution, and ρ is the density of liquid water. The optical thickness of a cloud is a measure of its brightness. A brighter cloud is more reflective to solar radiation. Changes in the cloud droplet size spectrum result in changes in the optical depth, and hence changes in the

brightness of the cloud. The cloud droplet number concentration depends mainly on the sub-cloud concentration of CCN, which in turn depends on the aerosol number concentration and aerosol chemical properties. Therefore, determining the number of aerosol particles, in addition to their mass and their chemical properties, is a key issue in estimating the indirect effects of aerosols on climate.

Twomey (1991, 1977) demonstrated that the clouds which are most susceptible to changes in droplet number concentration are those that have initially low number concentration and a reflectance of about 0.5, which means that 50% of the incident solar radiation is reflected. This characterizes typical marine stratus clouds in clean conditions. Since marine clouds cover a large percentage of the Earth's surface, and since marine clouds have low droplet concentrations compared with continental clouds, increases in the albedo of marine clouds can have a significant effect upon global climate.

Sulfur

Sulfur species in the atmosphere are formed by natural and anthropogenic processes. Sulfur species must undergo a reduction process in order to form volatile sulfur compounds, which are then released to the atmosphere.

Natural gaseous sulfur compounds originate from volcanoes, soils, plants, coastal wetlands, biomass burning, and the oceans. The largest of the natural gaseous emissions is associated with DMS (dimethylsulfide), which is released from soils, vegetation, and marine organisms (Andreae, 1992). Once in the atmosphere, DMS is oxidized to form SO_2 and MSA (methanesulfonic acid), which can both form submicron-sized aerosols. Carbonyl sulfide (COS) is the most abundant atmospheric sulfur species in the troposphere (Seinfeld, 1986; Andreae, 1992). COS is found mainly in the oceans, but is also found in small amounts in volcanoes, soils, plants,

wetlands, and biomass burning emissions. Emissions of SO_2 by combustion of fossil fuels represents a large fraction of the total flux of sulfur species to the atmosphere.

Sulfur particles have been shown to be a major constituent of atmospheric aerosols (Meszaros and Vissy, 1974; Gras and Ayers, 1983). Oxidation of gaseous sulfur compounds to form sulfate aerosols is thought to be a major source of CCN (Langner and Rodhe, 1991; Fitzgerald, 1991). In regions affected by anthropogenic sources, sulfate derived from SO_2 emissions is a major cause of acidic rainwater, while in remote marine regions, DMS is thought to be a precursor to CCN formation (Andreae *et al.*, 1983; Cline and Bates, 1983; Andreae, 1986; Kreidenweis *et al.*, 1991).

II. Large Scale Models of the Sulfur Cycle

Langner and Rodhe (1991) developed a three-dimensional global transport-chemistry model of the tropospheric sulfur cycle. The model includes mechanisms for emission, transport, loss, and chemical reactions. The model treats DMS and SO_2 as gases and treats the aerosol as sulfate. The model demonstrates that the current understanding of aspects of the sulfur cycle is consistent with observations, especially over Europe and North America where emissions are well known. In general, the model gives useful estimates of annually-averaged quantities but many simplifying assumptions were made and further work is needed. With respect to climate, one key aspect that their model needs is information regarding the number of particles; only sulfate mass is predicted.

Erickson *et al.* (1991) investigated the effect of anthropogenic sulfur emissions on CN concentrations using a three-dimensional global model of the sulfur cycle. Their model treats transport, convective and eddy mixing, deposition, and a simplified chemistry mechanism. The particles are assumed to have a diameter of 0.2 μm immediately upon formation. Mass and diameter are used to calculate the resulting number of particles. Oceanic DMS was concluded to be the dominant CN source over the oceans, while anthropogenic SO_2 influences marine CN concentration only in the

northern hemisphere winter where emissions are strong and sunlight needed for DMS formation is low. One important simplification in their model is the treatment of diameter. By assuming a particle diameter, the total number of particles is prescribed.

Calculations, such as those presented by Charlson *et al.* (1991), and Kiehl and Briegleb (1993), indicate the need for an improved understanding of the mechanisms regulating atmospheric aerosol formation and evolution before accurate assessments of the climate impacts of changes in aerosol precursor gases can be made. The importance of aerosols to climate suggests that the indirect and direct effects of aerosols must be included in general circulation models. To accomplish this, major sources of particles and precursor gases must be incorporated and a method developed for describing the conversion of gases to particulate matter, in order to estimate the effect of perturbations in aerosol sources and losses upon global atmospheric aerosol concentrations. Because of the importance of aerosol number concentration on climate, a method is needed to accurately predict the total aerosol number concentration in global models. The model developed here, BIMODAM, is such a mechanism for predicting aerosol number concentration. BIMODAM also gives information on the size of the particles which delineates CN from CCN, and therefore, may help to increase the understanding of how aerosols can influence climate. Because of their importance in the formation of CN and CCN, gas to particle conversion of sulfur species will be focused on here.

1.B. PREVIOUS WORK

I. Description of Techniques for Simulating the Formation of Aerosol

Goals of aerosol modeling

The goal of aerosol modeling is to follow the evolution of the aerosol size distribution through interactions with vapor-phase material and interactions with other

particles. The size distribution of all chemical species in the particle phase for each point in the time and space of interest is to be determined. The model must include a representation of the behavior of each species or material in each relevant phase. The effect of each process on the aerosol phase is represented by a rate expression which describes how the aerosol population changes with respect to that particular process.

A key factor in aerosol modeling is how the aerosol distribution is represented. The natural spectrum of aerosol sizes is tri-modal in nature (Seinfeld, 1986). The three modes are nucleation, accumulation, and coarse (Seinfeld, 1986). The most descriptive, yet still computationally feasible, representation of the three modes is with multiple continuous distribution functions. Other representations are approximations of the continuous form. The three representations of aerosol distributions which will be discussed here are modal, sectional, and monodisperse, represented pictorially in Figures 1.1-1.3. Only two modes of aerosol size ranges are shown because for the purposes of gas-to-particle conversion, which is the focus of this work, the third, coarse, mode does not play a large role.

The General Dynamic Equation

The processes which affect aerosol distributions in a cloud-free environment include nucleation from the vapor phase, condensation of vapor phase material onto the aerosol, coagulation, deposition, and chemical reactions within particles. For each of these processes, a mathematical expression is generated to describe the effect on the aerosol population. The General Dynamic Equation (GDE) describes the time-dependent size distribution of an aerosol (Friedlander, 1977). The discrete form of the GDE gives the most detailed information on the particle size distribution. The discrete form, however, leads to a large number of differential equations which limits its practical applications. The size distribution can be approximated by representing separate portions of the

complete distribution with analytical functions. The formulation of the GDE for an aerosol size distribution approximated as a continuous function is (Whitby, 1991):

$$(1.2) \qquad \frac{\partial}{\partial t} n(v_p) = \frac{1}{2}\int_0^{v_p} K(\bar{v}_p, v_p - \bar{v}_p) n(\bar{v}_p) n(v_p - \bar{v}_p) d\bar{v}_p - \int_0^{\infty} K(v_p, \bar{v}_p) n(v_p) n(\bar{v}_p) d\bar{v}_p + \left[\frac{\partial}{\partial t} n(v_p)\right]_s + \dot{n}_s(v_p),$$

where $n(v_p)$ is the continuous distribution function, v_p is particle volume, and K represents the coagulation kernel, which accounts for the number of collisions $cm^{-3}\ s^{-1}$. The first two terms on the right hand side represent coagulation, the third term represents particle growth, and the last term represents nucleation or other particle sources.

The sectional form of the GDE

When the distribution is approximated by dividing the particle size-space into X discrete sections, the GDE has the same form as for a continuous distribution, but only the distribution function for specific moments of the distribution are conserved within each section. Usually, mass is the chosen moment of the distribution because mass is a conserved property. The sectional approach is popular due, in part, to its ability to represent multicomponent aerosol distributions. Most sectional techniques assume that the section boundaries are invariant in time in order to simplify calculation of coagulation coefficients. This can, however, lead to numerical diffusion if an initially broad distribution becomes steep due to particle growth because sharply peaking distributions produce large differences between sections in the conserved quantity (Whitby, 1991).

The integral form of the GDE

When details of the distribution are not needed, the GDE can be simplified to an integral equation, where some of the integrals can be expressed in terms of other moments of the distribution. With a change of variable to diameter, the moment formulation of Equation (1.2) is (Whitby, 1991):

$$\frac{\partial M_k}{\partial t} = \int_0^{\infty} \frac{dD_p^k}{dv_p} \frac{\partial v_p}{\partial t} n(D_p) dD_p + \frac{1}{2} \int_0^{\infty} \int_0^{\infty} D_{p_{12}}^k K(D_{p_1}, D_{p_2}) n(D_{p_1}) n(D_{p_2}) dD_{p_1} dD_{p_2} - \frac{1}{2} \int_0^{\infty} \int_0^{\infty} (D_{p_1}^k + D_{p_2}^k) K(D_{p_1}, D_{p_2}) n(D_{p_1}) n(D_{p_2}) dD_{p_1} dD_{p_2} + \int_0^{\infty} D_p^k \dot{n}_S(D_p) dD_p, \quad (1.3)$$

The first term on the right hand side represents growth processes, the second and third terms represent coagulation, and the fourth term represents particle sources. Particle diameter is D_{pi}, v_p is particle volume, K is the coagulation kernel, and M_k represents the kth moment of the distribution and is defined by:

$$M_k = \int_0^{\infty} D_p^k n(D_p) dD_p \quad (1.4)$$

When the GDE is transformed into an integral equation, the resulting representation is termed 'modal'. In the modal representation, the population is represented by a small number of overlapping intervals, termed modes. Each mode is characterized by a

specific continuous distribution function. The function is arbitrary, but the log-normal distribution is a popular representation because it is capable of realistically representing the distribution of variables in a wide variety of systems (Whitby, 1991), and because it is mathematically tractable: only a few parameters are necessary to represent the entire distribution in the modal technique. One limitation of the modal representation is that a predetermined number of modes is usually required (Whitby, 1991).

The monodisperse approach

The simplest approach, which is a special case of the modal representation, is the monodisperse description in which the population is represented by particles of the same size. The representation is computationally efficient, but suffers from errors due to inaccuracies introduced by assuming that all particles have the same size. One method of minimizing such errors is to introduce multiple monodisperse modes, so that more than one particle size can be included (see Figure 1.3, for example).

II. Application of techniques

A monodisperse representation of the aerosol distribution will be developed in this work. This method was chosen for its simplicity and computational efficiency, thereby making it attractive for inclusion in global models. This section discusses previous work involving monodisperse, modal, and sectional models. Strengths and shortcomings of each are presented, and a course of work is proposed.

Sectional representation

Gelbard and Seinfeld (1980) developed a sectional model (MAEROS) for simulating the evolution of multicomponent aerosol size and chemical composition distributions resulting from coagulation, intra-particle chemical reaction, gas to particle conversion,

and particle sources and removal mechanisms. MAEROS is used in this study as a comparison tool and is discussed in more detail in Chapter 2.

An extension of MAEROS was developed by Warren and Seinfeld (1985). The code is called ESMAP and simulates formation, growth and coagulation processes. This code includes a mechanism for nucleation of particles from the vapor phase. Using ESMAP, the competition for vapor between nucleation and condensation was examined. Their treatment of nucleation and growth assumes that the nucleated aerosol is always monodisperse. The nucleation burst is eventually quenched by the subsequent condensational growth. Any preexisting particles exert an influence on the size distribution evolution and the nucleation rate. A simulation which began with 28 particles cm^{-3} resulted in 40 particles cm^{-3}, which is an order of magnitude reduction in particle number compared to the case without preexisting particles. The main development is the inclusion of algorithms for homogeneous nucleation and condensation which are coupled to the vapor phase, and accurately conserve number concentration.

Log-normal representation

Pratsinis (1988) developed a model of aerosol growth, nucleation, and coagulation in an aerosol reactor. Aerosol reactors are used in the production of ceramic powders and pigments. The model assumes a unimodal log-normal function to describe the shape of the distribution across the entire size spectrum. This log-normal model has been found to closely approximate important characteristics of the product aerosol from an aerosol reactor. The rate of change of the first three moments of the distribution, particle concentration, aerosol volume, and the second moment of the volume distribution, are derived. Five dimensionless groups are used as variables in the system: R, reaction rate group, Kn, Knudsen number, K, coagulation coefficient, Σ, surface tension group, and θ, reactor residence time. By comparing with an exact representation it is seen that the

log-normal model calculates particle concentration well, capturing the rise in N during nucleation, and subsequent condensational growth which suppresses nucleation. The log-normal model also predicts the particle diameter trends, though with slight overprediction in the numerical values.

Monodisperse representation

Kreidenweis and Seinfeld (1988) developed an integral model, based on the work of Warren and Seinfeld (1984), which included three variables, the saturation ratio, S, the total number of particles, N, and the total mass in the aerosol phase, M, to describe the vapor-aerosol system. The model was developed to allow for variable source rates of two condensable vapor species (sulfuric acid, H_2SO_4, and methanesulfonic acid, MSA), changes in the vapor concentration due to nucleation and growth, and competition for the vapor species between nucleation and condensation. The aerosol distribution is represented as a population of two monodisperse modes. The term 'mode' refers to an aerosol size which is distinguished from a second, separately treated, size present in the same volume sample. Each mode, i, is characterized by two moments: total mass in each mode, M_i, and total number in each mode, N_i. Together, M_i and N_i define a unique mean diameter for the ith mode. Results indicate that the formation of new particles is primarily due to the formation of H_2SO_4/H_2O particles, provided that initial seed particle concentrations are relatively low.

Warren and Seinfeld (1984) modeled nucleation and growth of an aerosol in a system in which the vapor concentration remained constant. This model employed classical homogeneous nucleation theory together with an expression for condensation and is cast in non-dimensional form. The aerosol is assumed to be monodisperse, where the number mean aerosol mass per particle is given by dividing the total aerosol mass by total aerosol number. This determines the mean particle diameter. Total aerosol mass is determined by both condensation and nucleation, while total aerosol number is

determined by nucleation only. This monodisperse representation overpredicts the condensation rate. The results from this model were compared with results from the detailed sectional model, MAEROS, which was modified to include homogeneous nucleation into the smallest aerosol size section. The results indicate that the monodisperse model predicts a particle number concentration which is half as large as the particle number concentration predicted by the sectional model, due to higher predicted condensation rates in the monodisperse model.

Comparison studies

In addition to the comparisons discussed above, a comparison of three representations of aerosol distributions was completed by Seigneur *et al.* (1986). Continuous, sectional, and log-normal models which simulated coagulation and condensation, separately, for clear, hazy, and urban conditions for 12 hours were reviewed. COAGUL and CONFEMM simulate coagulation and condensation, respectively, using a continuous distribution function. They are based on solution of the condensation and coagulation equations. ESMAP, discussed above, is the sectional model used. AGRO contains a log-normal representation of the particle size distribution and is based on parameterizations of the condensation and coagulation processes. The mass distributions from each simulation were compared, using the continuous distribution case as the control run.

The absolute averaged normalized percent errors are shown in Tables 1.1 and 1.2. ESMAP(39) represents the sectional model run with 39 sections, while ESMAP(12) represents the sectional model run with 12 sections. The time required to run each 12 hour simulation is shown in the last column of each table. The small errors resulting from the coagulation simulation for the clear and hazy conditions is attributed to the lack of coagulation that occurs. For the urban conditions, the log-normal representation produces the largest error in the coagulation simulation. However, this error is less than

20%, while requiring only 3% of the computational time. Table 1.2 shows that the log-normal representation outperforms the sectional representation in both the clear and the hazy condensation simulations.

Model	Percent Difference			Timing
	Clear	Hazy	Urban	
COAGUL	-	-	-	100-1000 s
ESMAP (39)	1	1	2	180-2500 s
ESMAP (12)	1	1	3	40-350 s
AGRO	2	2	18	< 1.0 s

Table 1.1 Comparison of model results for coagulation simulation (Seigneur, 1986)

Model	Percent Difference			Timing
	Clear	Hazy	Urban	
CONFEMM	-	-	-	150 s
ESMAP (39)	4	12	1	300 s
ESMAP (12)	13	35	4	90 s
AGRO	6	18	7	< 1.0 s

Table 1.2 Comparison of model results for condensation simulation (Seigneur, 1986)

1.C. OBJECTIVES AND METHODOLOGIES

Overview

The main objective of this work is the further development and testing of a simple model of aerosol formation from the vapor phase and evolution of aerosol size and number distributions by processes occurring in the atmosphere, specifically due to SO_2-to-sulfate conversion. The emphasis is on sulfur species because volatile sulfur

compounds are particularly important aerosol precursors and because sulfur species are very hygroscopic and, therefore, are an important component of CCN. The starting point is an existing time-dependent monodisperse integral model, BIMODAM I, with two modes which experience growth, nucleation, coagulation and loss processes associated with atmospheric conditions.

BIMODAM I objectives

BIMODAM I lacks a couple of important features so the first objective is to develop and test these. Because of the monodisperse representation, the condensation rate is overpredicted. The first development for BIMODAM I is the empirical derivation of correction factors for the condensation rate which account for the polydispersity in the of the actual aerosol population.

BIMODAM I lacks a method to describe mass and number transfer from mode 1 to mode 2. The second development in BIMODAM I is a method by which a criterion is developed which dictates when to merge the two modes.

BIMODAM I is calibrated against the more detailed sectional model, MAEROS, to derive these new parameters.

BIMODAM II objectives

BIMODAM I requires too much computational time to run in a global model and the differential equation solver is not vectorizable, so another objective is to develop simpler algorithms without losing information on the physics involved. This is done by solving the differential equations analytically, under simplifying assumptions, evaluating applicability of those assumptions, and developing parameterizations for the most computationally time-consuming processes involved.

The differential equations representing coagulation, and deposition are solved analytically, mass balance is applied to calculate particle growth, and a nucleation

parameterization is developed. The parameterizations and simplifications developed are incorporated into BIMODAM II and are compared with results from the original time-dependent integral model, BIMODAM I.

Chapter overview

Chapter 2 consists of a discussion of the mathematical formations of the models used in this study, BIMODAM and MAEROS. Chapter 3 includes development of the condensation rate factor, α, and the merging criteria, χ. In Chapter 4, analytical solutions are developed for the rate equations which represent condensation, coagulation, and deposition. A parameterization for the nucleation process is developed in Chapter 5. Chapter 6 is a collection of case studies of the complete BIMODAM II formulation, which is tested against BIMODAM I as well as against MAEROS. Chapter 7 includes summary and conclusions, as well as suggestions for future research.

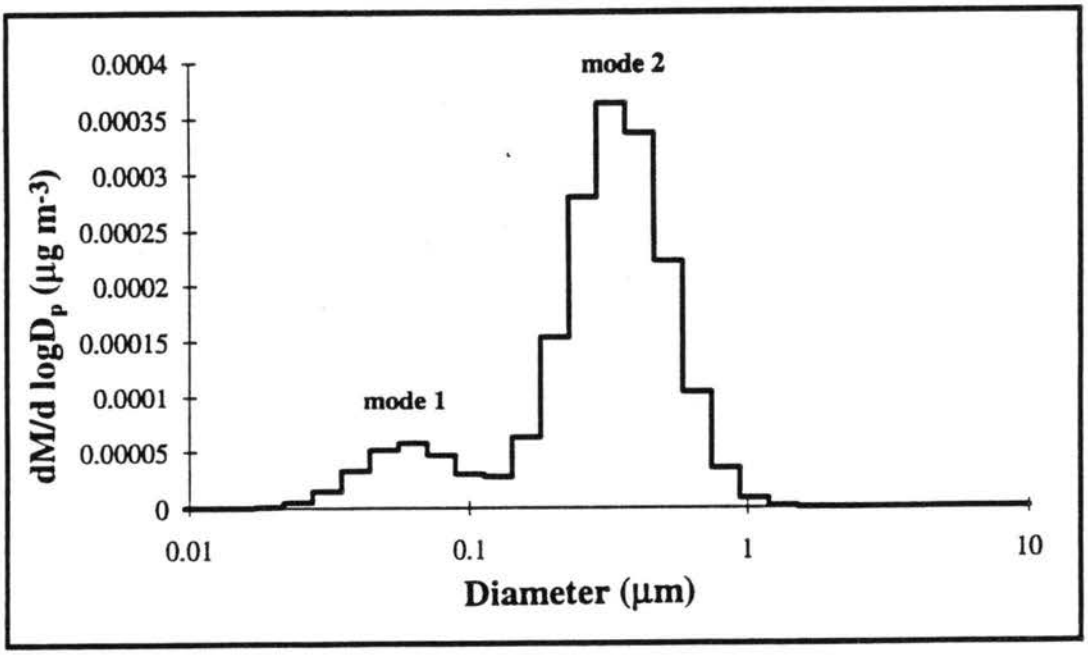

Figure 1.1. The sectional aerosol distribution with two modes.

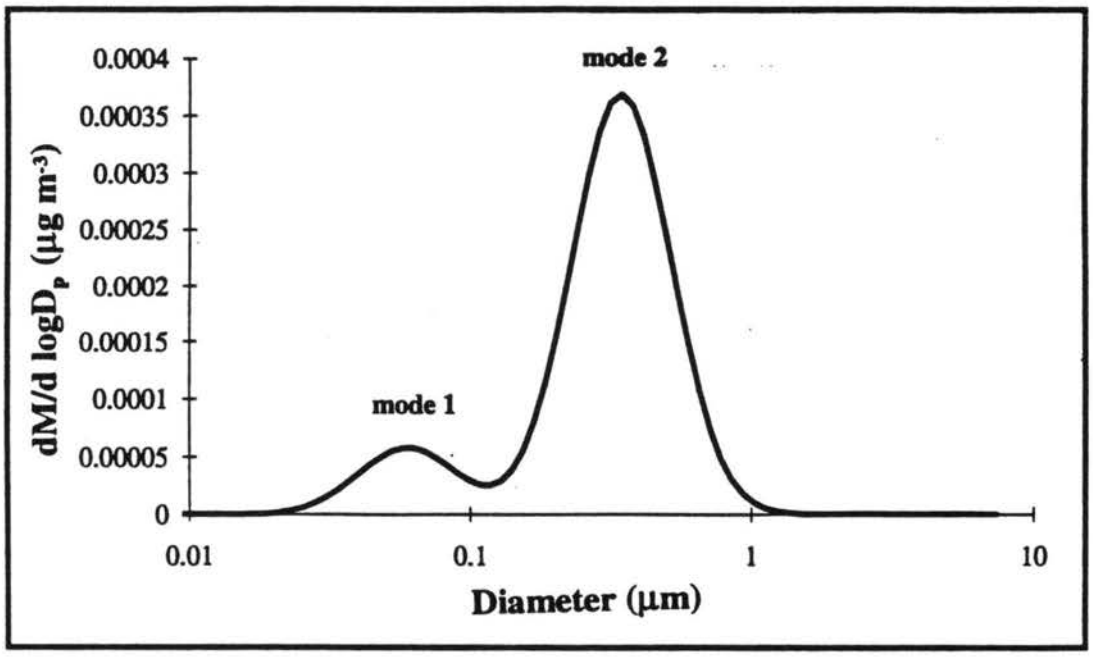

Figure 1.2. Two combined log-normal aerosol distribution functions.

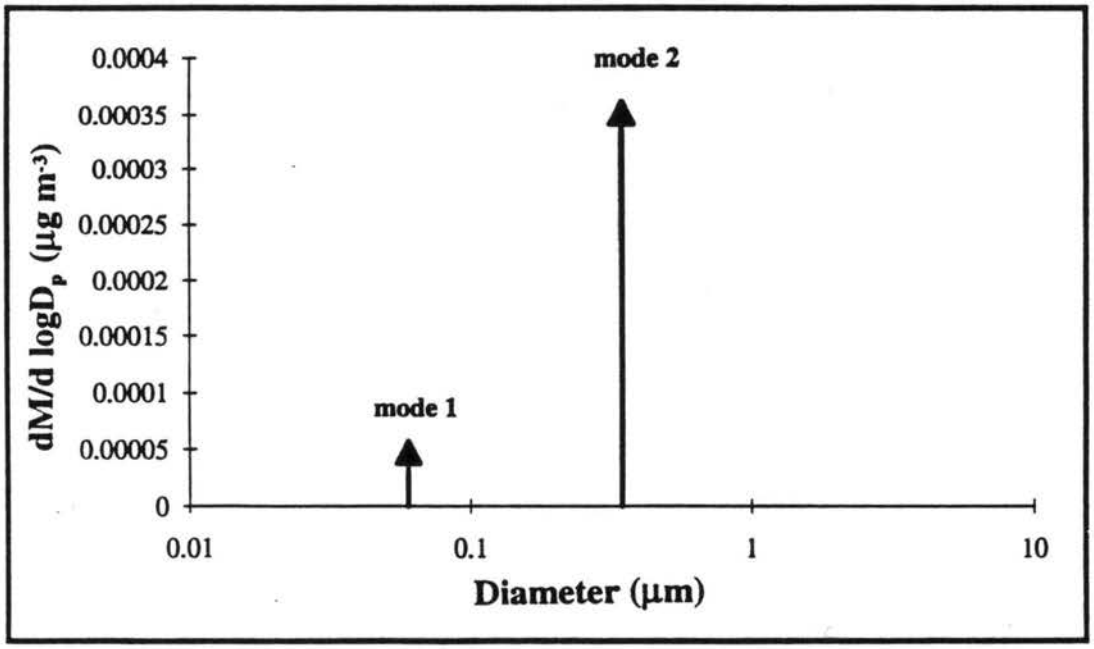

Figure 1.3. Two monodisperse aerosol distributions.

CHAPTER 2 MATHEMATICAL FORMULATION OF MODELS

2.A. AEROSOL AND GAS PHASE PROCESSES

In this section, the rate equations used in the aerosol models discussed in this study are presented. Formulations in both BIMODAM and MAEROS are shown.

I. Condensation

Condensation of vapor molecules onto particles occurs when the vapor pressure over the particle is less than the ambient vapor pressure. Condensation is a key factor in determining the aerosol size distribution. These models consider condensational growth by diffusion of H_2SO_4 to the particle surface, but treat the particle itself as composed of ammonium sulfate; thus the H_2SO_4 is assumed to be immediately neutralized.

By assuming negligible H_2SO_4 vapor pressure over the particle surface, the rate of condensation onto one spherical particle is approximated by a continuum expression modified for non-continuum effects (Okuyama *et al.*, 1988):

$$(2.1) \quad \frac{dM}{dt} = R_c = \frac{2\pi D_j p^o S \beta D_p}{RT},$$

where M is particle mass (molecules cm^{-3}), t is time (seconds), D_j is the molecular diffusion coefficient ($cm^2\ s^{-1}$), p^o is the vapor pressure of pure acid (dynes cm^{-2}), S is the saturation ratio, D_p is particle diameter (cm), R is the gas constant, T is temperature

(K), and β is a correction factor which extends the condensation rate expression through the transition and kinetic regimes following Dahneke's (1983) formulation:

$$\beta = \frac{(1+Kn)}{(1+2Kn(1+Kn/\psi))}, \quad (2.2)$$

where ψ is the sticking coefficient which is the fraction of vapor molecules encountering a particle that stick to the surface, and *Kn* is the Knudsen number. The Knudsen number defines the nature of the suspending fluid to the particle (Seinfeld, 1986):

$$Kn = \frac{2\lambda}{D_p}, \quad (2.3)$$

where λ is the mean free path of air (cm).

When the particle diameter is much greater than the mean free path ($Kn << 1$), the air appears as a continuous fluid to the particle, and the resulting regime is termed continuous. When the diameter is much smaller than the mean free path ($Kn >> 1$), the particle exists in a rarefied medium; this condition is termed the kinetic regime (Seinfeld, 1986). Intermediate between these two regimes is the transition regime.

The variation of β with diameter, computed from Equations (2.2) and (2.3), is shown in Figure 2.1. It is seen that β goes to 1.0 as diameter becomes large in the continuum regime, while on the other side of the spectrum in the kinetic regime, β becomes very small. Intermediate between these two regimes is the transition regime where β varies almost linearly with diameter.

For sulfuric acid in air, the parameters in Equations (2.1) and (2.3) are computed from:

(2.4) $D_j = (1.75x10^{-5})T^{1.5}$,

(2.5) $p^o = (1.167x10^{13})\exp(-10156/T)$,

and

(2.6) $\lambda = (2.383x10^{-8})T$.

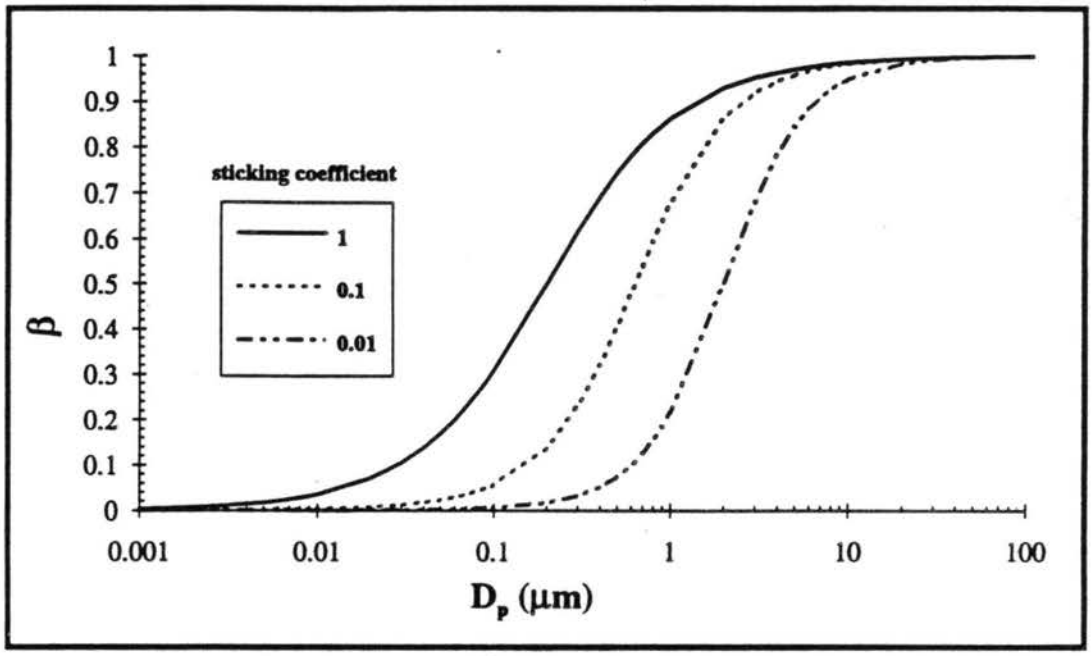

Figure 2.1. β, based on the transition regime formula, versus diameter, D_p, for three values of the sticking coefficient, ψ .

For condensation onto a spectrum of sizes, Equation (2.1) is integrated over diameter, D_p, so that the rate of condensation onto the particle size distribution, $n(D_p)$, is expressed by:

(2.7) $R_c(total) = \int_0^{\infty} R_c(D_p)n(D_p)dD_p$,

where $R_c(D_p)$ is the rate of condensation onto particles of size D_p and $n(D_p)dD_p$ is the number of particles per cm^3 of air with diameters between D_p and $D_p + dD_p$.

BIMODAM I

In BIMODAM I, all particles in the individual modes are assumed to have the same size, so the condensation rate onto each mode, *i*, is given by:

$$R_{ci} = \alpha_i 2\pi D_j N_i V \beta_i D_{pi}, \quad (2.8)$$

where α_i is a factor which corrects for the lack of polydispersity in the model, N_i is the total number of particles (cm^{-3}) in the mode, and V is the concentration of H_2SO_4 vapor (molecules cm^{-3}). The formulation for α_i will be discussed in Chapter 3.

Growth due to humidity

In BIMODAM I, since the relative humidity is considered constant during the simulation, water is not treated as a separate condensing species, but is taken into account when computing the particle size. The particle is assumed to be ammonium sulfate. Polynomial approximations of particle size as a function of aerosol mass and relative humidity that were developed for ammonium sulfate particles were used (Kreidenweis, personal communication).

MAEROS

Since MAEROS considers a distribution of particle sizes, which is divided into sections, the rate of mass addition for each chemical component in each section is calculated along with the rate of mass transfer between sections as particles grow out of a section. The limitation is made that only one chemical component can grow particles into another section and approximations were used for growth due to addition of water

vapor. MAEROS was modified to include the same condensation rate formulation as BIMODAM. A complete mathematical description is given in Gelbard and Seinfeld (1980).

II. Nucleation

The rate of new particle formation may be calculated by homogeneous nucleation theory. Homogeneous nucleation of particles occurs when the vapor phase becomes supersaturated; that is, when the vapor concentration reaches some critical value. For the special case of binary nucleation, particles can form at supersaturations of either chemical component which are insufficient to support homomolecular homogeneous nucleation (Okuyama *et al.*, 1988). In this study, the nucleation species of interest are sulfuric acid, H_2SO_4, and water, H_2O. The nucleation of H_2SO_4/H_2O particles at highly undersaturated conditions is well known (Seinfeld, 1986).

BIMODAM I

The mechanism of new particle formation can be described by the binary nucleation rate formulation, modified for hydrates, of Jaecker-Voirol *et al.* (1988). Figure 2.2 is a plot of the nucleation rate, J, versus sulfuric acid vapor concentration. It can be seen that even at low humidities, significant nucleation occurs, provided that the vapor concentration is high enough. Higher relative humidities require smaller vapor concentrations for nucleation to occur. For both high and low relative humidities, the curves of the nucleation rate are very steep. Because of the complicated nature of the nucleation rate dependence on RH, temperature, and vapor concentration, tables of the nucleation rate as a function of these parameters were compiled by Kreidenweis (personal communication). Tabulated values were fit to 5th order polynomials for use in BIMODAM and were used to generate Figure 2.2. The mean diameter of the freshly nucleated particles is equal to the mean diameter of MAEROS' section 6, approximately

0.004 μm. The number and diameter of the nucleated particles are used to calculate the nucleated mass, and are input into the smallest mode carried by BIMODAM.

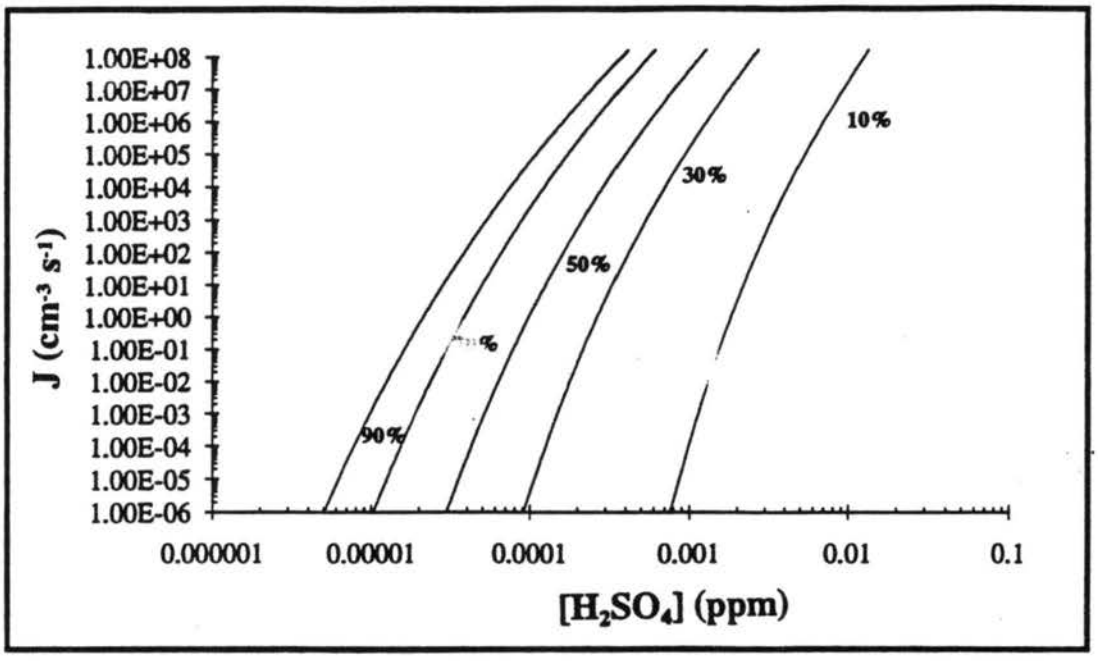

Figure 2.2. The nucleation rate, *J*, versus sulfuric acid vapor concentration, $[H_2SO_4]$, for five relative humidities.

MAEROS

In order to use MAEROS as a comparison tool, it was modified to incorporate the same nucleation rate calculation as that used in BIMODAM I. The particles are put into section 6 which has a mean diameter of approximately 0.004 μm. This corresponds to 291 molecules of sulfate added per each new particle which was calculated using:

$$(2.9) \quad m_p = N_{AV} \frac{\pi}{6} \frac{\rho}{MW} D_p^3,$$

where N_{AV} is avogadro's number (6.022 x 10^{23} molecules $mole^{-1}$), ρ is the density of H_2SO_4 (1.8 g cm^{-3}), MW is the molecular weight of H_2SO_4 (98.08 g $mole^{-1}$), and D_p is particle diameter (~ 4 x 10^{-7} cm).

III. Coagulation

Aerosol particles suspended in a fluid may coagulate because of their Brownian motion. The Fuchs form of the Brownian coagulation coefficient, K_{12}, is shown in Figure 2.3 and follows the formulation (Seinfeld, 1986):

$$(2.10)\quad K_{12} = 2\pi(D_1 + D_2)(D_{p1} + D_{p2})\left[\frac{D_{p1} + D_{p2}}{D_{p1} + D_{p2} + 2g_{12}} + \frac{8(D_1 + D_2)}{\bar{c}_{12}(D_{p1} + D_{p2})}\right]^{-1},$$

where

$$(2.11)\quad D_i = \frac{kT}{3\pi\mu D_{pi}}\left[\frac{5 + 4Kn_i + 6Kn_i^2 + 18Kn_i^3}{5 - Kn_i + (8+\pi)Kn_i^2}\right],$$

$$(2.12)\quad g_{12} = (g_1^2 + g_2^2)^{1/2},$$

$$(2.13)\quad g_i = (1/(D_{pi}l_i))\left[(D_{pi} + l_i)^3 - (D_{pi}^2 + l_i^2)^{3/2}\right] - D_{pi},$$

$$(2.14)\quad l_i = 8D_i / \pi\bar{c}_i,$$

$$(2.15)\quad \bar{c}_i = (8kT / \pi m_i)^{1/2},$$

$$(2.16)\quad \bar{c}_{12} = (\bar{c}_1^2 + \bar{c}_2^2)^{1/2},$$

where D_i is the diffusion coefficient ($cm^2\ s^{-1}$), D_{pi} is the diameter (cm), k is Boltzman's (1.38e-16 g $cm^2\ s^{-1}$ $molecule^{-1}\ K^{-1}$), T is temperature (K), μ is the viscosity of air (1.83e-4 g $cm^{-1}\ s^{-1}$), $\bar{c}_i$ is the molecular velocity (cm s^{-1}), and m_i is the particle mass (g). The values of K_{12} are used in evaluating the coagulation kernels in the GDE (Equation (1.2)). As seen in Figure 2.3, the lowest values of this coefficient occur when the collisions are between equally sized particles.

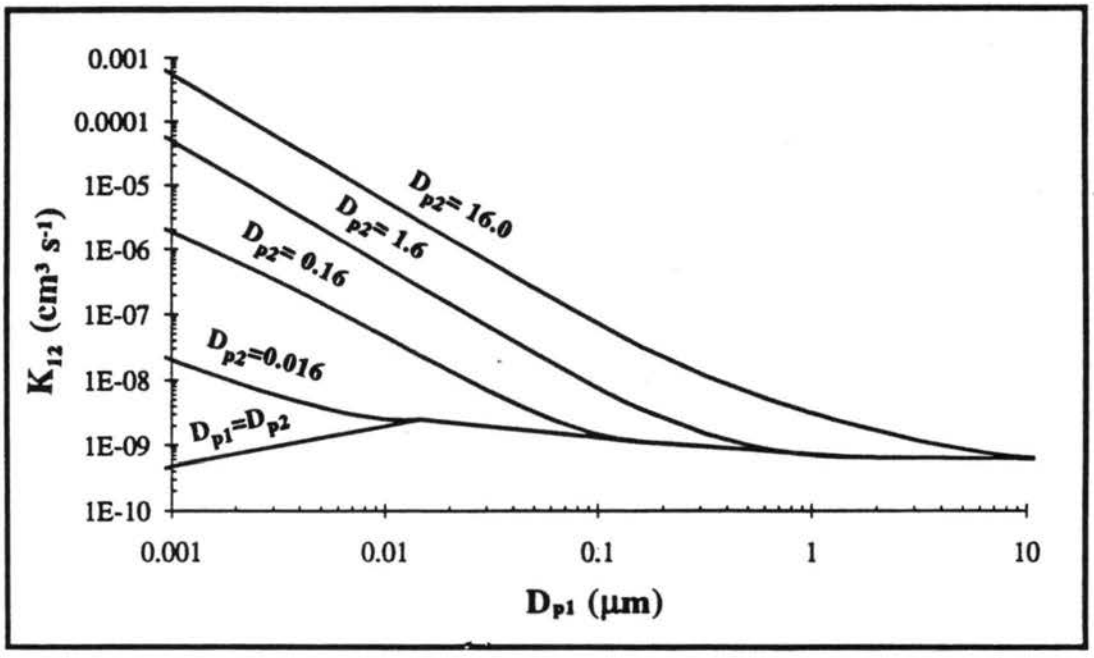

Figure 2.3. The Fuchs form of the Brownian coagulation coefficient, K_{12}.

BIMODAM I

For coagulation, Equation (2.10) is used to calculate the Brownian coagulation coefficient for collisions within mode 1 and mode 2, and for collisions between mode 1 and mode 2 particles so that:

$$\frac{dN_1}{dt} = -\frac{1}{2}K_{11}N_1^2 - K_{12}N_1N_2, \tag{2.17}$$

$$(2.18) \quad \frac{dN_2}{dt} = -\frac{1}{2} K_{22} N_2^2,$$

$$(2.19) \quad \frac{dM_1}{dt} = -K_{12} N_1 N_2 \left(\frac{M_1}{N_1} \right),$$

$$(2.20) \quad \frac{dM_2}{dt} = K_{12} N_1 N_2 \left(\frac{M_1}{N_1} \right).$$

Using this simple formulation, when particles in mode 1 coagulate together, the resulting particle remains in mode 1, regardless of the size of the coagulated particle. By this method, mode 1 particle number concentration decreases, while mode 1 mass is conserved, hence increasing the mean diameter of mode 1 particles. The same is true for coagulation within mode 2. When mode 1 particles collide with mode 2 particles, it is assumed that the resulting particle resides in mode 2, thereby increasing the mass in mode 2 while conserving mode 2 number.

MAEROS

For MAEROS, coagulation is more complicated due to the sectional form of the distribution. Coagulation is calculated according to the GDE (Equation (1.2)). The coagulation process must be evaluated for collisions within sections and between sections. For details of the mathematics, see Gelbard and Seinfeld (1980). MAEROS uses the following restriction on section boundary diameters:

$$(2.21) \quad v_{l+1} \geq 2 v_l.$$

This reduces computations by eliminating some of the coagulation integrals (Gelbard and Seinfeld, 1980).

IV. Loss terms

Assuming no net flow through a parcel of air, the primary particulate mass loss processes are dry and wet deposition. Dry deposition refers to removal of particles at the surface by gravitational settling, diffusion, or mixing. Wet deposition includes scavenging of particle within a cloud by cloud droplets (rainout) and scavenging of particles below the cloud by precipitation (washout).

BIMODAM I

In BIMODAM I wet deposition is ignored and it is assumed that the dry deposition rate is linearly proportional to N_i or M_i so that:

$$\frac{dN_i}{dt} = -K_d N_i, \tag{2.22}$$

and

$$\frac{dM_i}{dt} = -K_d M_i, \tag{2.23}$$

where K_d is the deposition rate constant (s^{-1}). A deposition rate constant of 8.96×10^{-6} s^{-1} was derived from the box model of the sulfur cycle given by Bates *et al.* (1990). The concentrations and fluxes of sulfur species (DMS, MSA, SO_2, and SO_4^{2-}), derived from measurements taken off the coast of Washington State, were used to generate a steady state box model. In order for the H_2SO_4 column burden (cb) of 3.1 μmol m^{-2} to remain in a steady state, the mass flux in must equal the mass flux out. The mass flux out is:

$$F_{out} = K_d [H_2SO_4]_{cb}, \tag{2.24}$$

where K_d is the deposition rate constant and $[H_2SO_4]_{cb}$ designates the column burden concentration (μmol m^{-2}) of H_2SO_4. Since $F_{out} = F_{in}$:

$$(2.25) \quad F_{in} = K_d[H_2SO_4]_{cb},$$

and therefore:

$$(2.26) \quad K_d = \frac{F_{in}}{(H_2SO_4)_{cb}},$$

where F_{in} is the mass flux in of H_2SO_4, measured as 2.4 μmol m^{-2} d^{-1}.

Usually, the dry deposition process is represented by a deposition velocity, which for sulfate particles varies between 0.01 and 1.0 cm s^{-1} (Seinfeld, 1986). Langner and Rodhe (1991) used a value of 0.2 cm s^{-1}. The deposition velocity is an empirically derived parameter which follows (Seinfeld, 1986):

$$(2.27) \quad v_d = \frac{F_{v_d}}{\left[M_{z_1}\right]},$$

where F_{v_d} is the vertical flux downward of the species and $\left[M_{z_1}\right]$ is the concentration of the material at some height, z_1, above the surface. The deposition velocity depends on the species being removed, the meteorological conditions of the surface layer, and the nature of the surface. The difference between Equations (2.26) and (2.27) is that Equation (2.26) considers the column burden of the material (mass/area), while Equation (2.27) considers the concentration of the material at a specific height (mass/vol). The deposition rate constant can be converted to a deposition velocity by multiplying by the depth of the boundary layer. Assuming a boundary layer depth of

1000 m converts K_d to a v_d value of 0.896 cm s^{-1}, which is within the range stated above.

MAEROS

MAEROS is designed to simulate a 1000 m^3 chamber volume. The leakage rate from the chamber volume was assumed equivalent to the deposition loss rate from BIMODAM I, and therefore, the same numerical value of 8.96×10^{-6} s^{-1} was used. In MAEROS, it is also assumed that the deposition is strictly dry deposition.

V. Vapor generation

The source rate of condensable species drives nucleation and condensation. These two processes will compete for available vapor. Typical H_2SO_4 generation rates in the atmosphere can be derived by considering how fast the reactions proceed to form H_2SO_4:

(2.28) $SO_2 + OH \xrightarrow{1} HSO_3$

(2.29) $HSO_3 + O_2 \xrightarrow{2} HO_2 + SO_3$

(2.30) $SO_3 + H_2O \xrightarrow{3} H_2SO_4$

The second and third steps of this reaction sequence are very fast, therefore, the first step will be the rate limiting step because it proceeds the slowest. The rate of production of H_2SO_4 is, therefore:

(2.31) $R_p = k[SO_2][OH]$,

where R_p is the rate of production of H_2SO_4, and k is the rate constant for this reaction which, for a temperature of 298 K, and a pressure of 1 atm, is 1.1×10^{-12} cm^3 molecules^{-1} s^{-1} (Seinfeld, 1986). The concentration of OH depends upon the amount of sunlight and the amount of water vapor in the atmosphere. The sunlight is necessary to photolyze ozone, which produces the excited singlet $\left(O\left(^1D\right)\right)$ oxygen atom:

(2.32) $O_3 + h\nu \rightarrow O\left(^1D\right) + O_2, \quad for\ \lambda < 315\ nm.$

The singlet oxygen atom then goes on to react with water vapor to produce OH:

(2.33) $O\left(^1D\right) + H_2O \rightarrow 2OH.$

Tropospheric chemical calculations indicate that the seasonally, diurnally, and globally averaged OH concentration ranges from 10^5 to 10^7 molecules cm^{-3} (Seinfeld, 1986). SO_2 concentrations vary from less than 1 ppb in clean areas up to 200 ppb in polluted areas. Tables 2.1 and 2.2 are matrices of these values and the resulting H_2SO_4 production rates computed from Equation (2.31).

$OH \setminus SO_2$	2×10^{10}	5×10^{11}	5×10^{12}
10^5	2×10^3	5.5×10^4	5.5×10^5
10^6	2×10^4	5.5×10^5	5.5×10^6
10^7	2×10^5	5.5×10^6	5.5×10^7

Table 2.1. Concentration ranges of SO_2 and OH (molecules cm^{-3}), and the resulting H_2SO_4 production rates (molecules cm^{-3} s^{-1}).

$OH \setminus SO_2$	7.84×10^{2}	1.96×10^{4}	1.96×10^{5}
3.92×10^{-3}	8.63×10^{-5}	2.16×10^{-3}	2.16×10^{-2}
3.92×10^{-2}	8.63×10^{-4}	2.16×10^{-2}	2.16×10^{-1}
3.92×10^{-1}	8.63×10^{-3}	2.16×10^{-1}	2.16×10^{0}

Table 2.2. Concentration ranges of SO_2 and OH (ppt), and the resulting H_2SO_4 production rates (ppt).

From these tables, the range of H_2SO_4 production rates is 2.2×10^3 up to 5.5×10^7 molecules cm^{-3}, which corresponds to 8.63×10^{-5} up to 2.16 ppt s^{-1}.

BIMODAM I

BIMODAM I can consider any vapor source rate. For this study the high values of the vapor production rates in Table 2.2 were used: 0.0024 up to 0.24 ppt/s. These rates were assumed constant for the duration of the simulations.

MAEROS

MAEROS may consider any vapor source rate. The vapor source rates used are the same as those used for BIMODAM I.

2.B COMPLETE BIMODAM FORMULATION

The model developed and tested in the first part of this study is the SNM model (Kreidenweis and Seinfeld, 1988), which is now called the BImodal MOnodisperse Aerosol Model, version 1 (BIMODAM I) . The complete formulation of the differential equations describing the aerosol and gas phase processes' effects on the aerosol distribution is:

$$(2.34) \quad \frac{dM_1}{dt} = J m_p + R_{c1} - K_{12} N_1 N_2 \overline{m}_{p1} - K_d M_1,$$

$$(2.35)\quad \frac{dN_1}{dt} = J - \frac{1}{2}K_{11}N_1^2 - K_{12}N_1N_2 - K_dN_1,$$

$$(2.36)\quad \frac{dM_2}{dt} = R_{c2} + K_{12}N_1N_2\,\overline{m}_{p1} - K_dM_2,$$

$$(2.37)\quad \frac{dN_2}{dt} = -\frac{1}{2}K_{22}N_2^2 - K_dN_2,$$

$$(2.38)\quad \frac{dV}{dt} = R_g - R_{c1} - R_{c2} - J\,m_p,$$

where M_1 and M_2 represent the mass concentration (molecules cm^{-3}) of the particles in mode 1 and mode 2, respectively. The number concentration (cm^{-3}) of the particles in mode 1 and mode 2 is represented by N_1 and N_2, respectively; V is the amount of H_2SO_4 (molecules cm^{-3}) in the vapor phase; J is the nucleation rate ($cm^{-3}\ s^{-1}$); m_p is the molecules of sulfate added per each nucleated particle; R_{c1} and R_{c2} are the condensation rates (molecules $cm^{-3}\ s^{-1}$) onto particles in mode 1 and mode 2, respectively; $\overline{m}_p$ is the mass per particle, and R_g is the chemical source rate (molecules $cm^{-3}\ s^{-1}$). K_{11}, K_{12}, and K_{22} are the coagulation coefficients ($cm^3\ s^{-1}$) for 1-1, 1-2, 2-2 collisions, respectively, and K_d is the deposition rate constant (s^{-1}).

Method of solution

The package used to solve the differential equations is VODE (Brown *et al.*, 1989). VODE is a variable coefficient ordinary differential equation solver which works for stiff and nonstiff systems. It utilizes the Adams Moulton and Backward Differentiation Formula methods in Nordsieck form, treating the Jacobian as full or banded. For this study, an internally generated full Jacobian was used.

2.C. COMPLETE MAEROS FORMULATION

MAEROS (Multi-component AEROSol model) is a sectional aerosol model (Gelbard and Seinfeld, 1980) which may be used to simulate the evolution of an aerosol distribution which contains more than one chemical component. The numerical method is based on dividing the particle size domain into X sections and imposing conservation of mass, $Q_i(t)$, for each chemical species and process considered.

The equation which represents the aerosol distribution is:

$$(2.39) \qquad Q_i(t) = \sum_{k=1}^{s} Q_{i,k}(t) = \int_{v_{i-1}}^{v_i} vn(v,t)dv,$$

where $Q_i(t)$ is the total mass of aerosol per unit volume of fluid in section i at time t, $n(v,t)dv$ is the number concentration of particles in the range $[v, v+dv]$ at time t, $Q_{i,k}(t)$ is the mass of chemical component k in section i, s is the total number of components and v_{i-1} and v_i denote the volume associated with the smallest and largest particles, respectively, in section i. The number in each section, $Qn_i(t)$, is diagnosed from the mass distribution according to:

$$(2.40) \qquad Qn_i(t) = Q_i(t)\frac{\dfrac{1}{v_i(t)} - \dfrac{1}{v_{i+1}(t)}}{\ln\left(\dfrac{v_{i+1}(t)}{v_i(t)}\right)}.$$

The MAEROS sections are formed based on the number of sections requested and the diameter range of interest. One simplification made is that the section boundaries are assumed to be invariant in time. Therefore, an estimate of the maximum diameter to which the particles will grow is required before the simulation begins. Increasing the number of sections to improve resolution of the distribution adds at least one additional

differential equation to be solved as well as another section for which to calculate intrasectional coagulation.

For the purposes of this study, MAEROS is run with 39 log-normally spaced sections which span 0.001 - 10 μm in particle diameter. The MAEROS output is analyzed by a post-processing code which calculates the mass mean diameter and the standard deviation of the distribution.

The method of solution

MAEROS employs the Fehlberg 4th-5th order Runge-Kutta method of solution for the differential equations. This method is described in Fehlberg (1970), and its performance is examined in Shampine *et al.* (1976).

2.D EXAMPLE SOLUTIONS

In a typical atmospheric scenario, the vapor concentration builds up due to chemical reaction and is simultaneously slowly depleted as it is scavenged by existing particles. If the vapor source rate is greater than the loss rates associated with particle growth, a 'critical' saturation ratio may be reached that is high enough to support new particle formation, which occurs as a nucleation 'burst'. The nucleation phenomenon occurs on a relatively short time scale, and results in rapid changes in the vapor saturation ratio; thus, during the 'burst' the ordinary differential equation (ODE) solver is forced to take many timesteps, resulting in more computational expense during the nucleation 'burst'. Figure 2.4 is an example of how the magnitude and duration of the nucleation burst changes in BIMODAM I in response to the chemical source rate, where $J(t)$ is the number of particles nucleated ($cm^{-3}\ s^{-1}$).

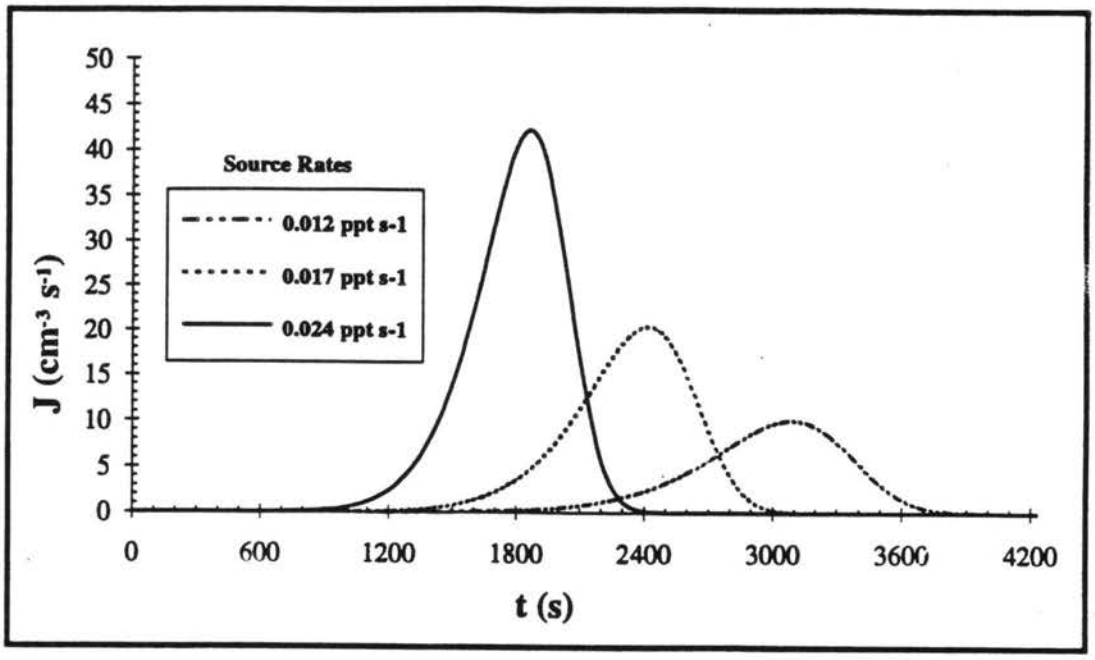

Figure 2.4. The nucleation rate, J, versus time, t, for three source rates, R_g. (RH = 70%).

BIMODAM I

An example application of a six-hour BIMODAM I simulation is shown in Figure 2.5. For this example, initial aerosol number and vapor concentration were set to zero. The particles were formed by the nucleation mechanism discussed previously, using a chemical source rate of 0.024 ppt s^{-1} and a relative humidity of 70%. Coagulation and deposition were not simulated. Particle mass (Figure 2.5b) begins at zero and exhibits a steep increase during the nucleation burst between 1400 and 2800 seconds. After the new particles are completely formed, and the production of number ceases, the aerosol mass increases steadily as the particles grow for the remainder of the simulation. Particle production ceases because of particle growth by condensation. At all times, condensation and nucleation compete for available vapor. During the burst, as the vapor concentration reaches its maximum value, nucleation takes most of the vapor, while the vapor concentration is rapidly depleted as condensation takes all of the vapor

as the particles grow after the burst. The diameter changes (Figure 2.5d) appear rapid in the first few second of the simulations. However, the number of particles in existence at this point is negligible. Diameter changes are then gradual as the first few significant particles form until the burst becomes strong. Once the burst has become strong, the rapid mass and number production cause a steep increase in particle diameter. After the burst, when condensation has quenched the nucleation burst and number concentration no longer changes, the diameter of the particles grows in a steady fashion.

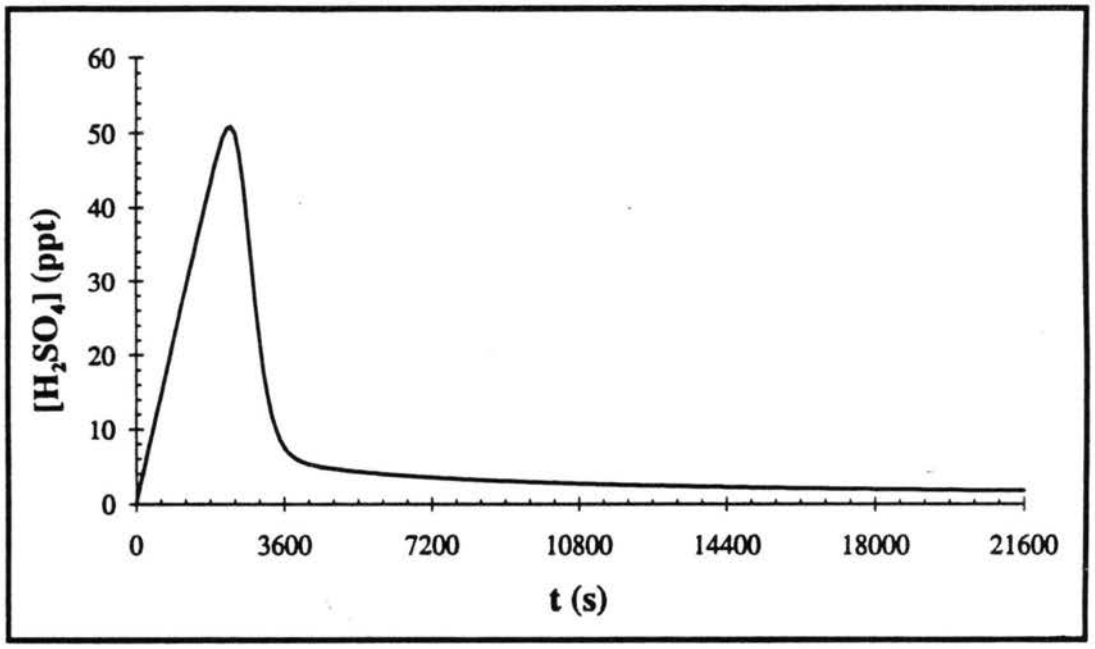

Figure 2.5a. Sulfuric acid vapor concentration, $[H_2SO_4]$, versus time, t, from a 6-hour BIMODAM I simulation, for a vapor source rate of 0.024 ppt s^{-1}, and a relative humidity of 70%.

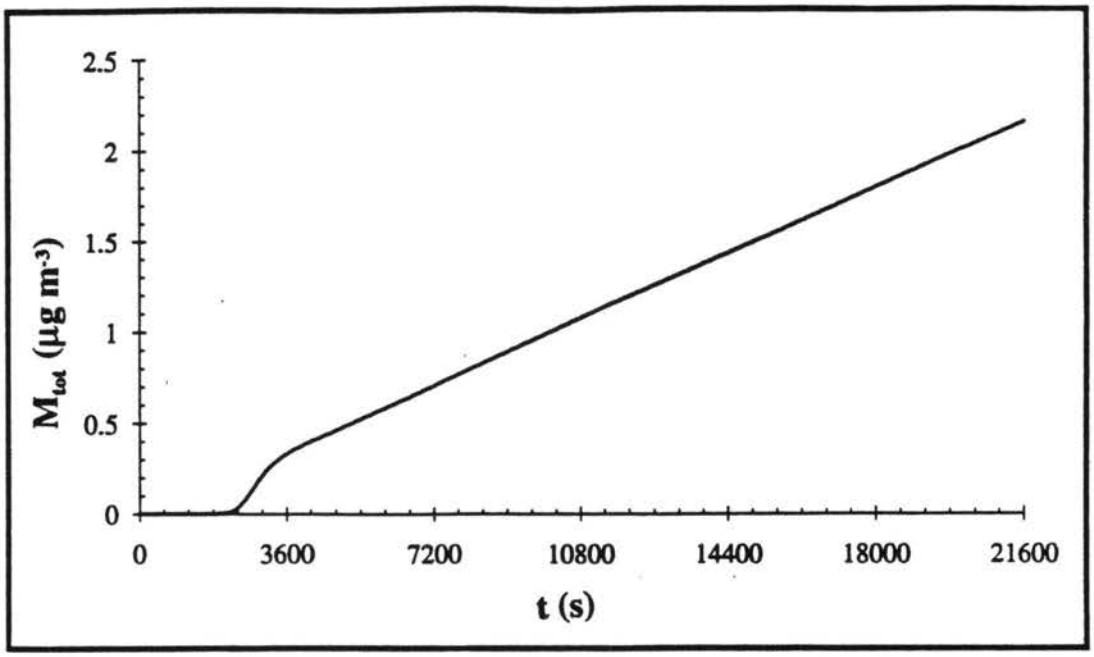

Figure 2.5b. Total aerosol mass concentration, M_{tot}, versus time, t, from a 6-hour BIMODAM I simulation, for a vapor source rate of 0.024 ppt s^{-1}, and a relative humidity of 70%.

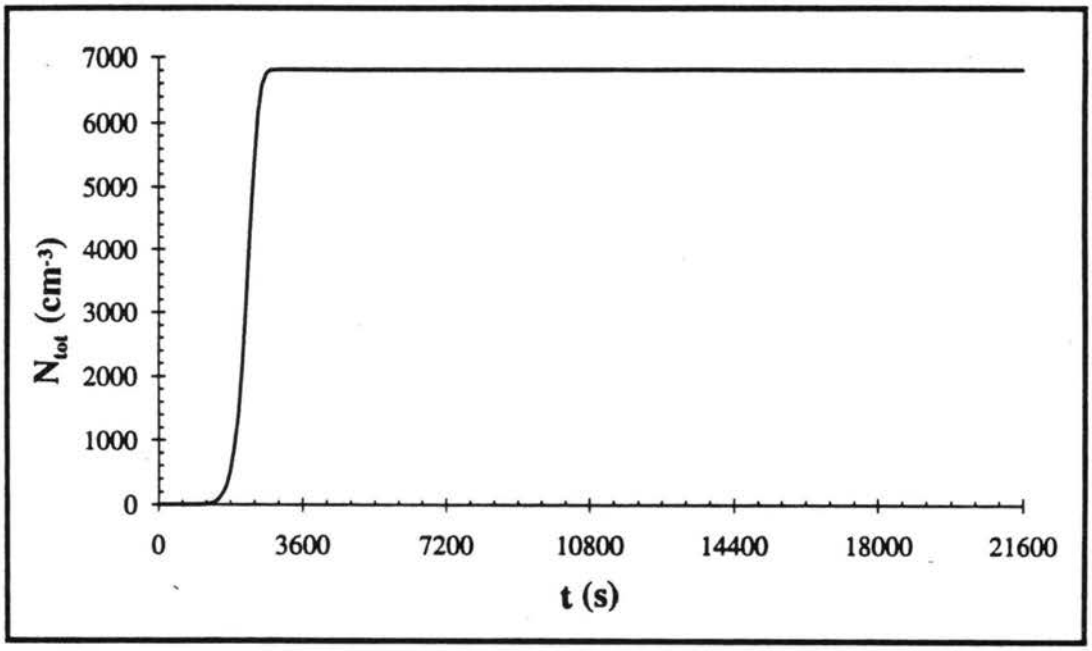

Figure 2.5c. Total aerosol number concentration, N_{tot}, versus time, t, from a 6-hour BIMODAM I simulation, for a vapor source rate of 0.024 ppt s^{-1}, and a relative humidity of 70%.

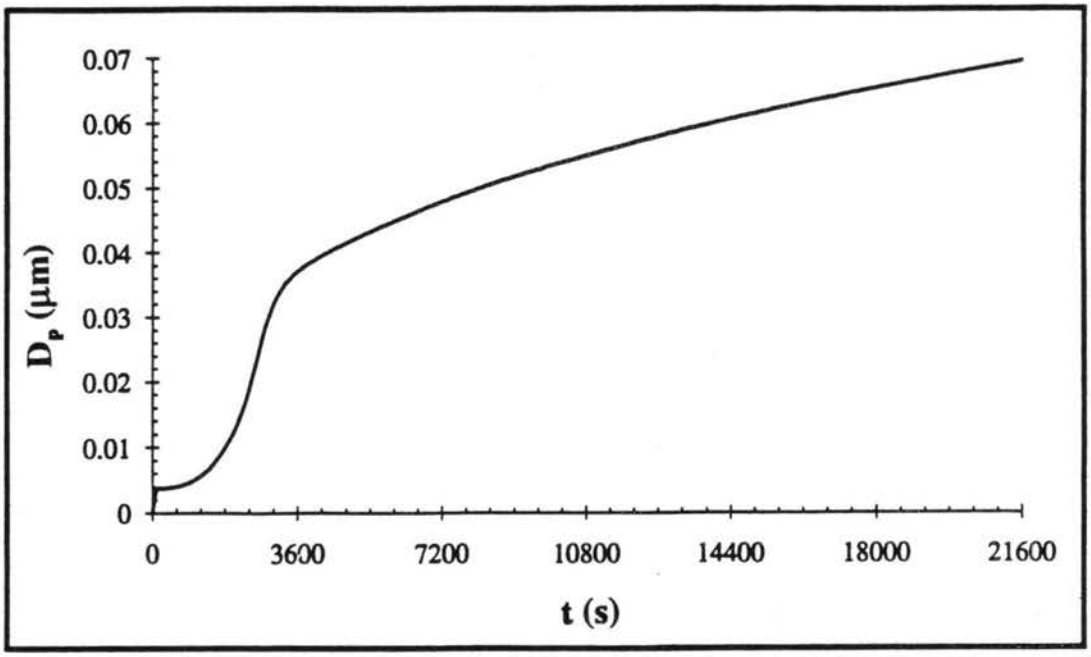

Figure 2.5d. Particle diameter, D_p, versus time, t, from a 6-hour BIMODAM I simulation, for a vapor source rate of 0.024 ppt s^{-1}, and a relative humidity of 70%.

MAEROS

A time history of MAEROS output for the same initial conditions is shown in Figure 2.6. As in the BIMODAM I example, the aerosol mass shows a sharp increase during the nucleation burst and then rises steadily as the particles grow. The vapor concentration peaks during the burst and is depleted rapidly as the particles grow. Aerosol number concentration jumps during the burst and remains constant during the remainder of the simulations. It can be seen by comparing Figures 2.5c and 2.6c that the final aerosol number concentration is lower in the BIMODAM I simulation. This is a result of overpredicting the condensation rate onto the monodisperse representation. When the condensation rate is overpredicted less vapor is available to nucleate more particles.

The MAEROS' mass distribution evolution is shown in Figures 2.7 and 2.8. The distributions which result during the nucleation burst are shown in Figure 2.7, while the

distribution at 1, 3, and 6 hours is shown in Figure 2.8. From these two figures, it can be seen that the distribution just after the start of the burst contains a little mass and spans a small range of diameters (0.01 - 0.05 μm). During the burst, the distribution grows and the diameter range is extended, so that at the end of the burst (3600 s), the diameter range of the distribution extends to 0.15 μm. As the distribution grows further, due to condensation, the diameter range shifts to larger sizes. At the end of the six hour simulation, the diameter range is from 0.02 μm - 0.2 μm.

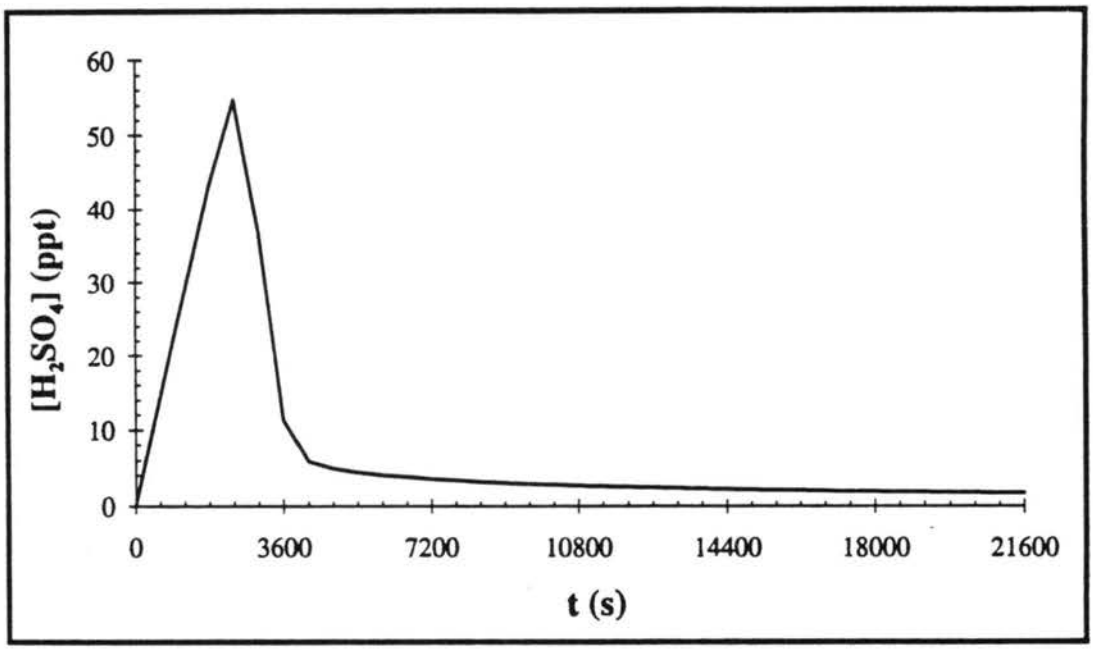

Figure 2.6a. Sulfuric acid vapor concentration, $[H_2SO_4]$, versus time, *t*, from a 6-hour MAEROS simulation, for a vapor source rate of 0.024 ppt s^{-1}, and a relative humidity of 70%.

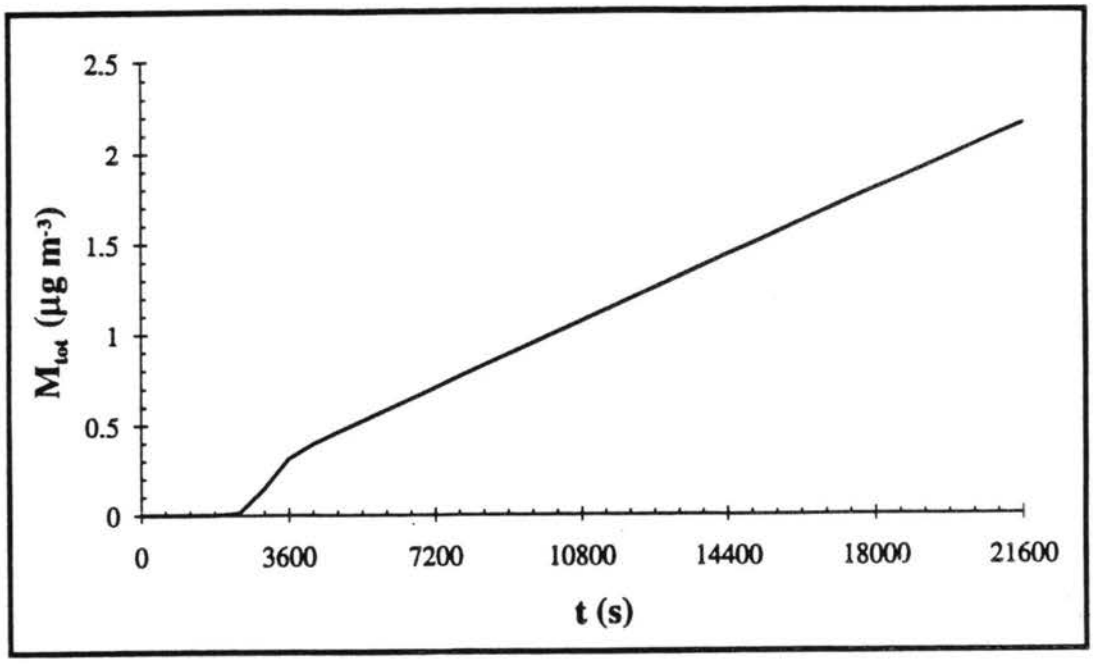

Figure 2.6b. Total aerosol mass concentration, M_{tot}, versus time, t, from a 6-hour MAEROS simulation, for a vapor source rate of 0.024 ppt s^{-1}, and a relative humidity of 70%.

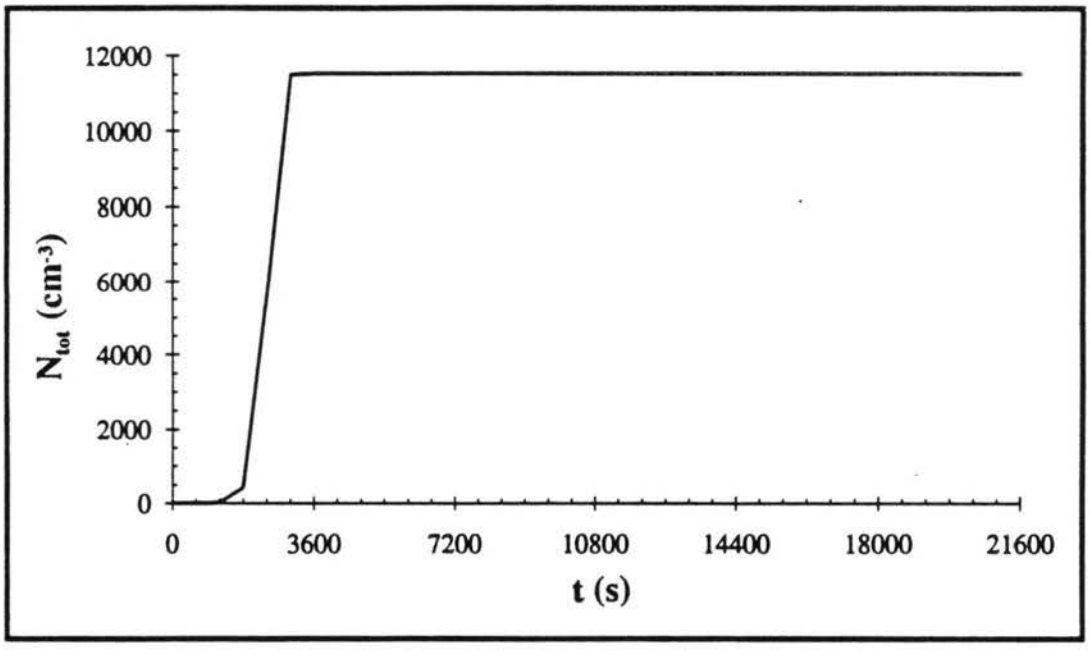

Figure 2.6c. Total aerosol number concentration, N_{tot}, versus time, t, from a 6-hour MAEROS simulation, for a vapor source rate of 0.024 ppt s^{-1}, and a relative humidity of 70%.

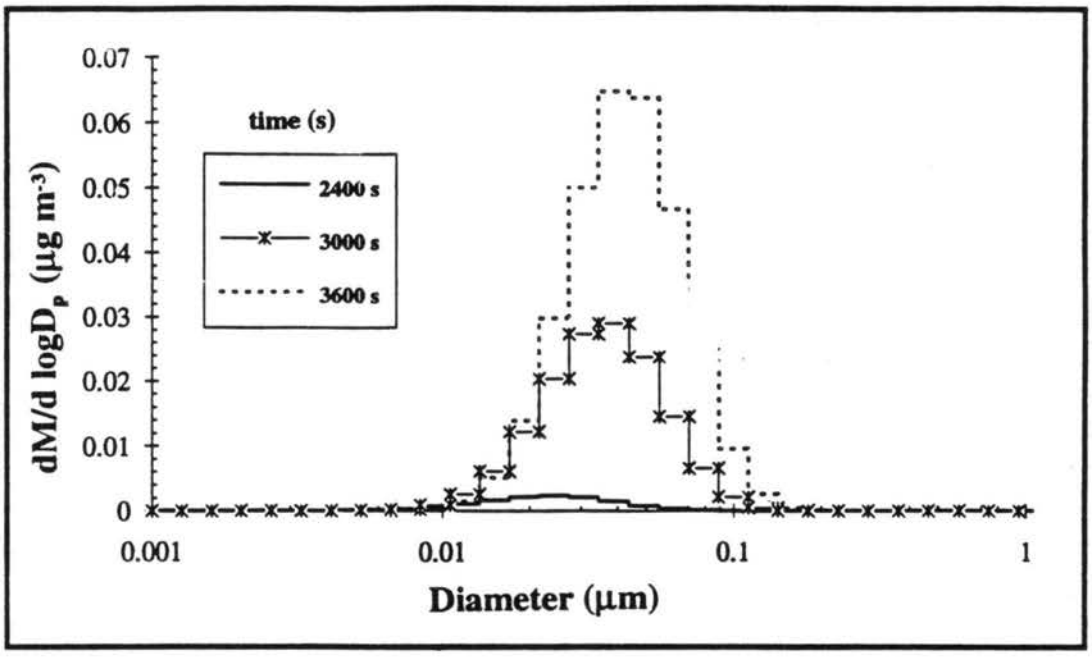

Figure 2.7. Mass distribution during the nucleation burst from the 6-hour MAEROS simulation, for a vapor source rate of 0.024 ppt s^{-1}, and relative humidity of 70%.

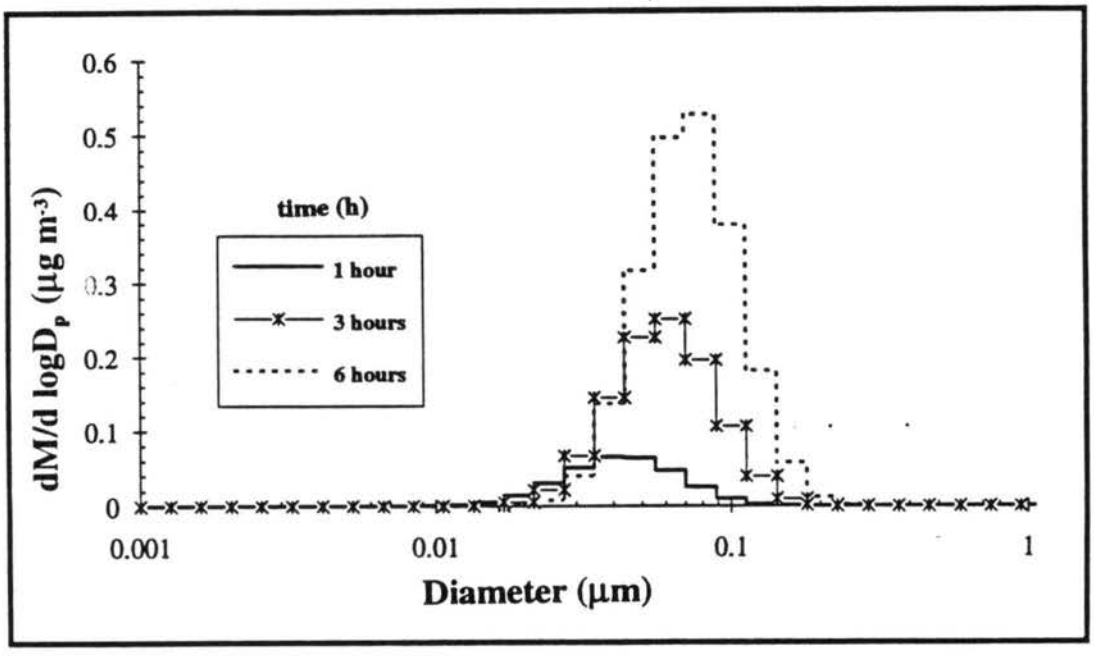

Figure 2.8. Mass distribution after the nucleation burst from the 6-hour MAEROS simulation, for a vapor source rate of 0.024 ppt s^{-1}, and a relative humidity of 70%.

2.E. WORK NEEDED ON BIMODAM I

Despite the fact that BIMODAM I is a simple model, further simplifications and parameterizations are necessary in order to make it suitable for inclusion in large-scale models.

Condensation rate factor

In a monodisperse representation, a method is needed to account for the lack of polydispersity of the simulated population. The rate of condensation onto a monodisperse population always exceeds that onto a polydisperse population (Okuyama *et al.*, 1988). The result is that the condensation rate is not described correctly, as discussed above in the previous BIMODAM I example solution. The condensation rate must therefore be modified to simulate the actual polydispersity of the distribution.

Mass and number transfer between modes

As described previously, the two modes are kept distinct during a simulation, with the exception of 1-2 coagulation. In order to include a method of mass and number transfer between modes, a merging process must be developed. In BIMODAM I, this is necessary because the new particles are assumed to have a diameter of 0.004 μm and they become part of mode 1 when they are formed. Since mode 1 may already have particles in it, adding these very small particles may skew the mean diameter towards the smaller particles.

Simplifications and parameterizations

In order to make this code more computationally efficient, it is necessary to eliminate the differential equation solver since, when conditions in the system are rapidly changing, the differential equation solver is forced to take computationally expensive small timesteps. Parameterization of the most rapidly changing processes in the code

would eliminate this problem, if the step size for the parameterization were chosen correctly.

CHAPTER 3 FURTHER DEVELOPMENT OF BIMODAM I

3.A. INTRODUCTION

In this chapter, two developments are completed and tested. First, appropriate values for the condensation rate factor are derived. This is done so that the condensation rate computed for the monodisperse representation will more closely approximate the condensation rate onto a polydisperse representation. Second, a process is included whereby the two modes are combined when a merging criterion has been met.

3.B CONDENSATION RATE FACTOR

I. Theoretical basis for α

The rate of condensation onto a particle size distribution, $n(D_p)$, was shown in Equation (2.7). For a monodisperse aerosol, this reduces to Equation (2.8) which includes the factor α which accounts for the polydispersity of the actual aerosol population. The condensation rate in Equation (2.8) is the condensation rate onto N particles of size D_p in the continuum regime corrected for non-continuum effects using the factor, β. Since the mass mean diameter is computed in BIMODAM I and is used to calculate the condensation rate, α is defined by:

$$(3.1) \quad \int_0^{\infty} R_c(D_p) n(D_p) dD_p = \alpha R_c(\overline{D}_p) N,$$

so that,

$$(3.2) \quad \alpha = \frac{\int_0^{\infty} R_c(D_p) n(D_p) dD_p}{R_c(\overline{D}_p) N},$$

which is the ratio of the condensation rate onto the total population to the condensation rate onto N particles of size $\overline{D}_p$.

For the special case of a log-normal aerosol distribution, α has the functional form (Okuyama *et al.*, 1988):

$$(3.3) \quad \alpha = \exp(-\ln^2 \sigma_g),$$

where σ_g is the geometric standard deviation. Figure 3.1 shows the variation of α with σ_g for the log-normal distribution. For a log-normal aerosol distribution with a σ_g of 1.3, α is 0.93, which means that the assumption of monodispersity (α = 1.0) results in a condensation rate about 7% too large.

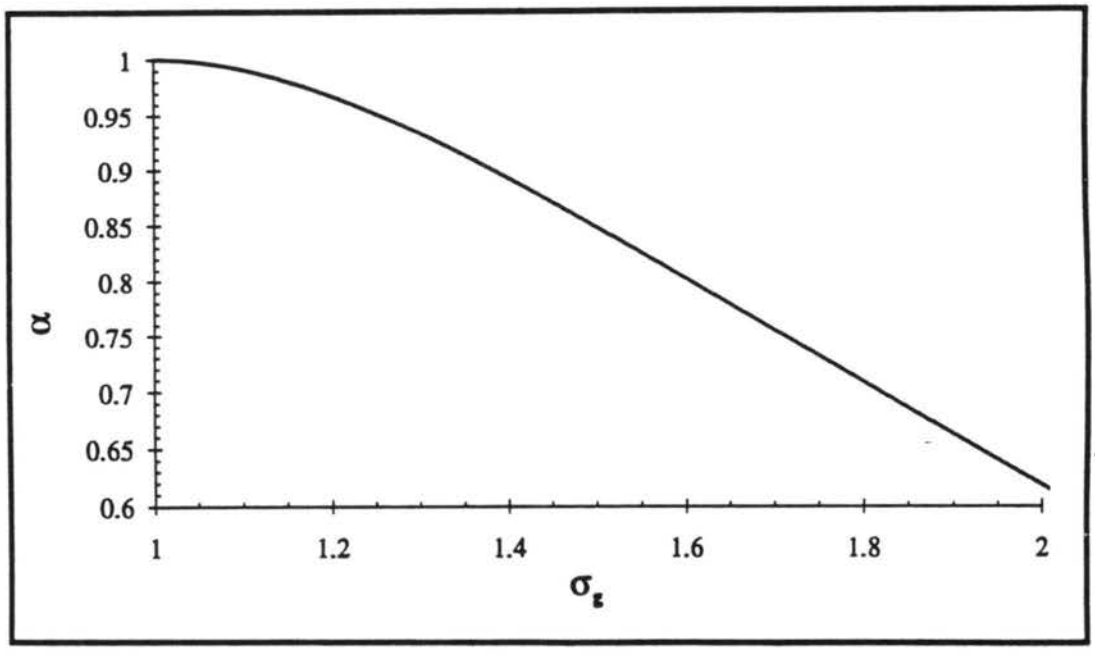

Figure 3.1. The condensation rate factor, α, versus the geometric standard deviation, σ_g, for a log-normal distribution, based on Equation (3.3).

II. Empirically-derived α

Introduction

The value of α_i is related to the spread of the true distribution, which is described by the variance, σ^2, and the geometric standard deviation, σ_g. An example of this relationship is shown in Figure 3.2. Figure 3.2a shows the time-varying results for α_i, as calculated by the MAEROS post-processing code, for three difference vapor source rates, while Figure 3.2b shows the corresponding values of σ_g. As the distribution broadens, during the nucleation burst, α_i decreases and σ_g increases (for a monodisperse distribution, σ_g is 1.0). After the nucleation burst is complete, and as the particles are simply growing, the distribution sharpens; indicated by the rise in α_i, and the decrease in σ_g. At the end of the simulation, the distributions from the three cases have similar values of α_i (0.84) and σ_g (1.4). This value for σ_g is consistent with aged aerosol distributions which have achieved a self-preserving form (Landgrebe and Pratsinis, 1989). However, since the details of the distribution are not known in BIMODAM I, an alternate method is needed to calculate appropriate values for α_i.

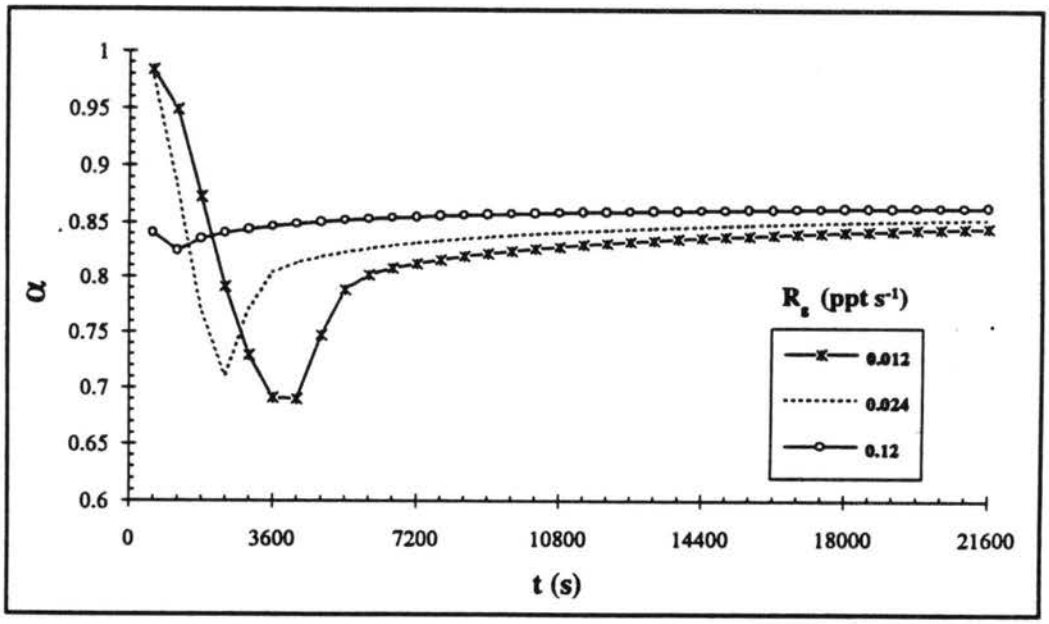

Figure 3.2a. The condensation rate factor, α, versus time, t, for three different source rates, R_g, from MAEROS simulations.

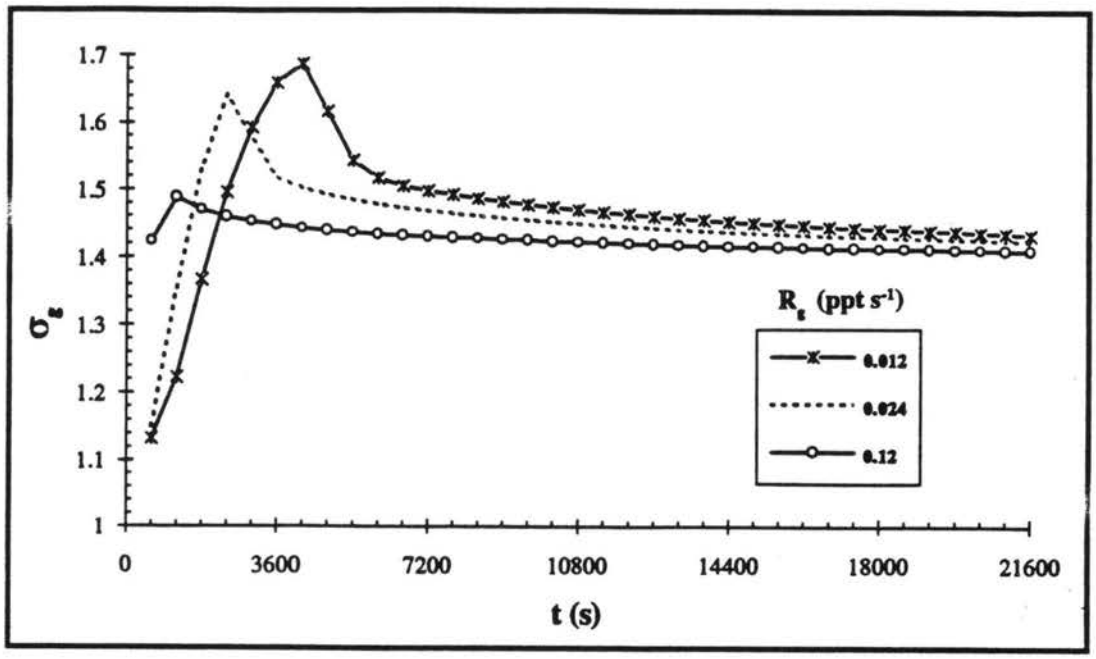

Figure 3.2b. Geometric standard deviation, σ_g, versus time, *t*, associated with Figure 3.2a.

The choice of value for the condensation rate factor, α, is important when nucleation and condensation are competing for the available vapor. If the condensation rate is not correct during a nucleation event, the result will be an incorrect number of nucleated particles. An example of how α affects total aerosol number is shown in Figure 3.3. These simulations were done with a source rate of 0.024 ppt s^{-1} and a relative humidity of 70%. It can be seen that the simulation completed with $\alpha = 1.0$ produces the lowest value of aerosol number concentration, due to the maximized condensation rate, while the simulation completed with $\alpha = 0.6$ produces the largest value of aerosol number concentration. The number nucleated from the MAEROS simulation was approximately 11500 particles cm^{-3}, and therefore, the appropriate α for this simulation is somewhere between 0.7 and 0.8.

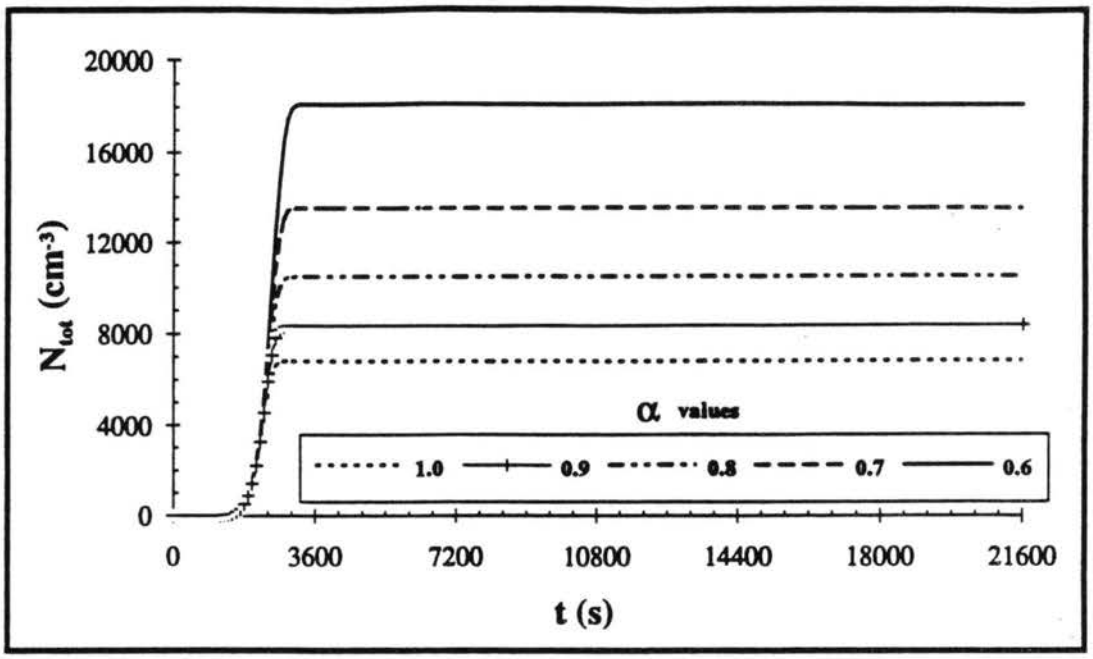

Figure 3.3. An example of the effect of α on total aerosol number, N_{tot}, resulting from a nucleation burst.

Since the most appropriate indicators of what α should be are not calculated in BIMODAM I, a method is needed to obtain a value for α during a nucleation event. Derivation of empirical values of α will be based on simulations in which nucleation and growth of new particles occurs in the presence of a chemical source rate and a depleting vapor concentration. The object is to use BIMODAM I to predict the correct number of particles (as determined by MAEROS) resulting from the nucleation burst.

Method

A number of MAEROS simulations were completed in order to quantify α as a function of source rate and relative humidity. As computed by the MAEROS post-processing code, α follows this formulation:

$$\alpha = \frac{\sum_{i=1}^{ns} D_p(i) N(D_p(i)) \beta(D_p(i))}{D_{p_*} \beta(D_{p_*}) N_{tot}}, \qquad (3.4)$$

where $D_p(i)$ is the mean diameter of section i, $N(D_p(i))$ is the number of particles in section i, D_{pv} is the mass mean diameter of the distribution, and N_{tot} is the total number of particles. This equation represents the ratio of condensation rates (with constant terms canceled), where the numerator is the sum of the condensation rates onto the particles in each section, and the denominator represents the condensation rate onto the mean mass particle. As the distribution evolves in time, the computed value of α changes, as shown in Figure 3.2a.

Values of α were derived from MAEROS simulations in which an aerosol distribution was nucleated and grown from a constant chemical source rate. For these simulations, there were no initial seed particles and the initial vapor concentration was zero. A BIMODAM I simulation was completed with the same initial conditions and active processes, using an α of 1.0. Total aerosol number from the two simulations was compared at the end of the burst. Subsequent BIMODAM I simulations were done using successively lower values of α until the number concentration of aerosol predicted by the two sets of output was different by less than 0.01%.

In order to complete these derivations, the nucleation burst must be finished; the total aerosol number must reach a steady value. For the conditions shown in Figure 3.5a, a six hour simulation was sufficiently long enough for the burst to be completed. In the case of low source rates, which are included in Figure 3.5b, the simulations required as much as 1 day for the burst to finish.

Resulting α values

Figure 3.2a showed how α changes with time as the nucleation burst proceeds. In a BIMODAM I simulation, α does not vary with time. Therefore, the α values derived and presented in this study are the average values, which are applicable during the

entire length of the burst. An example of how the average α compares with the time history of α is shown in Figure 3.4.

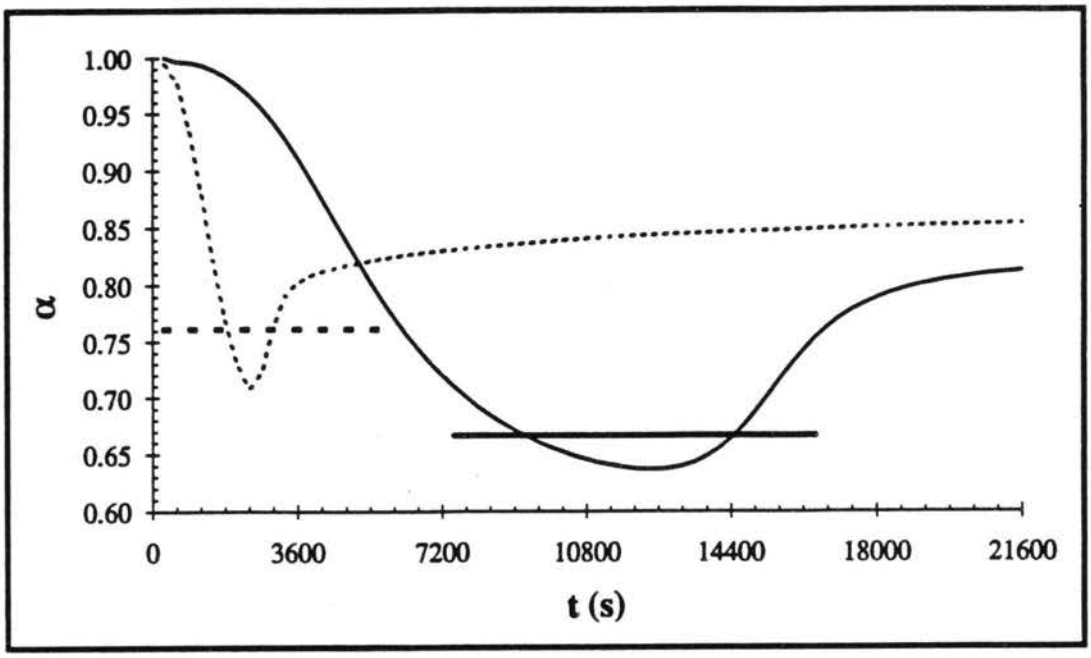

Figure 3.4. The average α used in BIMODAM I compared with the time-varying α computed from the MAEROS simulation (the dashed lines result from a source rate of 0.024 ppt s^{-1}; the solid lines result from a source rate of 0.0024 ppt s^{-1}).

In this manner, appropriate average values for α were derived for a variety of source rates and relative humidities; the results are shown in Figure 3.5. The data points, represented by the symbols in Figure 3.5a, were used to derive polynomial curve fits, represented by the lines, for calculation of α in the code, based on source rate and relative humidity. At high source rates, the nucleation burst occurs very quickly and the resulting distribution is close to monodisperse; hence, for a given relative humidity, the values of α get closer to 1.0 as the source rate increases. The same is true for a given source rate, as relative humidity increases. At low source rates, however, α begins to increase as relative humidity decreases, for a given source rate. This is partly due to the long duration of the bursts which occur at low source rates. With bursts

associated with low source rates, the distribution has time to narrow before the nucleation burst is done, therefore, the α values begin to rise at low source rates for a given relative humidity. For the low source rates, however, less than 1 particle per cubic centimeter is nucleated over approximately one day, so for most cases that will be considered, new particle production at these low source rates is negligible.

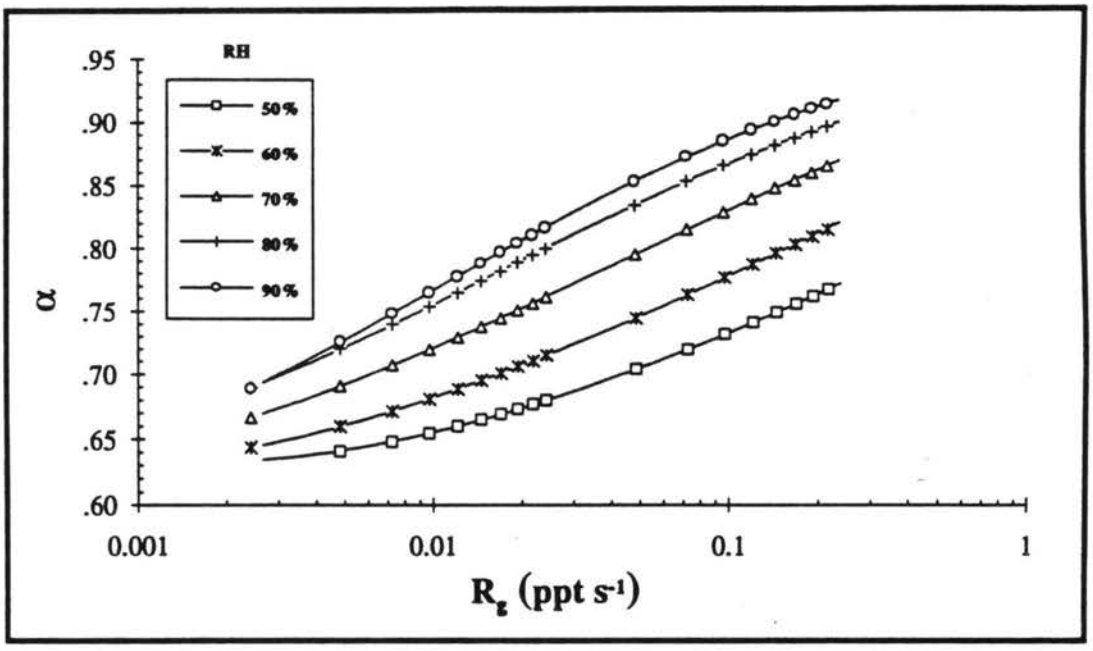

Figure 3.5a. The values of α used in BIMODAM I for a variety of source rates, R_g, and relative humidities, RH.

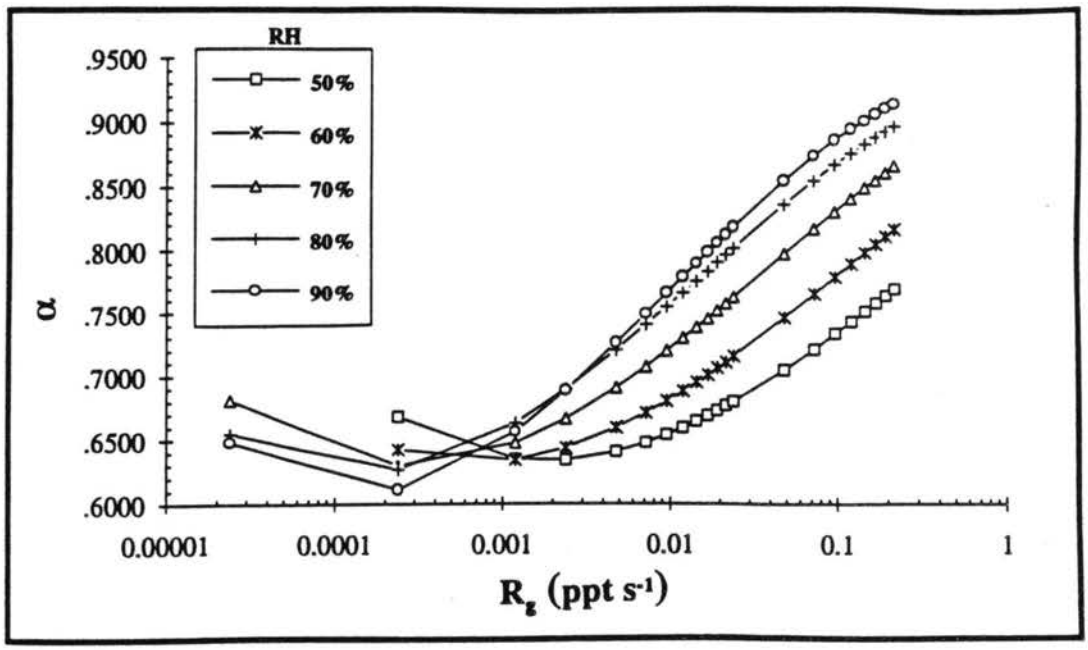

Figure 3.5b. Same as Figure 3.5a, but including low vapor source rates.

Evaluation of α performance

In order to generate accurate results from BIMODAM I, it is crucial to use the correct value of α during the nucleation burst(s), due to the competition between nucleation and condensation for vapor. If the correct α is not used during a nucleation burst, the number of particles nucleated will be incorrect, resulting in incorrect diameters for the entire simulation.

The following scheme is proposed for implementation in BIMODAM I. When there are particles existing in either mode at the beginning of a simulation, and condensation is the only process simulated, α_i is assumed to be 0.85. This value corresponds to a geometric standard deviation for the distribution of 1.5, which is consistent with those computed for self-preserving distributions by Landgrebe and Pratsinis (1989). When nucleation is simulated in the presence of preexisting particles, α_2 is assumed to be 0.85, while the value of α_1 is generated based on the effective source rate for nucleation, using the polynomial curve fits discussed previously.

Example 1

Figure 3.6 is an example of a six hour simulation in which a nucleation burst occurs, using different values of α in BIMODAM I. The source rate and relative humidity for this simulation were 0.024 ppt/s and 70%, respectively. The percent differences from the simulation done with the appropriate value of α , 0.76, are shown in Figure 3.7. Percent error was calculated by:

$$(3.5) \quad \%error = \frac{X_{maeros} - X_{BI}}{X_{maeros}} * 100,$$

where X_{maeros} represents the specific variable value from the MAEROS simulation and X_{BI} represents the specific variable value from the BIMODAM I simulation. It can be seen in the total aerosol number (Figure 3.6c) that α is most important during the nucleation burst (between 1800 and 3000 seconds) when the competition for vapor between nucleation and condensation is high. After the burst, the competition for the vapor between nucleation and condensation no longer exists, so the importance of α diminishes. The effect of α on vapor concentration for this type of simulation is to dictate the maximum vapor concentration reached. The effect of α on total aerosol mass is to overpredict (underpredict) mass when the condensation rate is too high (low), which occurs when α is too large (small). The effect of α on total aerosol number is more pronounced, since small errors in the condensation rate can result in large errors in number of nucleated particles. This is seen in Figure 3.6c. The errors in aerosol number nucleated are reflected in the diameter of the particles (Figure 3.6d), which depends on both mass and number.

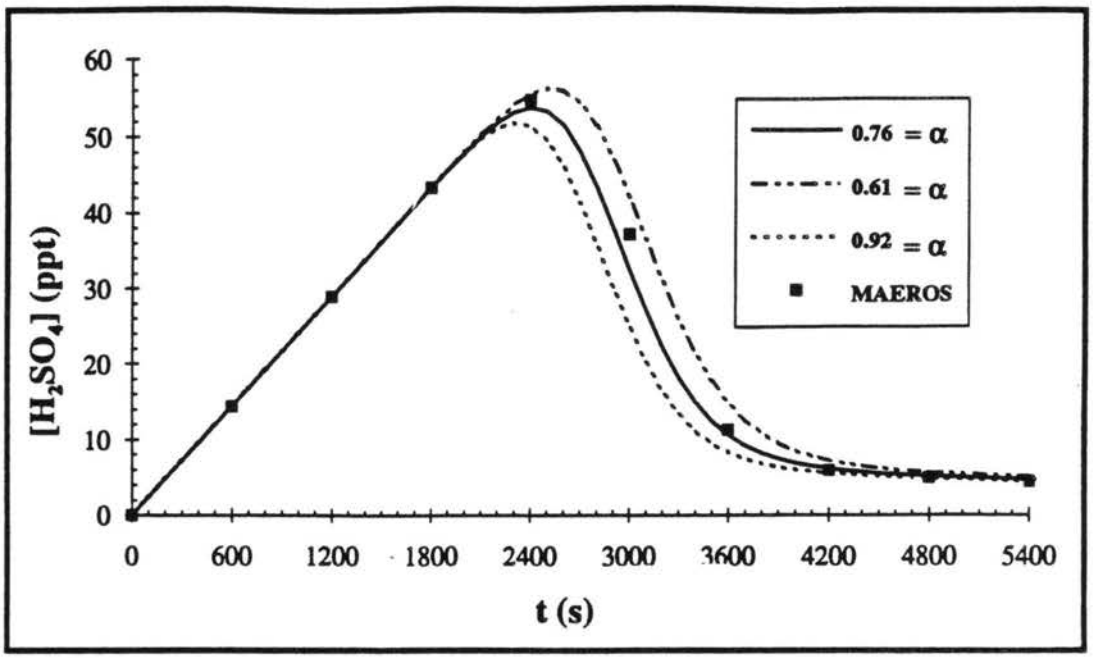

Figure 3.6a. Sulfuric acid vapor concentration, $[H_2SO_4]$, versus time, t, from a BIMODAM I simulation using different values of α. The calculated value of α for this source rate (0.024 ppt s^{-1}) and relative humidity (70%) is 0.76.

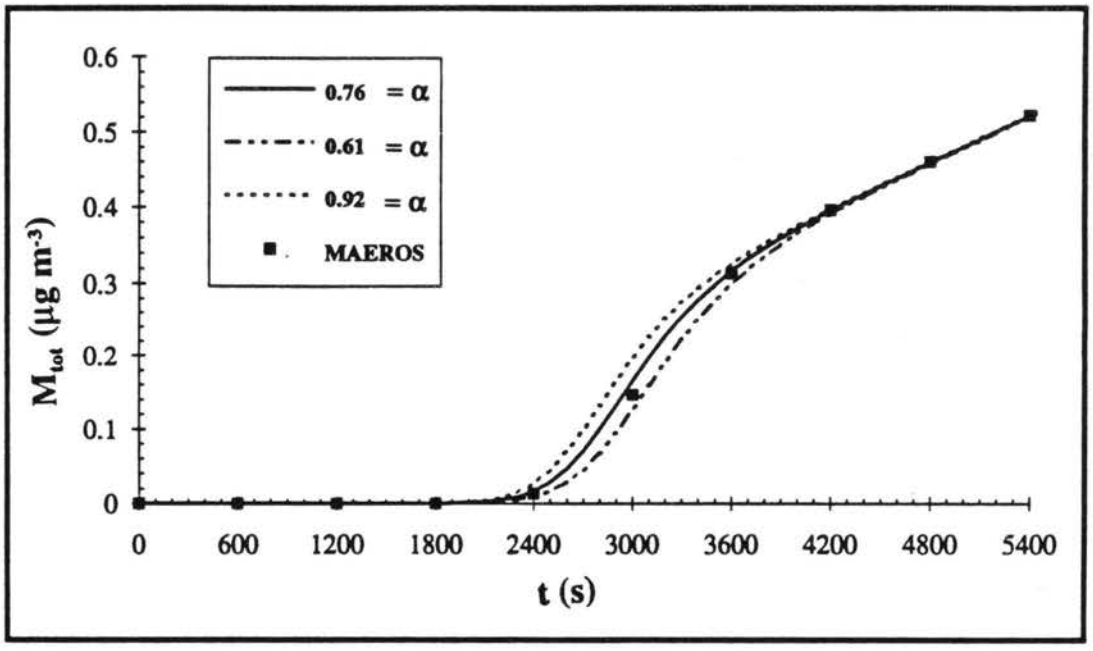

Figure 3.6b. Total aerosol mass, M_{tot}, versus time, t, from a BIMODAM I simulation using different values of α. The calculated value of α for this source rate (0.024 ppt s^{-1}) and relative humidity (70%) is 0.76.

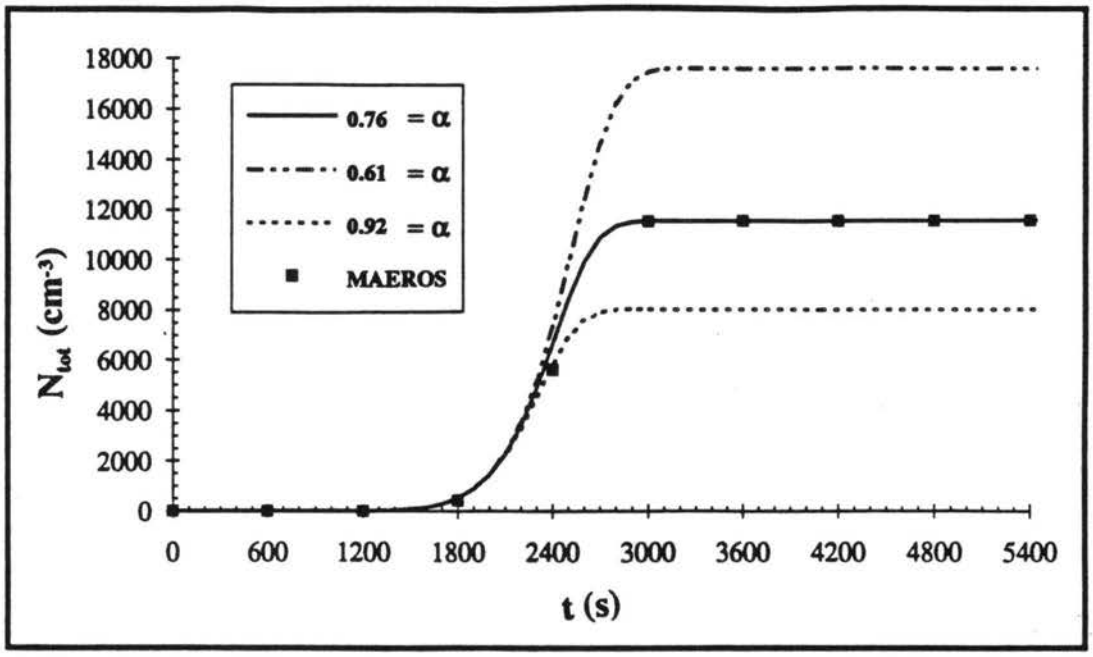

Figure 3.6c. Total aerosol number concentration, N_{tot}, versus time, t, from a BIMODAM I simulation using different values of α. The calculated value of α for this source rate (0.024 ppt s^{-1}) and relative humidity (70%) is 0.76.

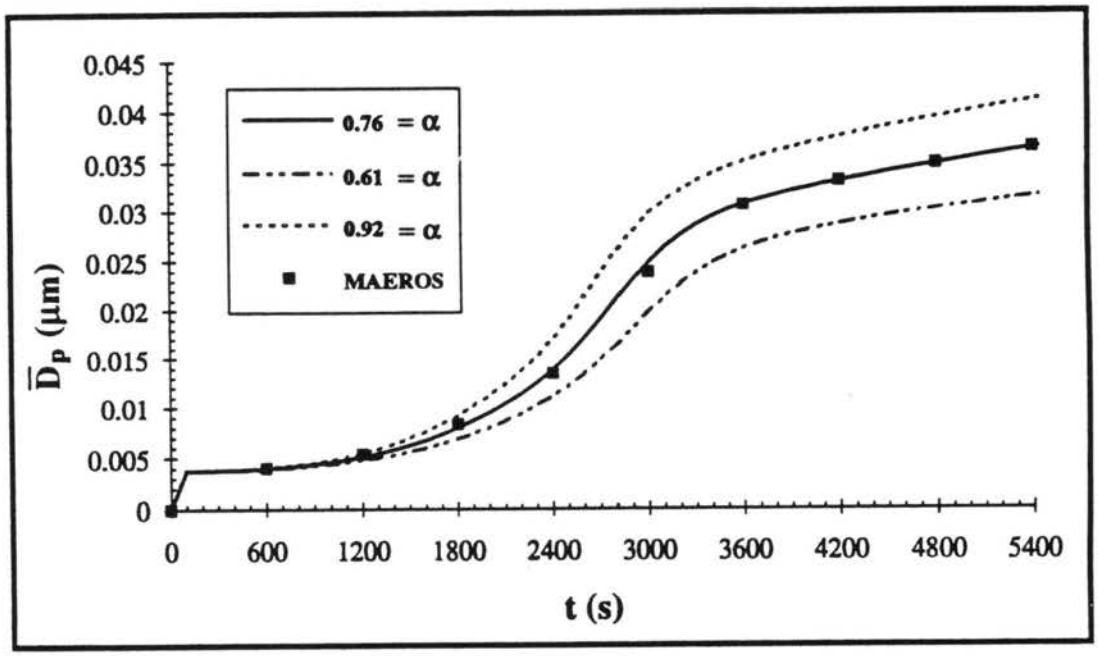

Figure 3.6d. Mass mean diameter, $\overline{D}_p$, versus time, t, from a BIMODAM I simulation using different values of α. The calculated value of α for this source rate (0.024 ppt s^{-1}) and relative humidity (70%) is 0.76.

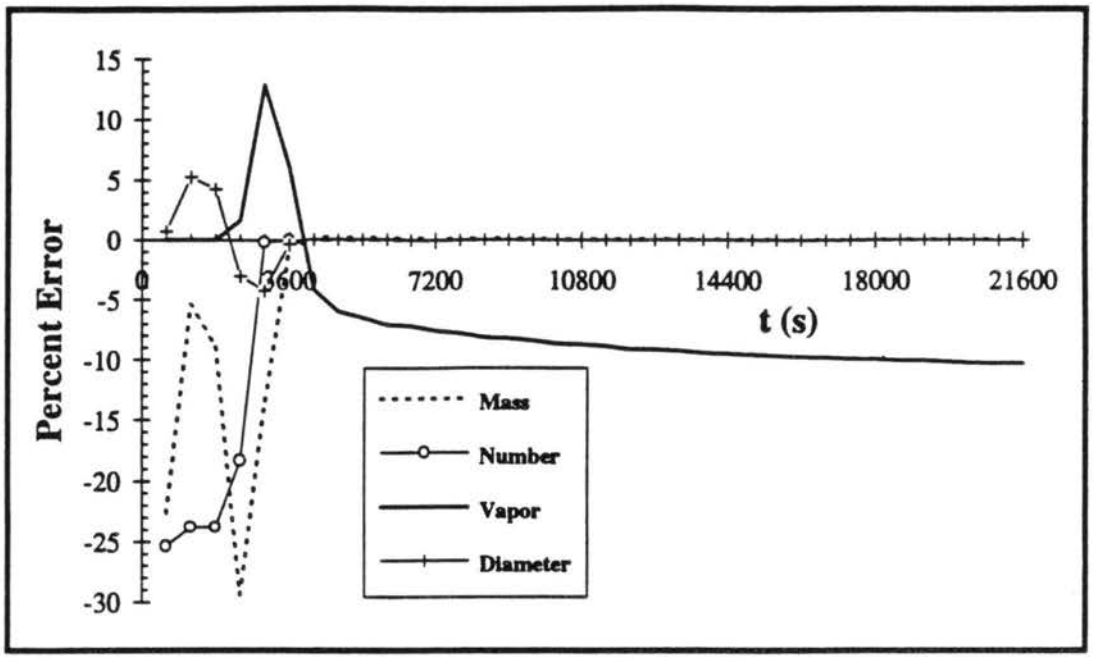

Figure 3.7. Percent errors associated with using the calculated value of α for this source rate (0.024 ppt s^{-1}) and relative humidity (70%).

Example 2

Figure 3.8 is an example of how the choice of α influences a three-hour growth simulation. For this case, a MAEROS simulation was completed with an initial mass distribution of .095 $\mu g\ m^{-3}$, which was log-normally distributed (σ_g=2.0). This corresponds to about 900 particles cm^{-3} with a mass mean diameter of approximately 0.1 μm. The simulation was completed with a relative humidity of 60% and a source rate of 0.002 ppt/s. Five BIMODAM I simulations were completed with α values ranging from 0.6 to 1.0.

It can be seen for this simulation that the value of α plays a large role in determining the vapor concentration; an α somewhere between 0.6 and 0.7 produces the best results, compared with MAEROS. This is consistent with the value of α computed by the post-processing code from the MAEROS distribution, shown in Figure 3.9. The value of α begins at less than 0.6 and rises to above 0.7 at the end of the simulation. The mass

change during this three hour simulation (0.1 $\mu g\ m^{-3}$) is small compared with that from the six hour nucleation simulation (0.5 $\mu g\ m^{-3}$) and, therefore, the value of α does not play such a large role in determining total aerosol mass for this case in which condensation is the only process simulated.

The small errors in total aerosol mass show up as large errors in vapor concentration, due to the orders of magnitude differences between the numbers. The large errors in vapor concentration will result in large errors in number of particles nucleated, if nucleation is simulated, since the nucleation process depends entirely on the vapor concentration. Errors in the vapor concentration will also affect subsequent nucleation bursts, because of the dependence of the nucleation rate on vapor concentration.

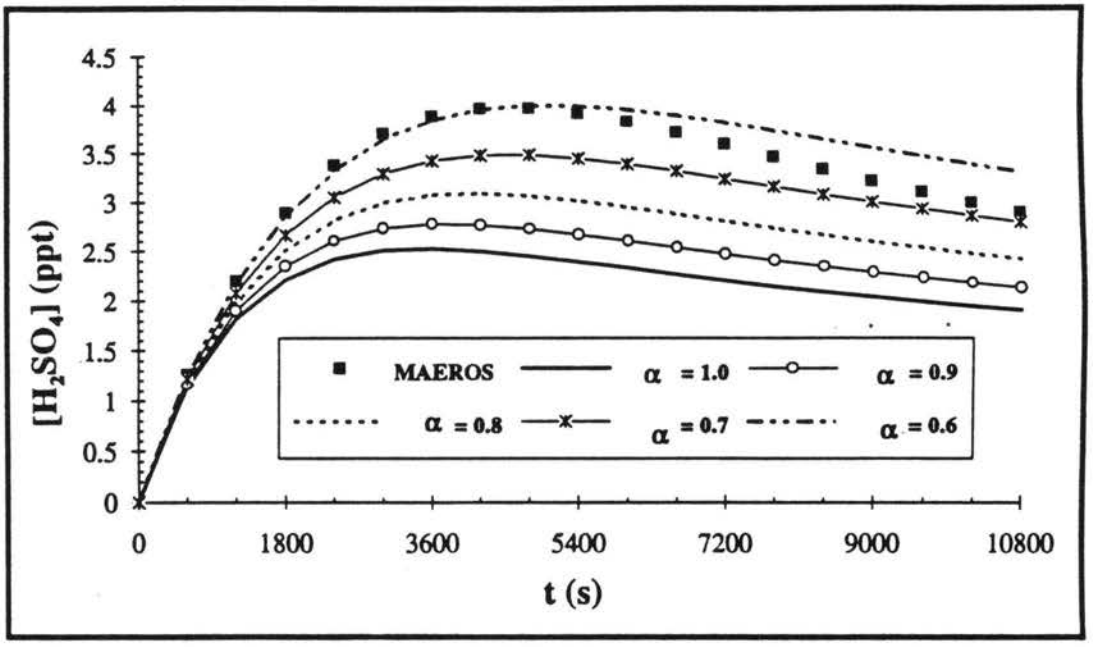

Figure 3.8a. Sulfuric acid vapor concentration, $[H_2SO_4]$, versus time, *t*, from BIMODAM I simulations of condensational growth, using different values of α.

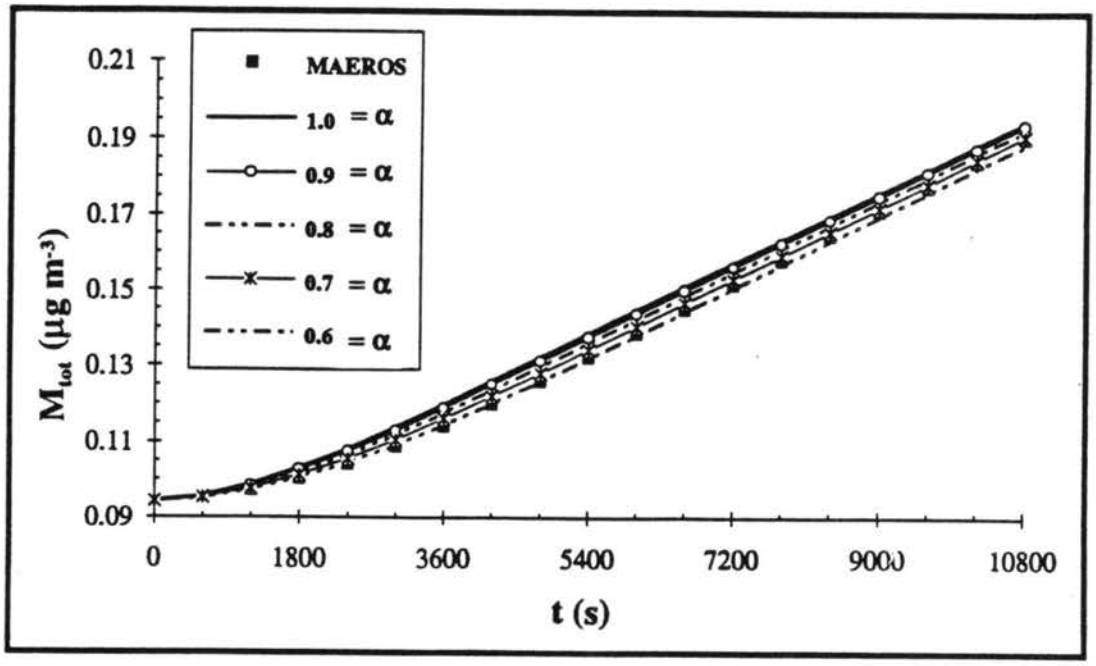

Figure 3.8b. Total aerosol mass, M_{tot}, versus time, t, from BIMODAM I simulations of condensational growth, using different values of α.

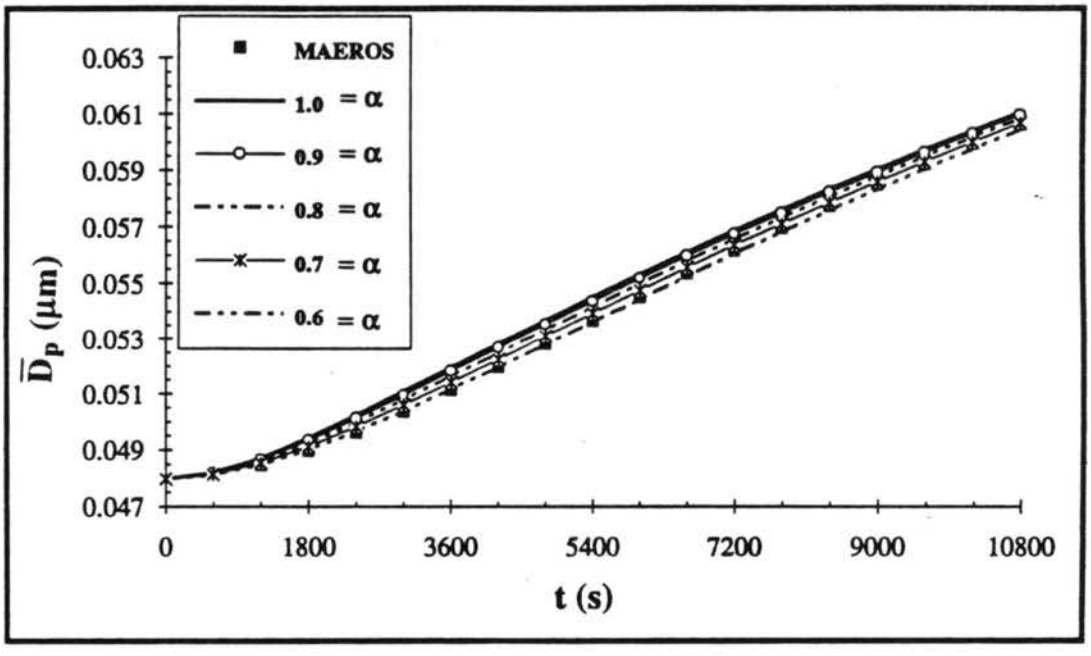

Figure 3.8c. Mass mean diameter, $\overline{D}_p$, versus time, t, from BIMODAM I simulations of condensational growth, using different values of α.

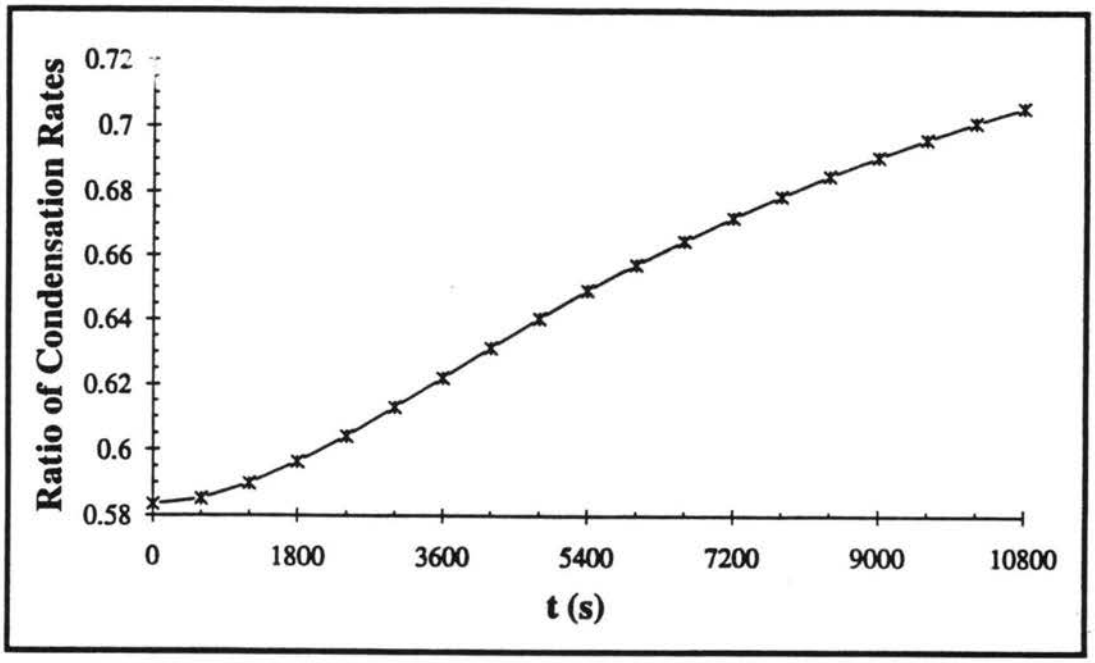

Figure 3.9. The ratio of condensation rates for the MAEROS simulation in Figures 3.8a-c.

Example 3

A nucleation burst in the presence of 100 preexisting particles with a mass mean diameter of 0.1 μm was simulated. The final aerosol number concentration was 3500 cm^{-3}. The value of α for mode 1 was calculated using the polynomial curve fits, discussed previously, where the source rate for nucleation, $\hat{R}_g$, was defined as:

$$\hat{R}_g = R_g - R_{c2} - R_{c1}, \quad (3.6)$$

where R_g is the total chemical source rate, R_{c2} is the condensation rate onto mode 2, and R_{c1} is the condensation rate onto mode 1. The value of $\hat{R}_g$ is determined at the beginning of the nucleation burst; generating a value for α_1 which is applied for the duration of the simulation. For mode 2, $\alpha = 1.0$ was assumed because the initial mass distribution was assigned to one section in MAEROS, which results in a monodisperse distribution.

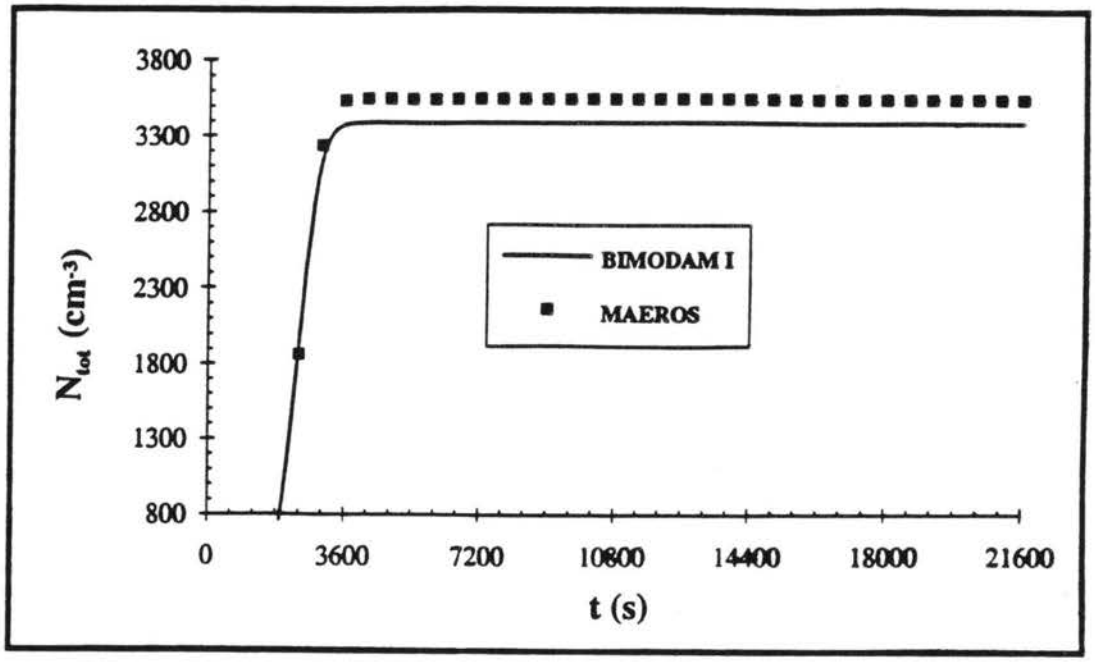

Figure 3.10a. Total aerosol number concentration, N_{tot}, versus time, t, resulting from a nucleation burst in the presence of preexisting particles.

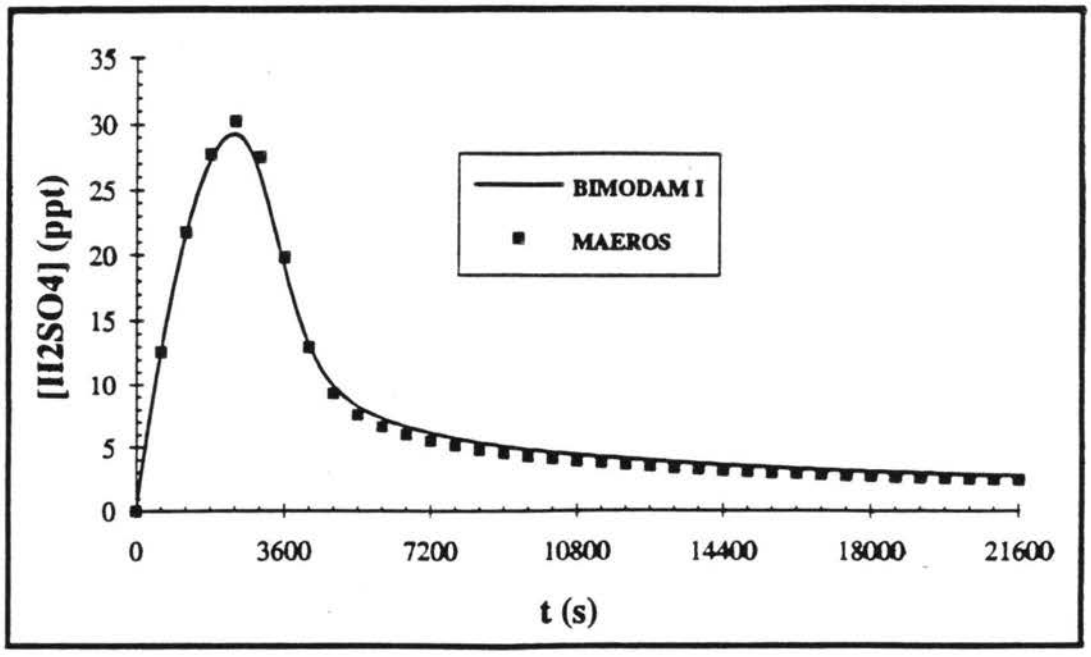

Figure 3.10b. Sulfuric acid vapor concentration, $[H_2SO_4]$, versus time, t, resulting from a nucleation burst in the presence of preexisting particles.

Figure 3.10a and 3.10b shows that this method of generating α_1 is successful in predicting the number of particles nucleated during a burst in the presence of preexisting particles.

3.C THE MERGING CRITERION

I. Introduction

Merging is an important process to include in the modal representation of the population because small particles grow more rapidly than large particles and therefore, the two modes may approach each other in size. When they are close to being the same size, mass and number from mode 1 should be transferred to mode 2, leaving mode 1 empty for acceptance of new particles.

For BIMODAM I, merging is an important control on the size of the individual modes. New particles are incorporated into mode 1 and are assumed to have a diameter of 0.004 μm. Depending on the diameter of particles existing in mode 1 prior to nucleation, the addition of new particles can shift the mass mean diameter towards the smaller particles, losing information about the preexisting particles in mode 1. If the preexisting particles in mode 1 are more similar to the diameter of particles in mode 2, the two modes should be combined.

Because the errors associated with merging are a result of errors in the condensation rate, an appropriate merging criterion will be based upon the condensation rate onto the merged mode, as compared with the combines rates onto unmerged modes.

II. Errors encountered by arbitrarily combining

If two modes are combined arbitrarily, large errors can result. Since the condensation rate onto one size of particles is always greater than that onto multiple sizes, to avoid large errors, merging of two modes into one cannot occur too early. An

example of the error incurred when two modes are merged arbitrarily is shown in Figure 3.11.

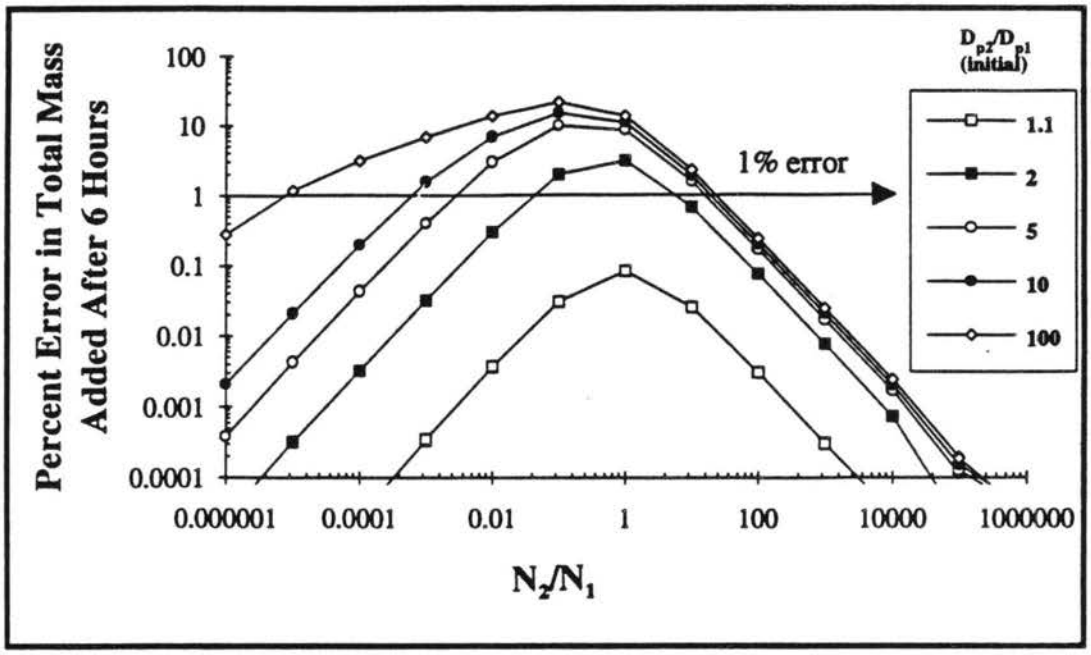

Figure 3.11a. Percent error due to merging for D_{p1} larger than D_{p2}.

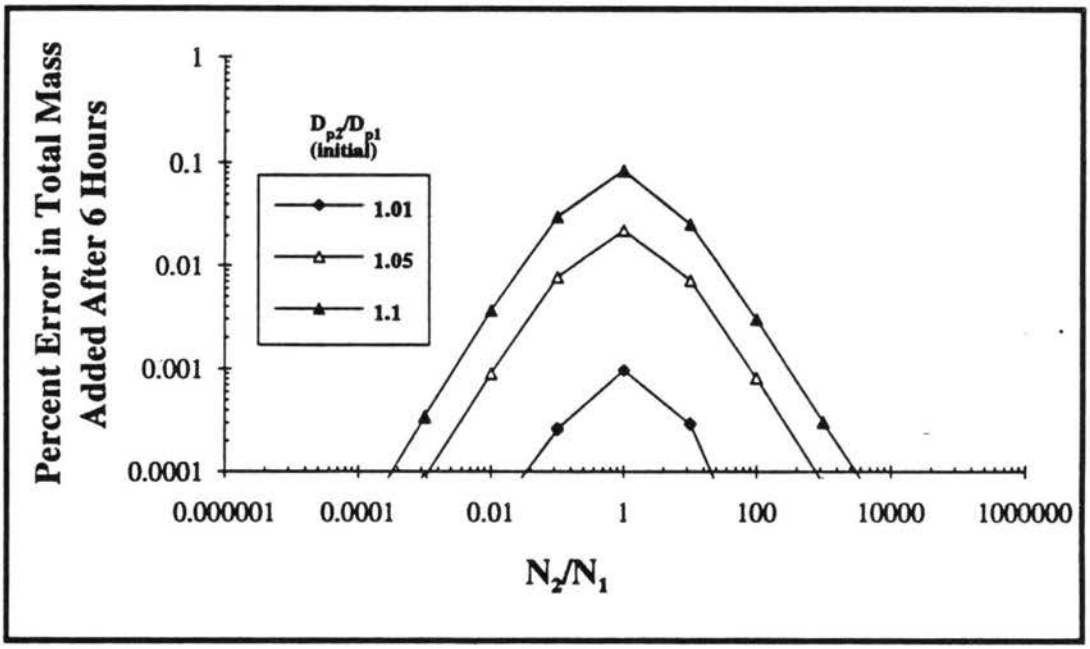

Figure 3.11b. Percent error due to merging for D_{p1} close to D_{p2}.

For this analysis, two simulations were completed. For the first simulation, two modes were grown separately for six hours, while for the second simulation, the two modes were combined into one mode at time at time zero and grown for six hours. For the separate mode simulation, mode 2 contained 100 monodisperse particles with an initial diameter of 0.1 μm, while the diameter and number of particles in mode 1 varied. Both simulations were completed with a relative humidity of 70% and a constant vapor concentration of 24 ppt.

The percent error in total mass added was calculated after six hours using:

$$(3.7) \quad \%error = \frac{(M_1 + M_2) - M_{merged}}{(M_1 + M_2)} * 100.$$

The error was plotted against the N_2/N_1 ratio for different D_{p2}/D_{p1} ratios. Recall from Equation (2.8) that with a constant vapor concentration, N_i and D_{pi} are the variables in the condensation rate. This analysis demonstrated that for the special case of D_{p2}=0.1 μm, in order to keep errors less than 1%, the ratio of mean diameters must be less than 2 when the two modes are combined into a single averaged mode. Therefore, the diameters of the two modes must be close for merging to be done without producing large errors. However, if the ratio of the number concentrations in each mode is greater than 10, errors associated with merging are always small, regardless of the diameters of the two modes. This is because combining a small number of small particles has little effect on the mass and number of the larger particles.

III. Development of merging mechanism

A mechanism was developed so that merging is only allowed when the errors in the condensation rate of the merged mode are small. The condensation rate of the merged

mode is compared with the sum of the condensation rates onto the individual modes. The factor, χ, is used as a criterion to determine if merging is appropriate.

Derivation of merging criterion

The merging criterion, χ, is the ratio of the condensation rate onto the two individual modes to the condensation rate onto the merged mode:

$$\chi = \frac{R_{c1} + R_{c2}}{R_c(merged)}. \tag{3.8}$$

Using the condensation rate formulation given by Equation (2.8), Equation (3.8) can be written:

$$\chi = \frac{\alpha_1 CVN_1 D_{p1}\beta_1 + \alpha_2 CVN_2 D_{p2}\beta_2}{\alpha_2 CVN_{merged} D_p^{'}\beta^{'}}. \tag{3.9}$$

where $D_p^{'}$ is the diameter of the merged mode, C is the collection of constants, and all other symbols have been previously defined. It is easily seen that the vapor concentration, V, and the collection of constants cancel out between the numerator and denominator, yielding:

$$\chi = \frac{\alpha_1 N_1 D_{p1}\beta_1 + \alpha_2 N_2 D_{p2}\beta_2}{\alpha_2 N_{merged} D_p^{'}\beta^{'}}. \tag{3.10}$$

This equation is simplified using the relationship between mass and diameter:

$$D_p = \left(\frac{6}{\pi\rho}\right)^{1/3} \frac{M^{1/3}}{N^{1/3}}, \tag{3.11}$$

so that Equation (3.9) may be written:

$$\chi = \frac{\alpha_1 N_1^{2/3} M_1^{1/3} \beta_1 + \alpha_2 N_2^{2/3} M_2^{1/3} \beta_2}{\alpha_2 N_{merged}^{2/3} M_{merged}^{1/3} \beta'}. \quad (3.12)$$

To further simplify, define the mass and number fractions, respectively, in each mode, *i*:

$$x_i = \frac{M_i}{M_{merged}}, \quad (3.13)$$

$$y_i = \frac{N_i}{N_{merged}}, \quad (3.14)$$

so that Equation (3.12) may be written:

$$\chi = \frac{\alpha_1}{\alpha_2} y_1^{2/3} x_1^{1/3} \frac{\beta_1}{\beta'} + y_2^{2/3} x_2^{1/3} \frac{\beta_2}{\beta'}. \quad (3.15)$$

By defining χ this way, its value will always be less than or equal to 1.

The criterion is applied by checking its value at every timestep, and if χ is equal to or greater than a designated value, the two modes are combined and remain as one mode for the remainder of the simulation.

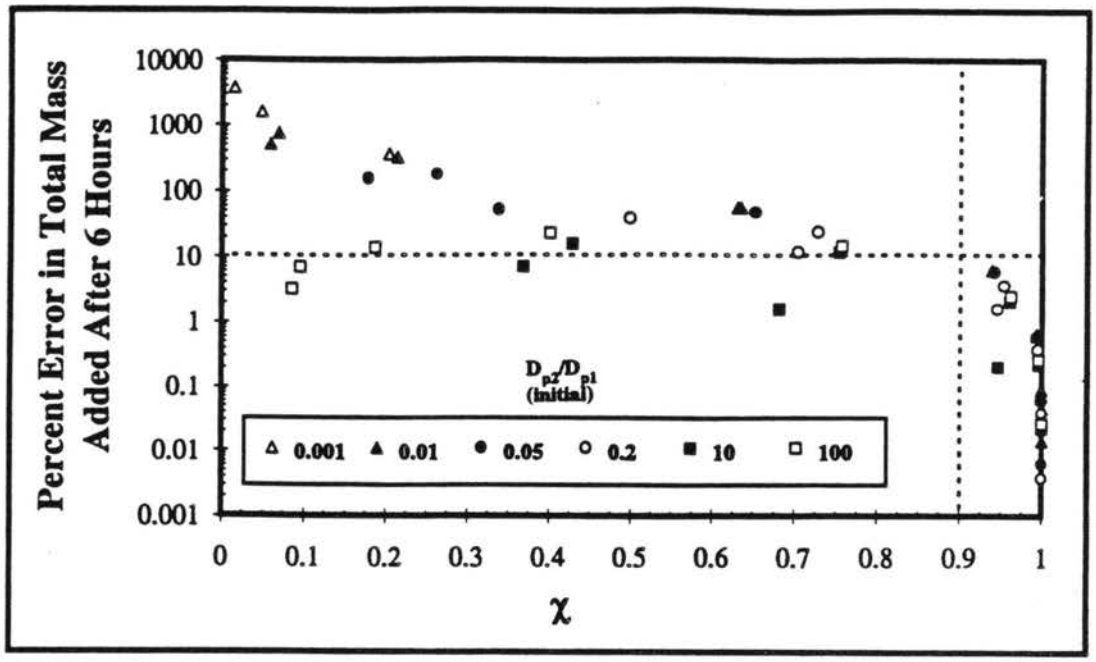

Figure 3.12. Percent error in condensed aerosol mass for various choices of χ and for different diameter and number ratios.

Determination of appropriate values for χ

Figure 3.12 is an example of how the percent error in mass added over six hours is related to the value of χ calculated based on the initial conditions. It can be seen that when χ is 0.9 or greater, the errors associated with merging are very small. This is because the condensation rate onto the merged mode is no more than 10% larger than the sum of the condensation rates onto the single modes.

For testing χ as a criterion for merging, the effect of merging and χ on total aerosol number during a nucleation burst in the presence of preexisting particles was examined.

Example 1

To examine the effect of the choice of χ during a simulation in which a nucleation mode grows along with a preexisting mode of particles, a MAEROS simulation was completed for three hours with 100 particles cm^{-3} initially residing in section 20,

corresponding to a mean diameter of about 0.1 μm. A vapor source rate of 0.024 ppt s^{-1} was used so that nucleation could be supported in the presence of the seed particles. The same initial conditions were used for a number of different BIMODAM I simulations. In the first BIMODAM I simulation, no merging was allowed, while for the other BIMODAM I simulations, merging was allowed according to three different χ values of 0.93, 0.95, and 0.97. The effect of the choice of χ on the aerosol and vapor properties is shown in Figure 3.13.

It is apparent from Figure 3.13h that low values of χ lead to values of D_{p2} which are too low. When χ is low, the two modes can merge earlier in the simulation. This results in a decrease of D_{p2} because the number of particles added to mode 2 from mode 1 is comparable to the number already residing in mode 2, while the accompanying mass is very small compared with mode 2 mass. Therefore, the diameter of particles in mode 2 decreases for a time. For larger values of χ, this effect diminishes because the merging criterion is more strict, and hence the two modes are merged later, when there is more mass in mode 1. The effect on aerosol mass in mode 2 (Figure 3.13g) is that it is overpredicted when merging occurs too early in the simulation.

Total aerosol number concentration (Figure 3.13c) is lower for the simulations using lower χ values because when merging occurs too soon, the condensation rate onto the lumped mode is overpredicted, which results in an underproduction of aerosol number concentration. Total aerosol mass is approximately the same for all simulations, as seen in Figure 3.13b. However, the mass in the vapor phase (Figure 3.13a) is not the same. When $\chi = 0.93$, merging occurs earlier so the condensation rate onto the merged mode is overpredicted because only one mode is simulated, when in fact there should be two. Since the condensation rate is overpredicted, the maximum vapor concentration is underpredicted.

The MAEROS distribution is shown in Figure 3.14 and the mean diameters, at each time, for each simulation, are shown in Tables 3.1 and 3.2.

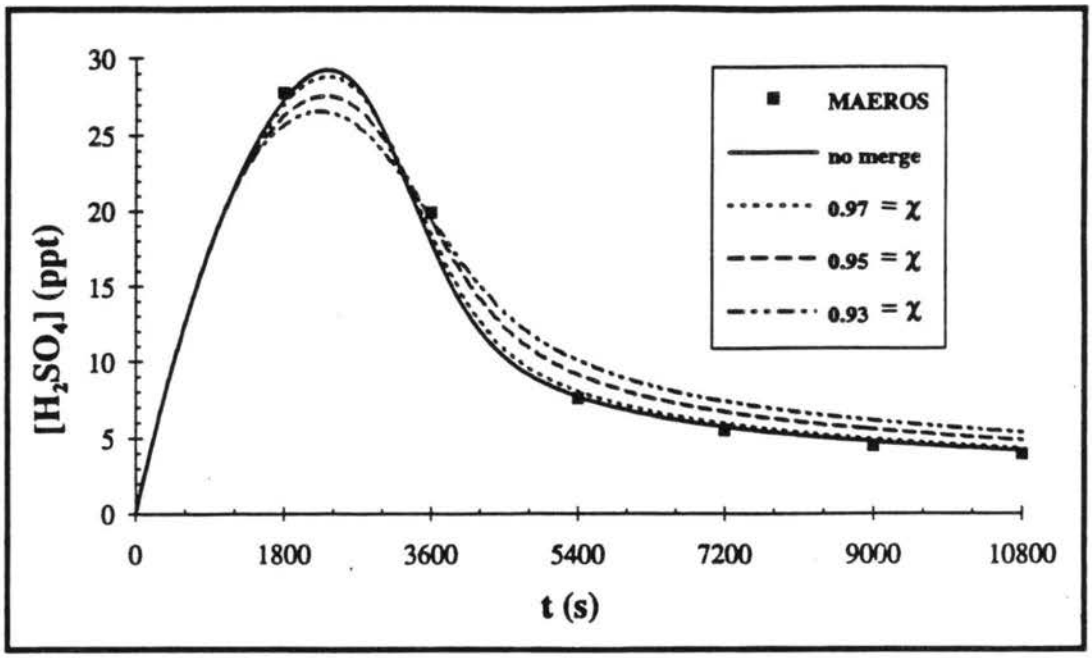

Figure 3.13a. Sulfuric acid vapor concentration,. $[H_2SO_4]$, versus time, t, computed using different values of χ. Initial conditions for Figures 3.13a-h are described in the text.

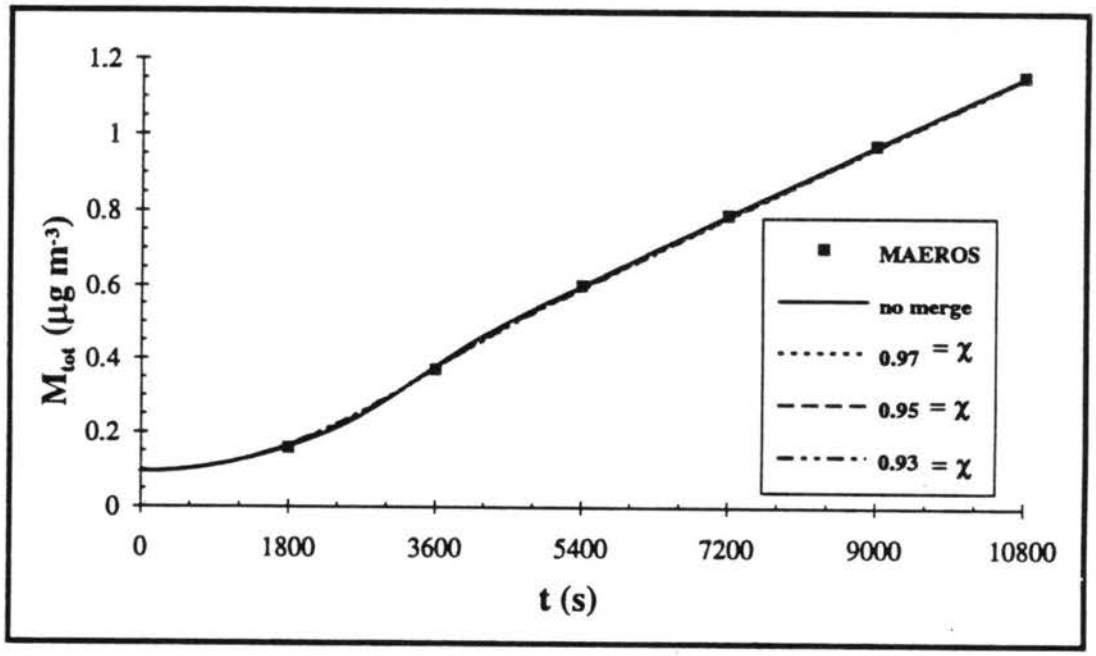

Figure 3.13b. Total aerosol mass, M_{tot}, versus time, t, computed using different values of χ.

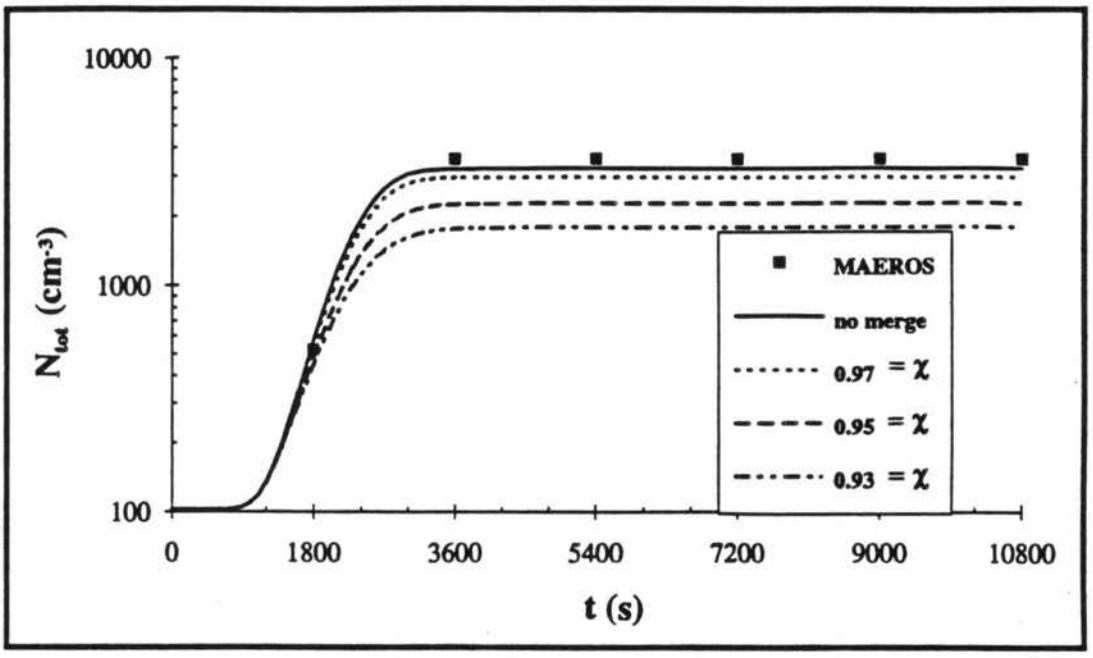

Figure 3.13c. Total aerosol number concentration, N_{tot}, versus time, t, computed using different values of χ.

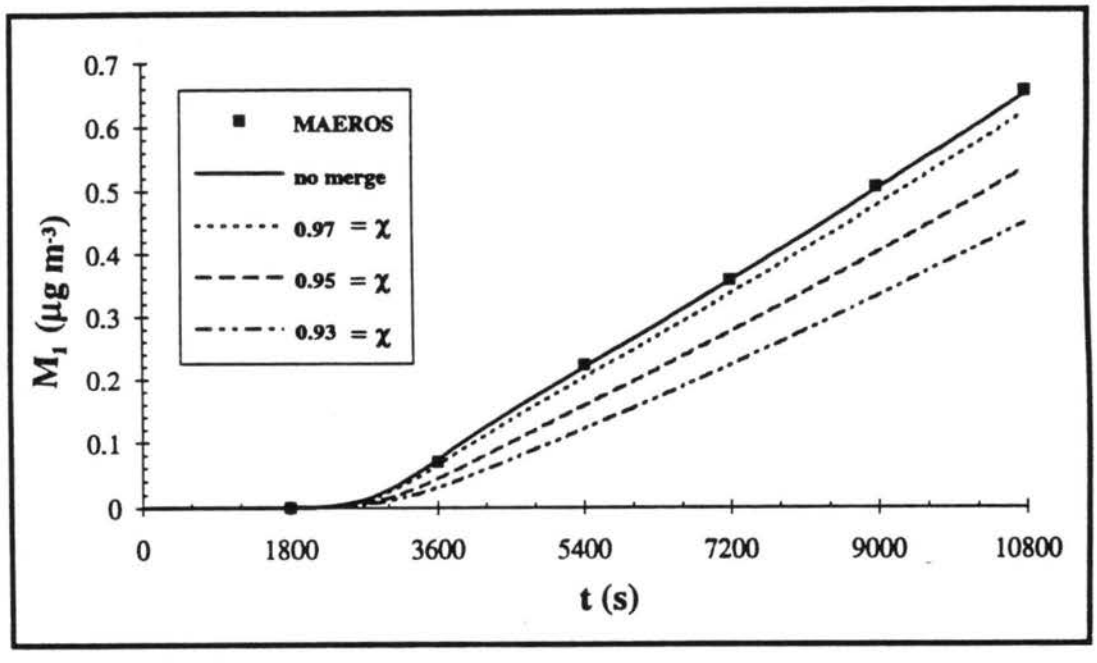

Figure 3.13d. Aerosol mass concentration in mode 1, M_1, versus time, t, computed using different values of χ.

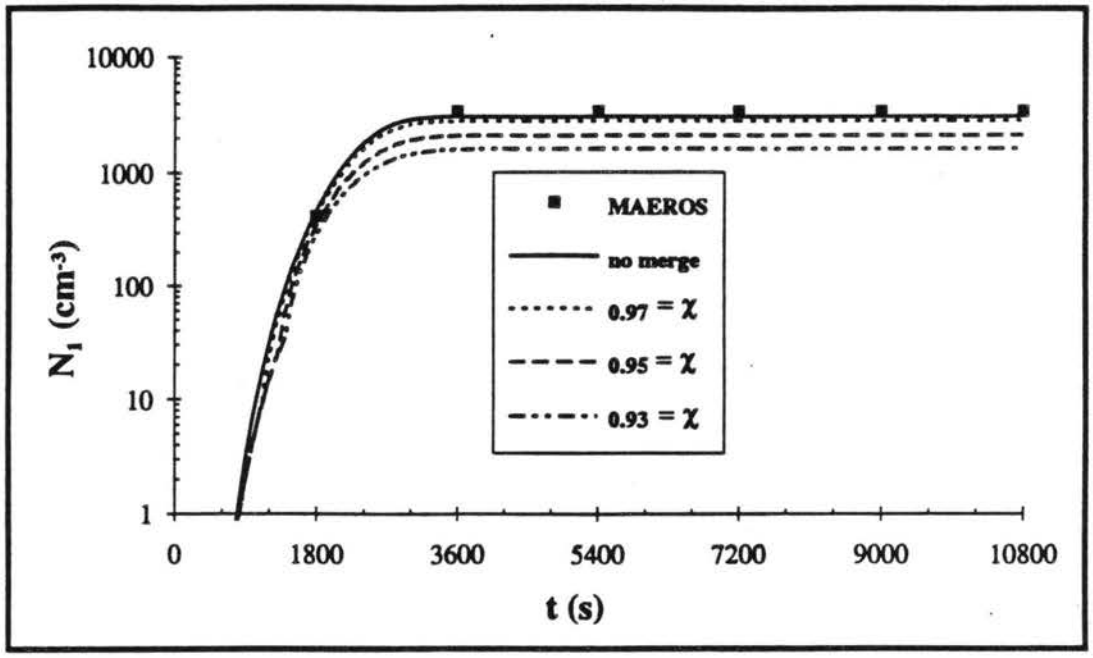

Figure 3.13e. Aerosol number concentration in mode 1, N_1, versus time, t, computed using different values of χ.

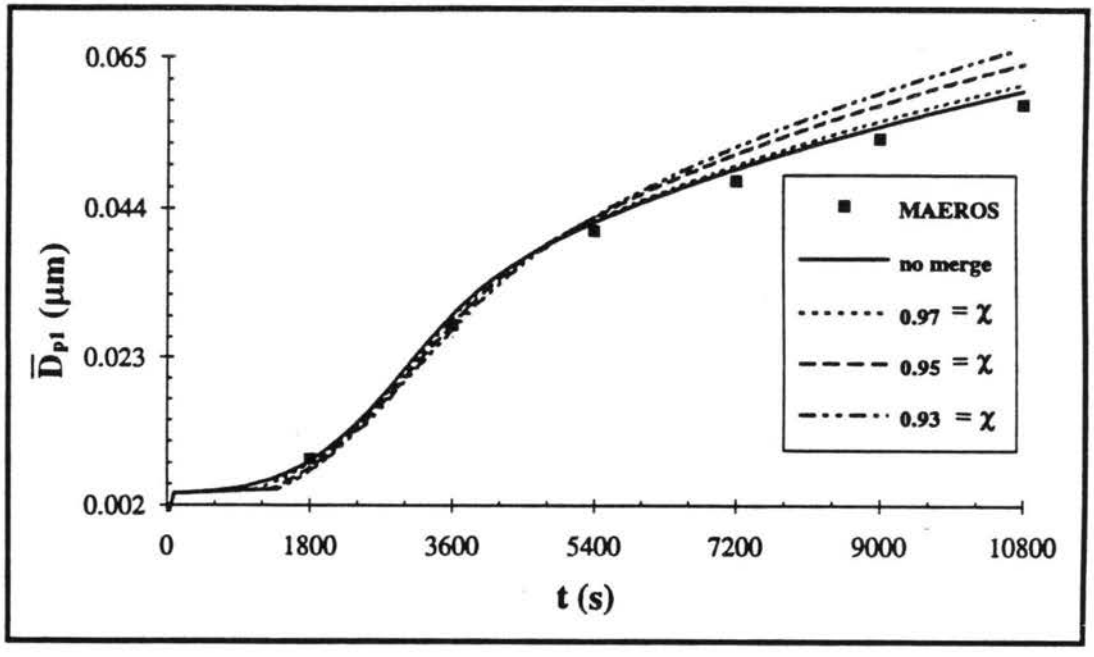

Figure 3.13f. Mass mean diameter of mode 1 particles, $\overline{D}_{p1}$, versus time, t, computed using different values of χ.

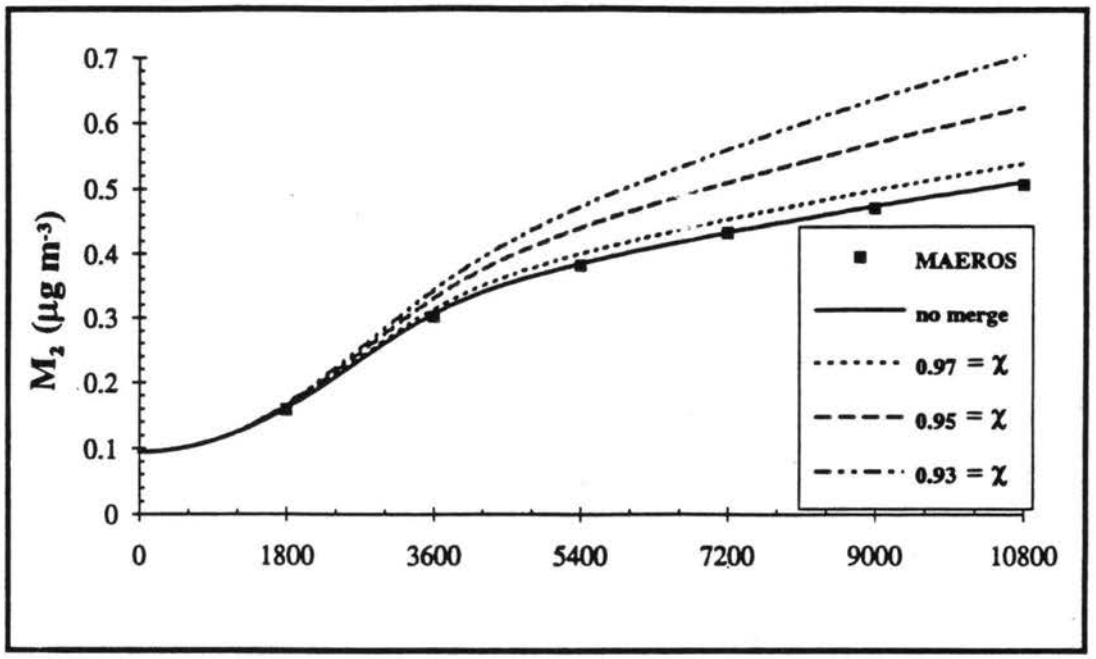

Figure 3.13g. Aerosol mass concentration in mode 2, M_2, versus time, t, computed using different values of χ.

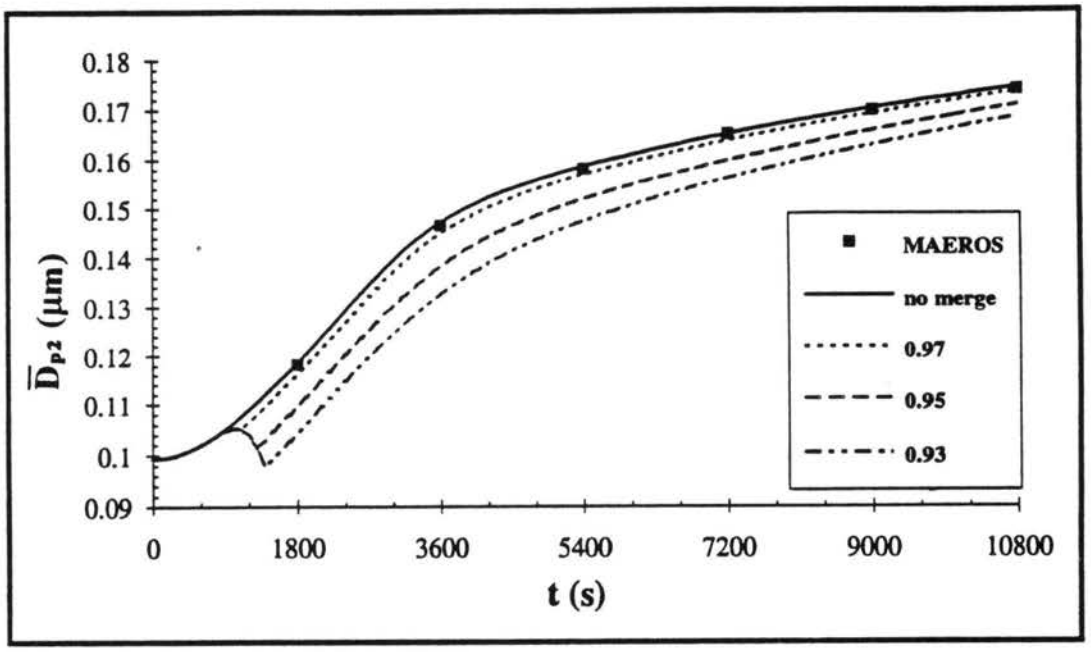

Figure 3.13h. Mass mean diameter of mode 2 particles, $\overline{D}_{p2}$, versus time, t, computed using different values of χ.

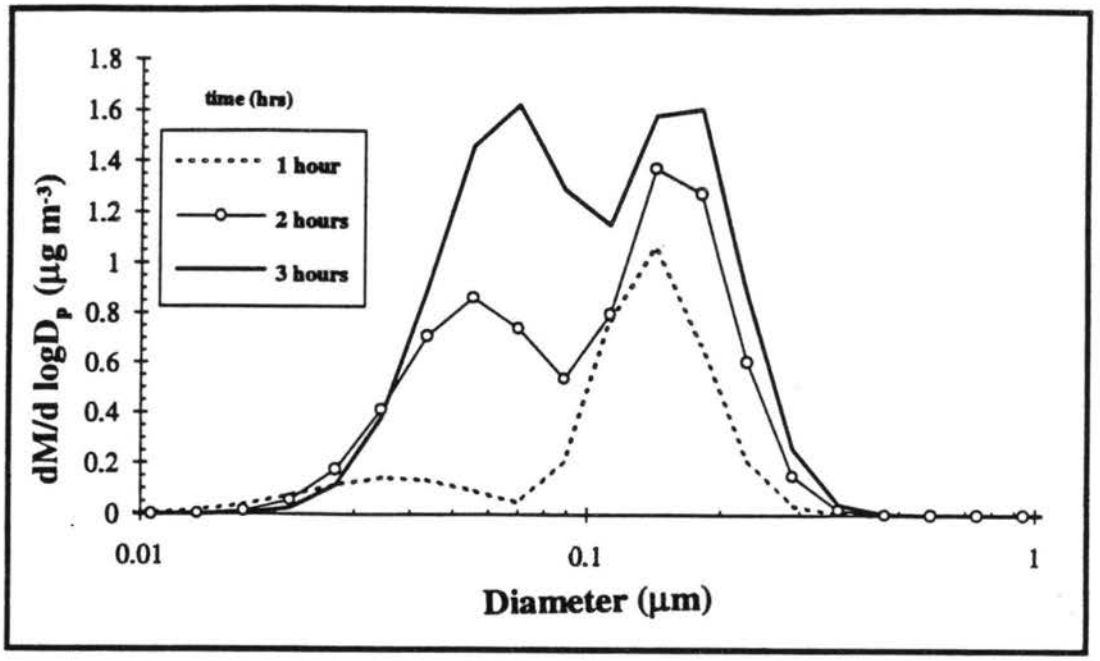

Figure 3.14. Mass distributions from the MAEROS simulation corresponding to Figures 3.13a-h.

		χ Values			
Time (hrs)	MAEROS	0.97	0.95	0.93	No Merge
1	0.028	0.029	0.028	0.027	0.029
2	0.048	0.049	0.052	0.053	0.049
3	0.058	0.060	0.064	0.064	0.060

Table 3.1. Diameter of particles in mode 1 (μm) for five simulations.

		χ Values			
Time (hrs)	MAEROS	0.97	0.95	0.93	No Merge
1	0.146	0.147	0.138	0.133	0.147
2	0.165	0.165	0.160	0.156	0.165
3	0.174	0.174	0.171	0.168	0.174

Table 3.2. Diameter of particles in mode 2 (μm) for five simulations.

CHAPTER 4 SIMPLIFICATION OF BIMODAM I

4.A. INTRODUCTION TO BIMODAM II

In order to use BIMODAM I as an effective tool in global chemical models, the differential equation solver must be eliminated. First, VODE is a variable time step solver, and is not vectorizable. Analytical solutions to the differential equations which represent each process in BIMODAM I are desirable. In this chapter, analytical solutions to the condensation, coagulation, and deposition equations will be derived.

Second, the shortest simulation time steps are required during nucleation bursts, when the vapor concentration and number concentration are rapidly changing. A method was sought whereby the explicit integration of Equations (2.34) - (2.38) during the burst could be eliminated, and the final number concentration of nucleated particles diagnosed from conditions at the start of the burst.

These new formulations are applied in BIMODAM II. In BIMODAM II, all processes occur sequentially, rather than simultaneously as in BIMODAM I. Figure 4.1 is the flowchart of operations for BIMODAM II. First, if mode 1 is not empty, the conditions in each mode are checked to see whether a merge is appropriate. If a merge does not occur then both modes are grown for the appropriate timestep, followed by coagulation and deposition. If mode 1 is empty, or if a merge has occurred, then the vapor phase conditions are analyzed to see if the vapor is supersaturated with respect to current conditions. If the vapor is supersaturated, new particles are formed in a nucleation burst. If a burst has been detected and predicted, the particles in mode 2 are grown for the length of the burst in mode 1, followed by coagulation and deposition for

the same timestep as the burst. If the vapor is not supersaturated, the existing modes are grown for an appropriate timestep, followed by coagulation and deposition.

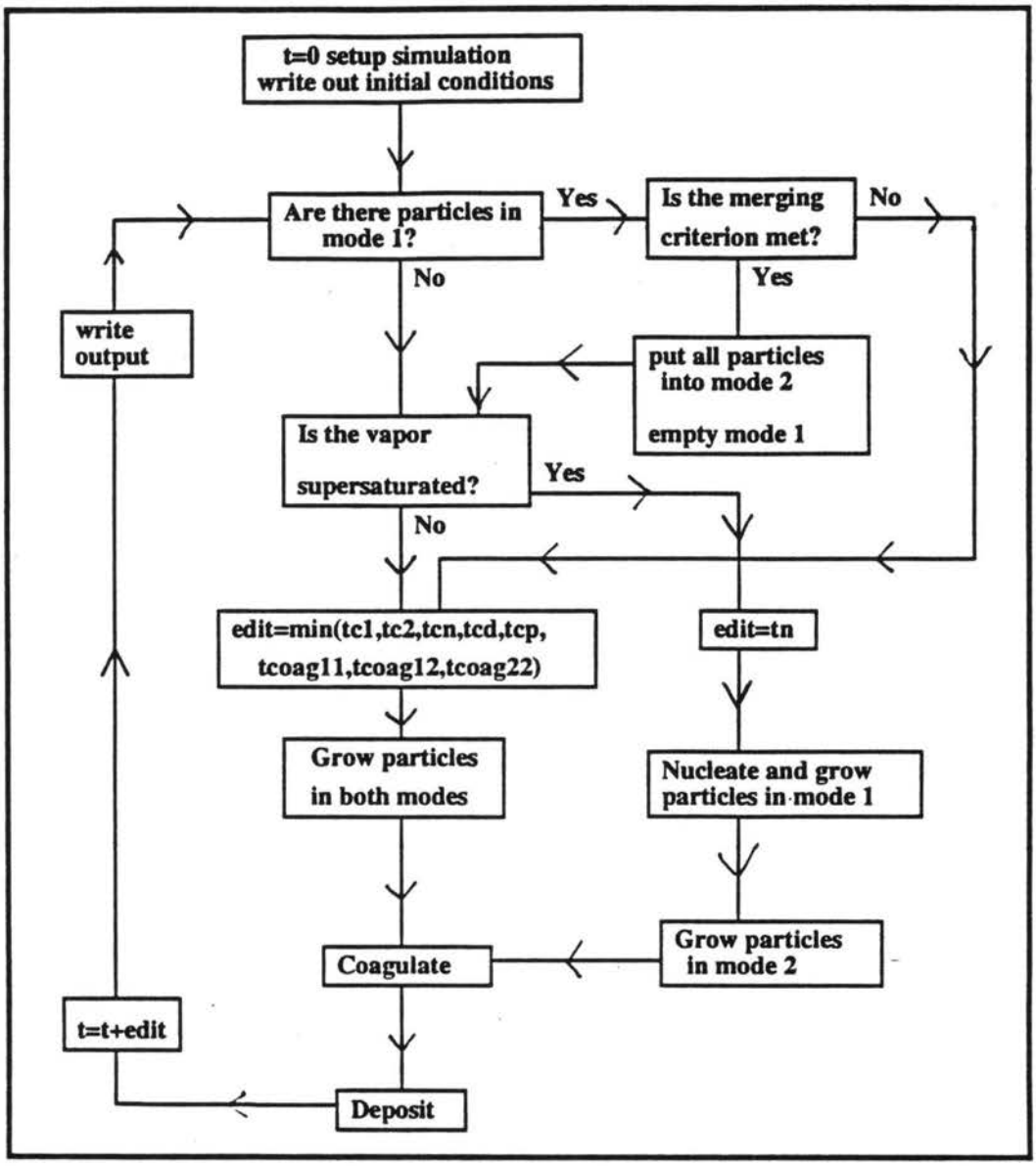

Figure 4.1. Flowchart of operations in BIMODAM II.

4.B. DEFINITION OF THE CHARACTERISTIC TIMES

The characteristic times for each process are derived here and will be used to determine appropriate time steps. The differential equations (Equations (2.34) - (2.38)) are non-dimensionalized in order to generate relationships for the characteristic times.

I. Vapor production

The production and loss of H_2SO_4 vapor is considered first. The only source of H_2SO_4 vapor is the preset chemical source rate, while the losses are due to nucleation of new particles, and growth of preexisting particles. The equation is written:

$$(4.1) \quad \frac{dV}{dt} = R_g - (Jm_p + R_{c1} + R_{c2}),$$

where all symbols have been previously defined. Using Equations (2.34) and (2.36) for R_{ci}:

$$(4.2) \quad \frac{dV}{dt} = R_g - \left(\frac{dM_1}{dt} + \frac{dM_2}{dt} + K_d (M_1 + M_2 \right),$$

where the terms for coagulation between mode 1 and mode 2 have canceled each other. Dividing through by V_o, which is a characteristic vapor concentration, and defining $\hat{V} = \frac{V}{V_o}$, $\hat{M}_1 = \frac{M_1}{V_o}$, and $\hat{M}_2 = \frac{M_2}{V_o}$, yields:

$$(4.3) \quad \frac{d\hat{V}}{dt} = \frac{R_g}{V_o} - \frac{d\hat{M}_1}{dt} - \frac{d\hat{M}_2}{dt} - K_d (\hat{M}_1 + \hat{M}_2).$$

Multiplying by V_o/R_g yields:

$$(4.4)\quad \frac{V_o}{R_g}\frac{d\hat{V}}{dt} = 1 - \frac{V_o}{R_g}\frac{d\hat{M}_1}{dt} - \frac{V_o}{R_g}\frac{d\hat{M}_2}{dt} - \frac{V_o}{R_g}K_d(\hat{M}_1 + \hat{M}_2).$$

A non-dimensional time for vapor production is defined as:

$$(4.5)\quad \tau_p = \frac{t}{V_o / R_g},$$

and a non-dimensional time for deposition is defined as:

$$(4.6)\quad \tau_d = K_d t,$$

so that Equation (4.4) becomes:

$$(4.7)\quad \frac{d\hat{V}}{d\tau_p} = 1 - \frac{d\hat{M}_1}{d\tau_p} - \frac{d\hat{M}_2}{d\tau_p} - \frac{\tau_d}{\tau_p}(\hat{M}_1 + \hat{M}_2).$$

By this analysis, the characteristic time for vapor production:

$$(4.8)\quad t_{c_p} = \frac{V_o}{R_g},$$

and the characteristic time for deposition:

$$(4.9)\quad t_{c_d} = \frac{1}{K_d}$$

are defined.

II. Nucleation

Beginning with the equation for change of number in mode 1 (Equation (2.35)):

$$(4.10)\quad \frac{dN_1}{dt} = J - \frac{1}{2}K_{11}N_1^2 - K_{12}N_1N_2 - K_dN_1.$$

The same procedure as above is followed by dividing by N_{1_o}, which is a characteristic number of particles in mode 1, and defining $\hat{N}_1 = \frac{N_1}{N_{1_o}}$ yields:

$$(4.11)\quad \frac{d\hat{N}_1}{dt} = \frac{J}{N_{1_o}} - \frac{1}{2}K_{11}N_1\hat{N}_1 - K_{12}N_2\hat{N}_1 - K_d\hat{N}_1.$$

Now, multiplying by V_o/R_g, and applying the definitions of τ_p and τ_d yields:

$$(4.12)\quad \frac{d\hat{N}_1}{d\tau_p} = \frac{t}{\tau_p}\frac{J}{N_{1_o}} - \frac{1}{2}\frac{t}{\tau_p}K_{11}N_1\hat{N}_1 - \frac{t}{\tau_p}K_{12}N_2\hat{N}_1 - \frac{t_d}{\tau_p}\hat{N}_1.$$

Defining $N_{1_o} = J_{\max}t_n$, where t_n is the length of the burst and J_{max} is the maximum nucleation rate, and using $\hat{J} = \frac{J}{J_{\max}}$ yields:

$$(4.13)\quad \frac{d\hat{N}_1}{dt_p} = \frac{t}{\tau_p}\frac{\hat{J}}{t_n} - \frac{1}{2}\frac{t}{\tau_p}K_{11}N_1\hat{N}_1 - \frac{t}{\tau_p}K_{12}N_2\hat{N}_1 - \frac{\tau_d}{\tau_p}\hat{N}_1.$$

If a non-dimensional time for nucleation is defined by:

$$(4.14)\quad \tau_n = \frac{t}{t_n},$$

Equation (4.13) becomes:

$$(4.15)\quad \frac{d\hat{N}_1}{d\tau_p} = \frac{\tau_n}{\tau_p}\hat{J} - \frac{1}{2}\frac{t}{\tau_p}K_{11}N_1\hat{N}_1 - \frac{t}{\tau_p}K_{12}N_2\hat{N}_1 - \frac{\tau_d}{\tau_p}\hat{N}_1.$$

Non-dimensional times for coagulation between mode 1 and mode 1 particles, and between mode 1 and mode 2 particles are defined by:

$$(4.16)\quad \tau_{coag_{11}} = tK_{11}N_{1_o},$$

$$(4.17)\quad \tau_{coag_{12}} = tK_{12}N_{2_o},$$

so that Equation (4.15) becomes:

$$(4.18)\quad \frac{d\hat{N}_1}{d\tau_p} = \frac{\tau_n}{\tau_p}\hat{J} - \frac{\tau_{coag_{11}}}{\tau_p}\hat{N}_1^2 - \frac{\tau_{coag_{12}}}{\tau_p}\hat{N}_2\hat{N}_1 - \frac{\tau_d}{\tau_p}\hat{N}_1.$$

By this analysis, the characteristic time for nucleation:

$$(4.19)\quad t_{c_n} = t_n,$$

and the characteristic time for coagulation within mode 1:

$$(4.20)\quad t_{coag_{11}} = \frac{1}{K_{11}N_{1_o}},$$

and the characteristic time for coagulation between modes 1 and 2:

$$(4.21) \quad t_{coag22} = \frac{1}{K_{12} N_{2_o}}$$

are defined.

Examination of N_2 equation

The balance equation for N_2 is (Equation (2.37)):

$$(4.22) \quad \frac{dN_2}{dt} = -\frac{1}{2} K_{22} N_2^2 - K_d N_2 .$$

Dividing by N_{2_o} and defining $\hat{N}_2 = N_2 / N_{2_o}$, where N_{2_o} is a characteristic number of particles in mode 2, yields:

$$(4.23) \quad \frac{d\hat{N}_2}{dt} = -\frac{1}{2} K_{22} \hat{N}_2 N_2 - K_d \hat{N}_2 .$$

Multiplying by V_d/R_g and applying the definition for τ_p yields:

$$(4.24) \quad \frac{d\hat{N}_2}{d\tau_p} = -\frac{1}{2} \frac{t}{\tau_p} K_{22} \hat{N}_2 N_2 - \frac{t}{\tau_p} K_d \hat{N}_2 .$$

Using $K_d = \tau_d / t$, and $N_2 = \hat{N}_2 N_{2_o}$ yields:

$$(4.25) \quad \frac{d\hat{N}_2}{d\tau_p} = -\frac{1}{2} \frac{t}{\tau_p} K_{22} \hat{N}_2^2 N_{2_o} - \frac{\tau_d}{\tau_p} \hat{N}_2 .$$

A non-dimensional time for coagulation within mode 2 may be defined by:

(4.26) $\tau_{coag_{22}} = tK_{22}N_{2_o}$,

so that:

(4.27) $$\frac{d\hat{N}_2}{d\tau_p} = -\frac{1}{2}\frac{\tau_{coag_{22}}}{\tau_p}\hat{N}_2^2 - \frac{\tau_d}{\tau_p}\hat{N}_2.$$

In this analysis, a characteristic time for coagulation within mode 2 has been defined:

(4.28) $$t_{coag_{22}} = \frac{1}{K_{22}N_{2_o}}.$$

III. Growth

Mode 1

The equation for the change of mass in mode 1 (Equation (2.34)) is:

(4.29) $$\frac{dM_1}{dt} = Jm_p + R_{c1} - K_{12}N_1N_2\overline{m}_{p1} - K_dM_1.$$

Using the definition of τ_p, and $\hat{M}_1 = \frac{M_1}{V_o}$ in the first term yields:

(4.30) $$R_g\frac{dM_1}{d\tau_p} = Jm_p + R_{c1} - K_{12}N_1N_2\overline{m}_{p1} - K_dM_1.$$

Dividing by R_g and using $M_1 = \hat{M}_1 V_o$ in the last term yields:

(4.31) $$\frac{dM_1}{d\tau_p} = \frac{Jm_p}{R_g} + \frac{R_{c1}}{R_g} - \frac{K_{12}}{R_g}N_1N_2\overline{m}_{p1} - K_d\hat{M}_1\frac{V_o}{R_g}.$$

Substitute $J = \hat{J} J_{\max}$, $K_d = \tau_d / t$, and $V_o / R_g = t / \tau_p$ to obtain:

$$(4.32) \quad \frac{d\hat{M}_1}{d\tau_p} = \frac{\hat{J} J_{\max} m_p}{R_g} + \frac{R_{c1}}{R_g} - \frac{K_{12}}{R_g} N_1 N_2 \overline{m}_{p1} - \frac{\tau_d}{\tau_p} \hat{M}_1.$$

Each term on the right hand side of this equation will now be considered separately.

Using the definition of τ_n and τ_p and solving for R_g yields:

$$(4.33) \quad R_g = \frac{V_o \tau_p}{t_n \tau_n}.$$

This expression may be substituted into the first term in Equation (4.32) so that:

$$(4.34) \quad \frac{\hat{J} J_{\max} m_p}{R_g} = \hat{J} J_{\max} m_p \frac{t_n \tau_n}{V_o \tau_p}.$$

Let $m_{p_o} = m_p J_{\max} t_n = m_p N_{1_o}$, where m_{p_o} is the mass carried by a characteristic number of particles, to get:

$$(4.35) \quad \frac{\hat{J} J_{\max} m_p}{R_g} = \hat{J} \frac{m_{p_o}}{V_o} \frac{\tau_n}{\tau_p}.$$

Using the definition for R_{c1}, and the relationship for τ_p, term 2 may be written:

$$(4.36) \quad \frac{R_{c1}}{R_g} = C N_1 V \beta_1 D_{p1} \frac{t}{V_o \tau_p} = \frac{t}{\tau_p} C N_1 \hat{V} \beta_1 D_{p1}.$$

Using the definition for D_{p1} yields:

$$(4.37)\quad \frac{R_{c1}}{R_g} = \frac{t}{\tau_p} C N_1 \hat{V} \beta_1 \left[\left(\frac{6}{\pi \rho} \right)^{1/3} N_1^{-1/3} M_1^{1/3} \right].$$

Combining the N_1 terms, and combining the constant terms yields:

$$(4.38)\quad \frac{R_{c1}}{R_g} = \frac{t}{\tau_p} C_1 N_1^{2/3} \hat{V} \beta_1 M_1^{1/3}.$$

Using the definition, $N_1 = \hat{N}_1 J_{max} t_n$ and $M_1 = \hat{M}_1 V_o$ yields:

$$(4.39)\quad \frac{R_{c1}}{R_g} = \frac{t}{\tau_p} C_1 \hat{N}_1^{2/3} J_{max}^{2/3} t_n^{2/3} \hat{V} \beta_1 \hat{M}_1^{1/3} V_o^{1/3}.$$

Substituting the definition of $\tau_n = t / t_n$ yields:

$$(4.40)\quad \frac{R_{c1}}{R_g} = \frac{t}{\tau_p} C_1 \hat{N}_1^{2/3} J_{max}^{2/3} \frac{t^{2/3}}{\tau_n^{2/3}} \hat{V} \beta_1 \hat{M}_1^{1/3} V_o^{1/3}.$$

A non-dimensional time for mode 1 growth may be defined based on the quantities remaining which carry units:

$$(4.41)\quad \tau_{c_1}^{5/3} = t^{5/3} C_1 J_{max}^{2/3} V_o^{1/3},$$

so that:

$$(4.42)\quad \frac{R_{c1}}{R_g} = \frac{\tau_{c_1}^{5/3}}{\tau_p \tau_n^{2/3}} \hat{N}_1^{2/3} \hat{V} \beta_1 \hat{M}_1^{1/3}.$$

In term 3 of Equation (4.32), $\overline{m}_{p1}$ is just the mass per particle in mode 1 transferred to mode 2 when coagulation between the two modes occurs:

$$(4.43) \quad \frac{K_{12}N_1N_2}{R_g}\overline{m}_{p1} = \frac{K_{12}N_1N_2}{R_g}\frac{M_1}{N_1} = \frac{K_{12}M_1N_2}{R_g}.$$

Using the relationship for R_g yields:

$$(4.44) \quad \frac{K_{12}N_1N_2}{R_g}\overline{m}_{p1} = K_{12}M_1N_2\frac{t_n\tau_n}{V_o\tau_p}.$$

Using the definition for $\tau_{coag_{12}}$, involving K_{12} yields:

$$(4.45) \quad \frac{K_{12}N_1N_2}{R_g}\overline{m}_{p1} = \frac{\tau_{coag_{12}}}{tN_{2_o}}M_1N_2\frac{t_n\tau_n}{V_o\tau_p} = \frac{\tau_{coag_{12}}}{\tau_p}\frac{\hat{N}_2\,M_1}{V_o} = \frac{\tau_{coag_{12}}}{\tau_p}\hat{N}_2\,\hat{M}_1.$$

The fourth term is already in non-dimensional form.

Putting all four terms back into the original equation yields:

$$(4.46) \quad \frac{d\hat{M}_1}{d\tau_p} = \hat{J}\frac{m_{p_o}}{V_o}\frac{\tau_n}{\tau_p} + \frac{\tau_{c1}^{5/3}\hat{N}_1^{2/3}}{\tau_p\tau_n^{2/3}}\hat{V}\beta_1\hat{M}_1^{1/3} - \frac{\tau_{coag_{12}}}{\tau_p}\hat{N}_2\,\hat{M}_1 - \frac{\tau_d}{\tau_p}\hat{M}_1.$$

In this analysis, a characteristic time for mass change in mode 1 has been determined:

$$(4.47) \quad t_{c1} = C_1^{-3/5}J_{\max}^{-2/5}V_o^{-1/5}.$$

Mode 2

The equation for the change of mass in mode 2 (Equation (2.36)) is:

$$(4.48)\quad \frac{dM_2}{dt} = R_{c2} + K_{12} N_1 N_2 \overline{m}_{p1} - K_d M_2.$$

Dividing by V_o and defining $\hat{M}_2 = M_2 / V_o$ yields:

$$(4.49)\quad \frac{d\hat{M}_2}{dt} = \frac{R_{c2}}{V_o} + \frac{K_{12}}{V_o} N_1 N_2 \overline{m}_{p1} - K_d \hat{M}_2.$$

Multiplying by V_o/R_g and applying the definition of τ_p yields:

$$(4.50)\quad \frac{d\hat{M}_2}{d\tau_p} = \frac{R_{c2}}{R_g} + \frac{K_{12}}{R_g} N_1 N_2 \overline{m}_{p1} - \frac{K_d V_o}{R_g} \hat{M}_2.$$

Looking at each term separately produces results similar to the mode 1 analysis, except that the subscript 1 will be replaced by the subscript 2, and the nucleation term is not included. Because of the lack of the nucleation term, the non-dimensional time for mass change in mode 2 takes on a slightly different form:

$$(4.51)\quad \tau_{c2} = t C_1 N_{2_o}^{2/3} V_o^{1/3},$$

so that the resulting equation is:

$$(4.52)\quad \frac{d\hat{M}_2}{d\tau_p} = \frac{\tau_{c_2}}{\tau_p} \hat{N}_2^{2/3} \hat{V} \beta_2 \hat{M}_2^{1/3} + \frac{\tau_{coag_{12}}}{\tau_p} \hat{N}_2 \hat{M}_1 - \frac{\tau_d}{\tau_p} \hat{M}_2.$$

In this analysis, a characteristic time for mass change in mode 2 has been defined:

(4.53) $t_{c_2} = C_1^{-1} N_{2_o}^{-2/3} V_o^{-1/3}$.

Tables 4.1 and 4.2 summarize the dimensionless variables and the characteristic times derived in this section.

Variable	*Formulation*
$\hat{V}$	V / V_o
$\hat{M}_1$	M_1 / V_o
$\hat{M}_2$	M_2 / V_o
$\hat{N}_1$	N_1 / N_{1_o}
$\hat{N}_2$	N_2 / N_{2_o}
$\hat{J}$	$J / J_{\max}$

Table 4.1 Dimensionless variables defined in this section

Characteristic Time	*Formulation*
t_{c_p}	V_o / R_g
t_{c_d}	$1 / K_d$
t_{c_n}	t_n
t_{c_1}	$C_1^{-3/5} J_{\max}^{-2/5} V_o^{-1/5}$
t_{c_2}	$C_1^{-1} N_{2_o}^{-2/3} V_o^{-1/3}$
$t_{coag_{11}}$	$1 / K_{11} N_{1_o}$
$t_{coag_{22}}$	$1 / K_{22} N_{2_o}$
$t_{coag_{12}}$	$1 / K_{12} N_{2_o}$

Table 4.2 Characteristic times derived in this section

4.C. CONDENSATIONAL GROWTH IN BIMODAM II

For particle growth, a simple algebraic calculation was implemented. At any time, the amount of H_2SO_4 in the gas phase is calculated. The remaining acid produced over a time step is assumed to condense onto the particles.

I. *Derivation of expression for gas phase concentration*

To calculate the amount of mass in the aerosol and vapor phases, mass balance is applied between the chemical source rate and the changes in the aerosol mass and vapor concentrations:

$$(4.54) \quad R_g = \frac{dM_1}{dt} + \frac{dM_2}{dt} + \frac{dV}{dt},$$

where R_g is the chemical source rate, $\frac{dM_1}{dt}$ and $\frac{dM_2}{dt}$ are the condensation rates onto the particles in mode 1 and mode 2, respectively, and $\frac{dV}{dt}$ is the change in the vapor concentration. Recall from Chapter 2 (Equation (2.8)) that the change in mass due to aerosol growth alone is written:

$$(4.55) \quad \frac{dM}{dt} = R_c = CNV\beta D_p.$$

Substituting Equation (4.55) into Equation (4.54) yields:

$$(4.56) \quad R_g = (CN_1\beta_1 D_{p1} + CN_2\beta_2 D_{p2})V(t) + \frac{dV}{dt}.$$

Equation (4.56) is a linear first order differential equation for which the method of solution is:

$$(4.57) \quad Ve^{\int F dt} = \int R_g e^{\int F dt} dt + c,$$

where F is,

$$(4.58) \quad F = CN_1\beta_1 D_{p1} + CN_2\beta_2 D_{p2} = F_1 + F_2.$$

For this study, R_g is always assumed constant, and is therefore, independent of time. If short enough time steps are taken, then it is approximately true that F is also independent of time. Using this and the fact that at the beginning of the time step, V has the value $V(t)$, Equation (4.57) has the solution:

$$(4.59) \quad V(t+\Delta t) = \frac{R_g}{F}\left(1 - e^{-F\Delta t}\right) + V(t)e^{-F\Delta t},$$

which can be written in terms of ΔV:

$$(4.60) \quad \begin{aligned} V(t+\Delta t) - V(t) = \Delta V &= \frac{R_g}{F}\left(1 - e^{-F\Delta t}\right) + V(t)(e^{-F\Delta t} - 1) \\ &= \left(\frac{R_g}{F} - V(t)\right)\left(1 - e^{-F\Delta t}\right). \end{aligned}$$

If $V(t)$ is zero, the solution reduces to:

$$(4.61) \quad \Delta V = \frac{R_g}{F}\left(1 - e^{-F\Delta t}\right).$$

Because of the approximation that F and therefore, D_p, are constant over a timestep, Δt, this equation will be very sensitive to the timestep used. An example of this is shown in Figure 4.2. The situation modeled is condensation onto 1000 cm^{-3}, 0.2 μm particles,

using various chemical source rates, and a relative humidity of 70%. The corresponding solution for $V(t)$, generated by the VODE package is indicated by the solid circles. It can be seen that, using Equation (4.59), if the timestep is too large, the maximum concentration of mass in the gas phase is overpredicted. The effect of timestep is magnified for high source rates, because things change rapidly over a timestep, and this change is not captured using Equation (4.59) with large timestep. Application of the characteristic times which were derived in the previous section to the choice of timestep will be discussed at the end of this chapter.

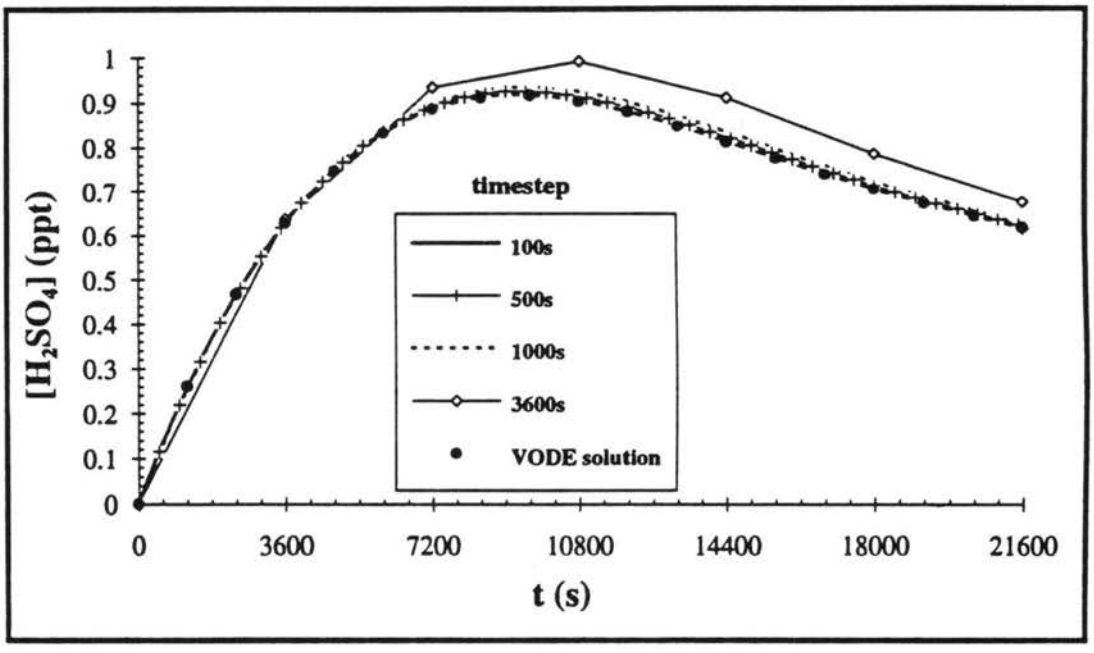

Figure 4.2a. Example of how the timestep affects the $V(t)$ calculation in BIMODAM II, compared with the VODE solution for a source rate of 0.00024 ppt s^{-1}.

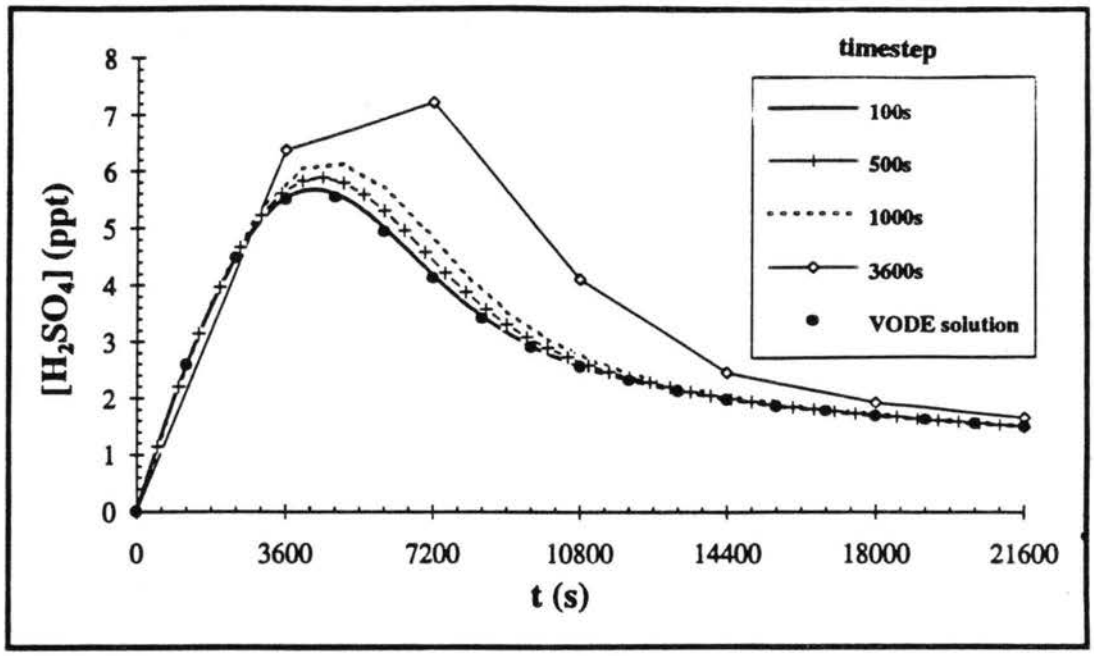

Figure 4.2b. Example of how the timestep affects the *V(t)* calculation in BIMODAM II, compared with the VODE solution for a source rate of 0.0024 ppt s^{-1}.

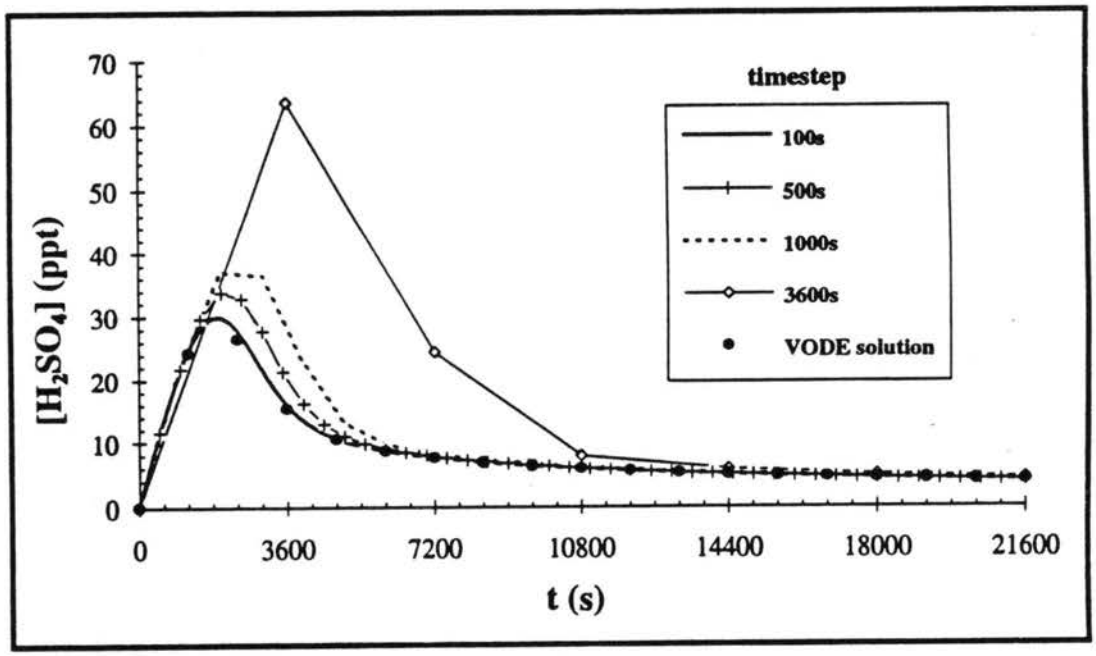

Figure 4.2c. Example of how the timestep affects the *V(t)* calculation in BIMODAM II, compared with the VODE solution for a source rate of 0.024 ppt s^{-1}.

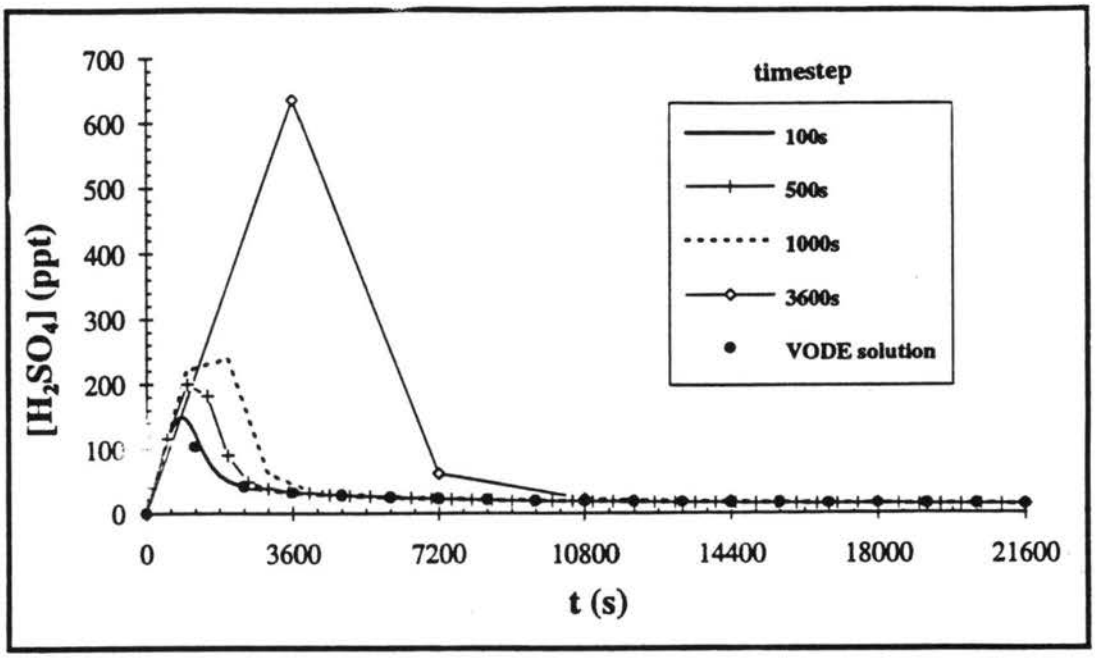

Figure 4.2d. Example of how the timestep affects the *V(t)* calculation in BIMODAM II, compared with the VODE solution for a source rate of 0.24 ppt s^{-1}.

II. ***Determination of mass in the aerosol phase***

At any time, *t*, the amount of mass in the vapor phase is calculated using Equation (4.59). The amount of vapor mass scavenged by the particles is then calculated by subtracting the vapor mass from the mass of H_2SO_4 which is produced during the timestep:

$$\Delta M = R_g \Delta t - \Delta V, \tag{4.62}$$

where ΔM is the mass added to the particles over a timestep. When only one mode exists, all of the mass added to the particle phase goes to that one mode. For this case, *F* in Equation (4.58) includes only the portion with information on the appropriate mode. When two modes exist, the added particle mass is calculated in the same manner, using Equations (4.59) and (4.62). This total aerosol mass is then partitioned

according to the fractional condensation rate in each mode at the beginning of the timestep. The fractional condensation rates are represented by:

$$(4.63) \quad F_{m1} = \frac{F_1}{F_1 + F_2},$$

and

$$(4.64) \quad F_{m2} = \frac{F_2}{F_1 + F_2},$$

so that the new masses after growth are:

$$(4.65) \quad M_1 = M_1 + F_{m1}\Delta M_{tot}$$

$$(4.66) \quad M_2 = M_2 + F_{m2}\Delta M_{tot}.$$

4.D. COAGULATION AND DEPOSITION IN BIMODAM II

I. Coagulation

The coagulation mechanism in BIMODAM I was discussed in Chapter 2. For BIMODAM II, the differential equations representing the changes due to coagulation are solved analytically. The differential coagulation equations and their analytical solutions are written:

$$(4.67) \quad \frac{dN_1}{dt} = -\frac{1}{2}K_{11}N_1^2 - K_{12}N_1N_2; \qquad N_1(t+\Delta t) = \frac{K_{12}N_{2_o}N_{1_o}}{(K_{12}N_{2_o} + \frac{1}{2}K_{11}N_{1_o})e^{\Delta t K_{12}N_{2_o}} - \frac{1}{2}K_{11}N_{1_o}}$$

(4.68) $$\frac{dN_2}{dt} = -\frac{1}{2}K_{22}N_2^2; \qquad N_2(t+\Delta t) = \frac{N_{2_o}}{1+\Delta t\frac{1}{2}K_{22}N_{2_o}}$$

(4.69) $$\frac{dM_1}{dt} = -K_{12}N_2M_1; \qquad M_1(t+\Delta t) = M_{1_o}e^{-\Delta tK_{12}N_{2_o}}$$

(4.70) $$\frac{dM_2}{dt} = K_{12}N_2M_1; \qquad M_2(t+\Delta t) = \Delta tK_{12}N_{2_o}M_{1_o} + M_{2_o}.$$

All values on the right hand side of the analytical solutions are those at the beginning of the calculations, indicated by the subscript, *o*. The calculation for the coagulation coefficients is the same as that used in BIMODAM I.

I. Deposition

The deposition equation, for particle number, and its analytical solution are:

(4.71) $$\frac{dN_i}{dt} = -K_dN_i,$$

(4.72) $$N_i(t+\Delta t) = N_i(t)e^{-K_d\Delta t},$$

where i represents the appropriate mode, and K_d is the deposition rate constant derived in chapter 2. Equation (4.72) is used to calculate the number of particles remaining at the end of the timestep, Δt, so that ΔN_i, is:

(4.73) $$\Delta N_i = N_i(t+\Delta t) - N_i(t) = N_i(t)(e^{-K_d\Delta t} - 1).$$

Once the number of particles which have been lost is calculated, the amount of mass which goes with them is calculated. First, a mass per particle ratio is calculated:

$$(4.74) \quad m_{pi} = \frac{M_i(t)}{N_i(t)},$$

so that the amount of mass remaining after deposition is:

$$(4.75) \quad M_i(t+\Delta t) = M(t) - (m_{pi}\Delta N_i)$$

At each timestep, coagulation and deposition are the last calculations done.

4.E. TIMESTEP ISSUE

I. Choosing the appropriate timestep

In order for BIMODAM II to run most efficiently in a global model, the timestep must be chosen appropriately. There are two key issues in the development of these equations which dictate the need for the correct timestep. First, the value of the vapor mass concentration, V, must be watched very closely in order to predict the nucleation burst correctly. Second, in the derivation of the equation for $V(t)$, it was assumed that the diameters are invariant over the timestep, in order to obtain an analytical solution.

In section 4.B, the characteristic times associated with each process were derived by non-dimensionalizing the five prognostic equations for M_1, M_2, N_1, N_2, and V. These characteristic times are calculated at every timestep to analyze the most rapidly changing process. Examples of typical characteristic times for production, nucleation, and condensation are shown in Figure 4.3. The five plots represent 5 different relative humidities, 50, 60, 70, 80, and 90%. The characteristic value for V_o was defined as the critical vapor concentration at which a nucleation burst begins. It can be seen that in these five examples, the characteristic time for condensation onto mode 2 (*tc2*) is very

dependent on how the characteristic number of particles in mode 2 (N_{2o}) is defined, where N_{2o} is indicated by the number in parenthesis next to *tc2*. When N_{2o} is large, *tc2* is small because of the large mass changes which result. The characteristic times for condensation (*tc1* and *tc2*) are the shortest characteristic times for all five cases. It can also be seen that the characteristic time for each process decreases for a given source rate, as relative humidity increases, which follows from the fact that when there is more vapor production, the processes of nucleation and growth can happen much faster. Therefore, a small timestep should be chosen.

II. Choosing the optimal timestep

For using BIMODAM II in a global model, such as GRANTOUR, the smallest timestep suggested by the analysis presented in 4.E.I. may sometimes be too computationally expensive. Therefore, the choice of timestep must be a compromise between computational feasibility and accuracy.

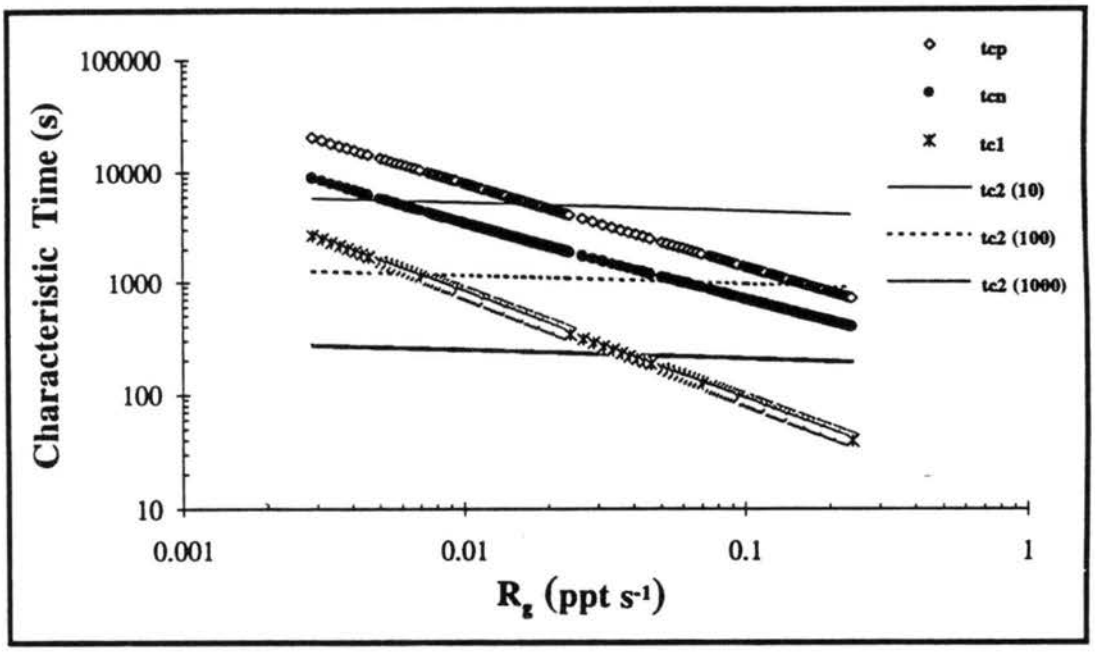

Figure 4.3a. Characteristic times for vapor production, nucleation, and condensation for a nucleation simulation. Relative humidity is 50%.

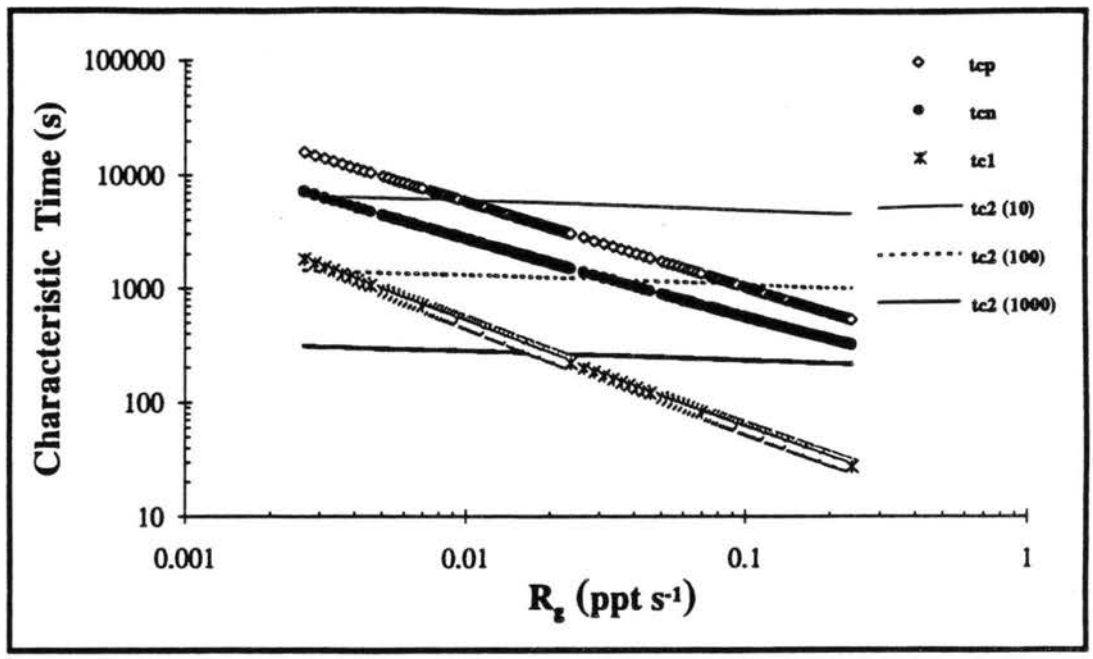

Figure 4.3b. Characteristic times for vapor production, nucleation, and condensation for a nucleation simulation. Relative humidity is 60%.

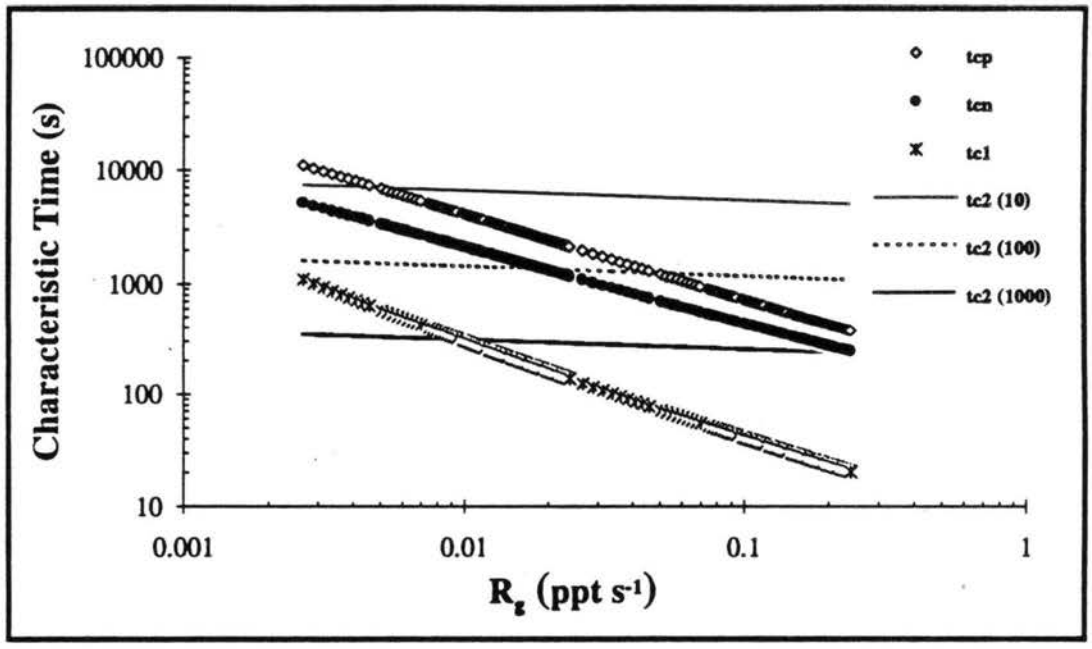

Figure 4.3c. Characteristic times for vapor production, nucleation, and condensation for a nucleation simulation. Relative humidity is 70%.

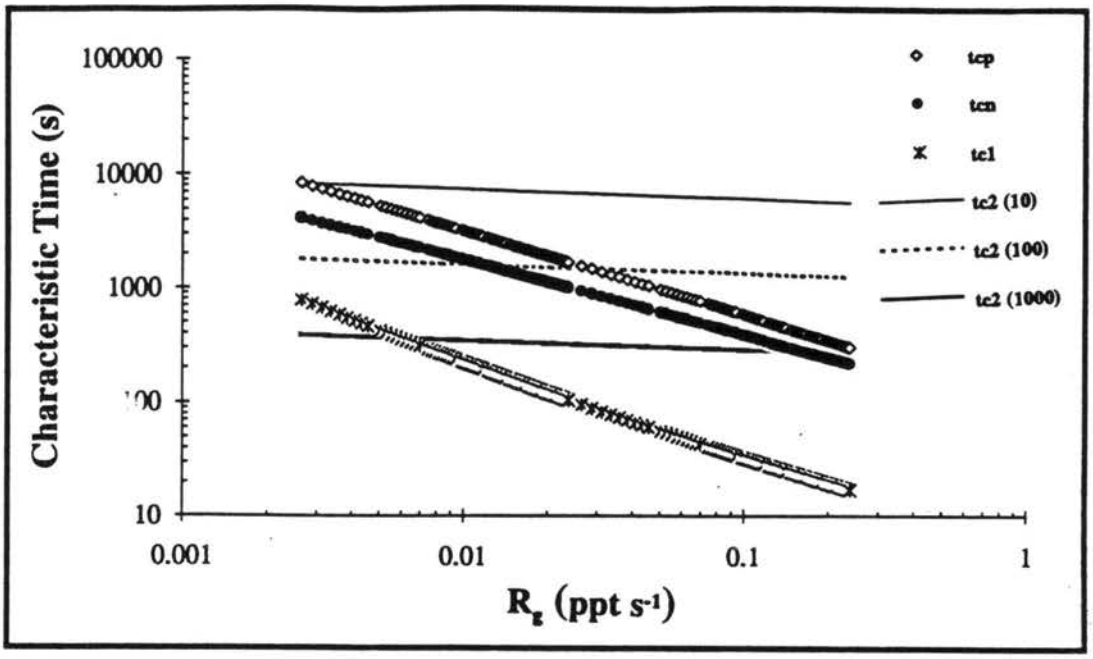

Figure 4.3d. Characteristic times for vapor production, nucleation, and condensation for a nucleation simulation. Relative humidity is 80%.

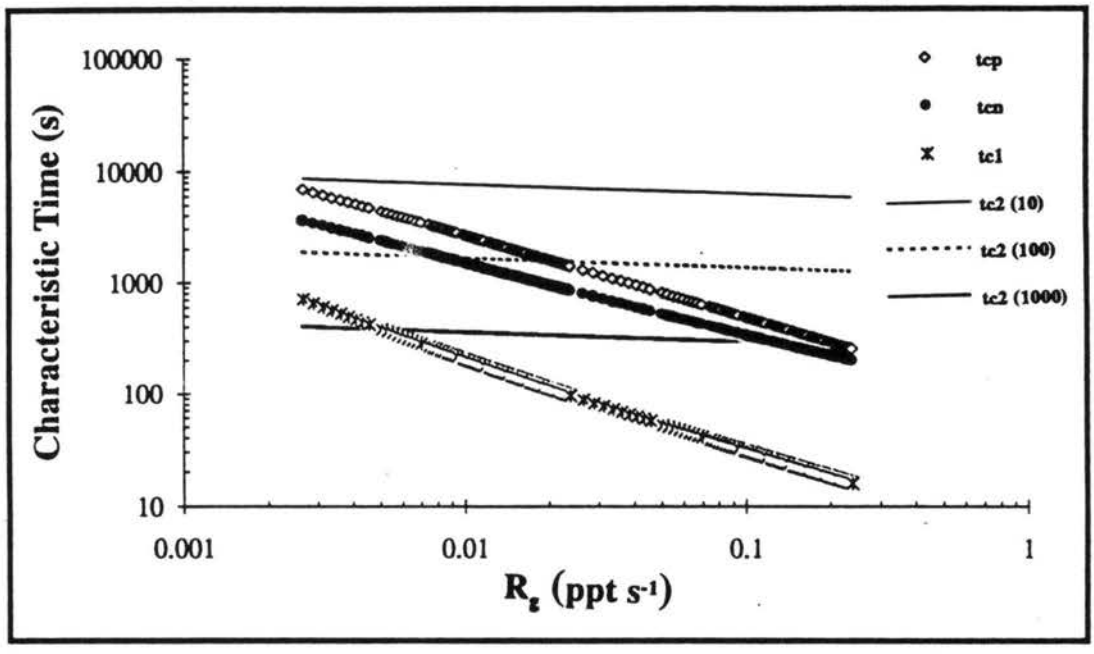

Figure 4.3e. Characteristic times for vapor production, nucleation, and condensation for a nucleation simulation. Relative humidity is 90%.

CHAPTER 5 THE NUCLEATION PARAMETERIZATION

5.A. INTRODUCTION TO NUCLEATION

I. Previous Work

McMurry and Friedlander (1979) carried out experiments and theoretical studies to examine aerosol dynamics in a system in which nucleation occurs in the presence of preexisting particles. A criterion is developed for determining whether or not a burst will occur in the presence of any preexisting particles. The criterion consists of a parameter, L, which is the products of two ratios of rates. The first ratio is the rate at which condensable molecules (monomers) collide with preexisting aerosol to the rate at which monomers are produced. This ratio is maximized at 1, when all vapor molecules are consumed by condensation. The second ratio is the rate at which monomers collide with preexisting aerosol to the rate at which monomers collide with themselves. It is large compared to 1 when condensation is the dominant process. By plotting the fraction of new aerosol volume which appears in the form of new particles versus L, it was determined that L=0.01 is the criterion below which nucleation is important and above which nucleation falls off rapidly.

Shaw (1989) developed a scheme to explain the high concentrations of condensation nuclei observed in polar regions and over central oceans in air that has no continental influence. The particles are assumed to be composed exclusively of H_2SO_4 and are produced by homogeneous nucleation from the vapor phase. Shaw derives a balanced equation for the number of acid molecules, which includes terms for source, nucleation, and condensation. The assumption is made that 1 embryo cm^{-3} s^{-1} defines the beginning of the nucleation burst. The conclusion is made that in order to achieve the observed

number concentration of particles, the air in which the burst occurs must be free of particles; otherwise, the preexisting aerosol will scavenge the available vapor.

Barrett and Clement (1991) derived coupled equations which give number and supersaturation changes during a nucleation burst. They considered a uniform vapor-gas mixture with an initial non-dimensional saturation value of 4. They compared an exact solution, their analytical solution and the approximate solution of Warren and Seinfeld (1985). The approximation of Warren and Seinfeld is that the nucleated aerosol is initially monodisperse. The approximation underpredicts total aerosol number and saturation ratio, while overpredicting aerosol diameter. The conclusions were that the analytical expression for number is in good agreement with the approximate and exact solutions.

5.B. NUCLEATION IN BIMODAM II

I. Development of prediction of total aerosol number

In this work, an approach has been developed to predict the number of new particles nucleated and the duration of the nucleation burst from knowledge of the vapor source rate and relative humidity.

Triangular function approach

The method is based upon the approximation of the time-dependent nucleation rate during the burst as a triangular function (Figure 5.1). The function is oriented so that the left hand side of the triangle lies tangent to the *J(t)* curve at the point of $\dot{J}_{max}$, where $\dot{J}_{max}$ is the slope of the left-hand side of the triangle. The area under the curve, and hence the area under the triangle, represents the total number of particles nucleated:

$$(5.1) \qquad N = Area = \int_{t_1}^{t_2} J(t)dt = \int_{t_1}^{t_2} \frac{dN}{dt}dt,$$

where N is total particle number concentration nucleated, $J(t)$ is the nucleation rate, t_1 is the time at the beginning of the burst and t_2 is the time at the end of the burst. The area of the triangle is, therefore, an approximation to the total number of particles nucleated. Written simply, the area of the triangle is:

$$(5.2) \quad Area = N = \frac{1}{2}bh = \frac{1}{2}(2\Delta t)J^*,$$

where $2\Delta t$ is the length of the burst ($\Delta t = t_2 - t_1$) and J^* is the height of the triangle. From Figure 5.1, it can be seen that Δt is determined from the slope of the left-hand side of the triangle:

$$(5.3) \quad \Delta t = \frac{J^*}{\dot{J}_{max}}.$$

By substituting Equation (5.3) into (5.2), the calculation of N becomes:

$$(5.4) \quad N = \frac{(J^*)^2}{\dot{J}_{max}}.$$

Simulations were done with a variety of relative humidities and source rates (R_g), in order to quantify the relationship in Figure 5.1, and therefore, obtain relationships between J^* and $\dot{J}_{max}$. From these simulations, it was determined that J^* can be related to the value of J at the point of $\dot{J}_{max}$ by the factor 1.60. The value of J at the point of $\dot{J}_{max}$ is termed J_{crit}. This relationship is shown in Figure 5.2. Therefore, N can be defined in terms of J_{crit} and $\dot{J}_{max}$:

$$(5.5)\quad N = \Delta t J^* = \frac{J^*}{\dot{J}_{max}} J^* = \frac{(1.6 J_{crit})^2}{\dot{J}_{max}}.$$

In this way, N is simply related to the value of the time-dependent nucleation rate and its derivative at one point in time. The value of J_{crit} is uniquely related to a critical saturation ratio, or vapor concentration, V_{crit} (see Figure 2.2), which, along with $\dot{J}_{max}$ has been correlated to the two independent parameters, relative humidity and source rate, from the results of a large number of simulations.

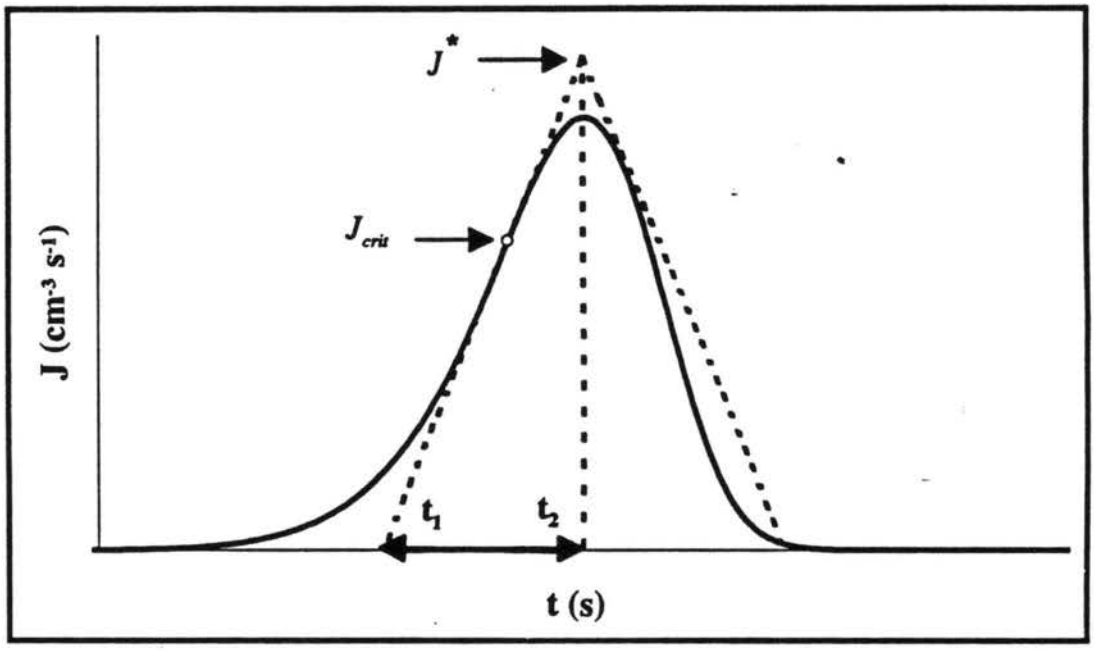

Figure 5.1. The triangular function.

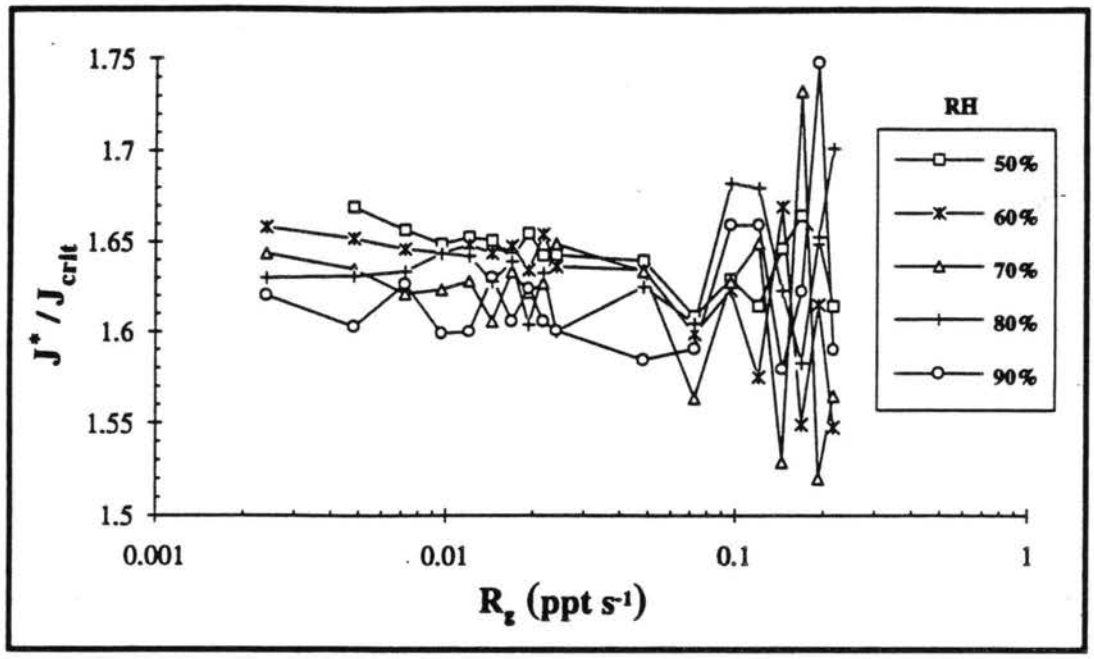

Figure 5.2. The $\frac{J^*}{J_{crit}}$ ratio.

For a given relative humidity, J_{max} and the slope of the time-dependent nucleation rate ($\dot{J}$) vary with source rate (see Figure 2.4). With higher source rates, the nucleation burst occurs very quickly and hence, the slope of *J(t)* is very steep. J_{max} reaches a larger value as a result of the larger available chemical source rate. Because of these variations with source rate and relative humidity, correlations are necessary for the two parameters, V_{crit} and $\dot{J}_{max}$.

Correlations

The correlations for V_{crit} and $\dot{J}_{max}$ were derived from a large number of simulations in which relative humidity and source rate were varied. BIMODAM I was executed for the duration of a nucleation burst with 10 second timesteps in order to closely follow *V(t)* and *J(t)*. The values of α used in each simulation were taken from Figure 3.5a, which depends on total source rate and relative humidity. The output from these simulations was analyzed to identify $\dot{J}_{max}$ and V_{crit} where V_{crit} is the value of *V* at the

time of $\dot{J}_{max}$. This analysis was completed for source rates between 0.0024 and 0.216 ppt/s for each relative humidity: 50, 60, 70, 80, and 90%. The data are represented by the symbols in Figure 5.3a.

A least-squares fit for $\ln(V_{crit})$ versus $\ln(R_g)$ and for $\ln(\dot{J}_{max})$ vs $\ln(R_g)$ was generated from the data for each relative humidity. The data are close to falling onto straight lines on a log-log plot and therefore, fairly easy to fit an accurate polynomial to. A variety of polynomial fits was tried for each parameter, V_{crit} and $\dot{J}_{max}$. Each fit was used to predict V_{crit}, $\dot{J}_{max}$, and N_{tot}. For each attempted fit, the results were compared with the original data. From this analysis, it was determined that quadratic fits give the best results for V_{crit} and $\dot{J}_{max}$. The resulting fits are represented by the solid lines in Figure 5.3. An interpolation scheme is used to calculate $\dot{J}_{max}$ and V_{crit} for relative humidities between the five for which there are equations.

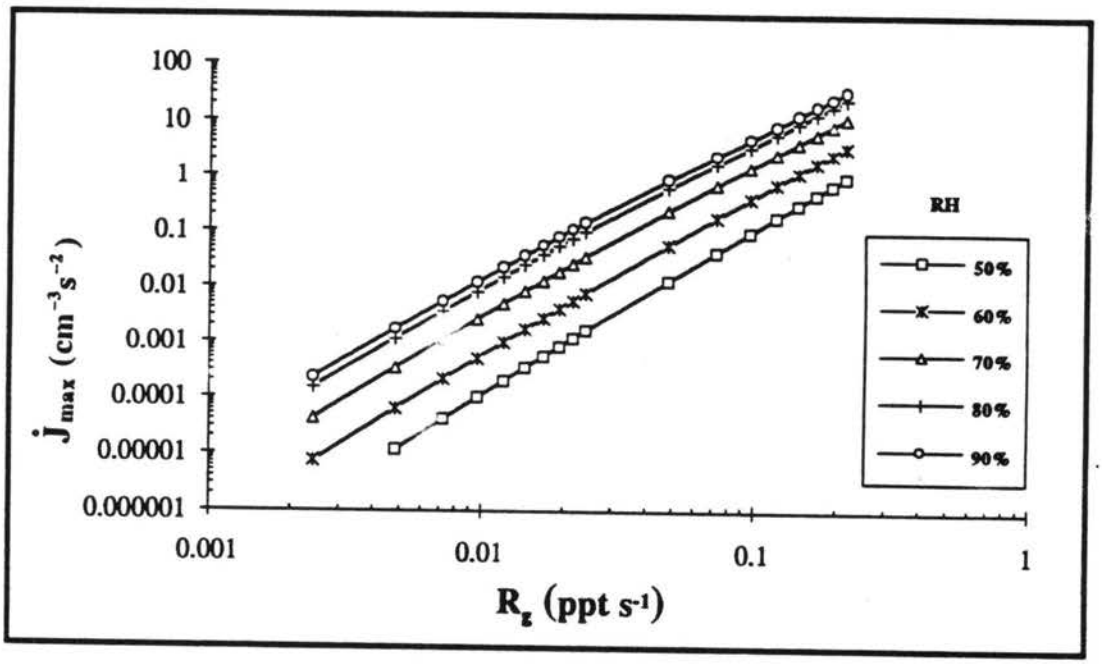

Figure 5.3a. Correlations for $\dot{J}_{max}$

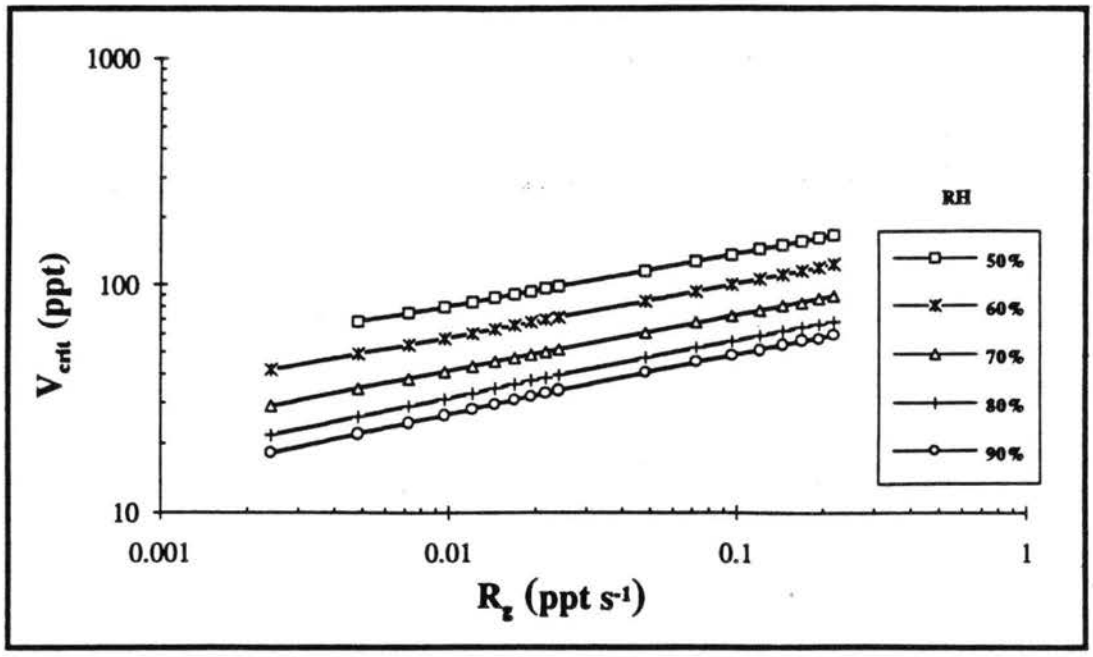

Figure 5.3b. Correlations for V_{crit}.

Mass calculation

During the nucleation burst, when there are no preexisting particles, it is assumed that all vapor produced during the time of the burst is scavenged by the nucleating particles:

(5.6) $$M_1 = R_g 2\Delta t$$

where $2\Delta t$ is the length of the burst, R_g is the chemical source rate and M_1 is the aerosol mass concentration. This is an assumption similar to that used in cloud droplet condensation calculation scheme, in which if the saturation ratio exceeds 1.0, the entire amount of 'excess' water vapor is added to the droplets.

Implementation

Implementation of this scheme in the absence of preexisting particles involves calculating a value for V_{crit}, using the correlations discussed above. This value of V_{crit} is compared with the value of V at the beginning of each timestep. The nucleation burst should begin when V is equal to V_{crit}. There is, however, very little possibility of finding a value of V exactly equal to V_{crit}. Therefore, a value of V within 10% of V_{crit} is accepted. When the value of V is within 10% of V_{crit}, the nucleation burst begins and the number of new particles is calculated using Equation (5.5). The corresponding amount of mass apportioned to the particles is calculated using Equation (5.6). It is important to note that following V until it is within 10% of V_{crit} only defines the time at which the burst begins. For calculating particle number concentration resulting from the burst, Equation (5.5) is used with the 'true' V_{crit} and $\dot{J}_{max}$, based on the correlations with source rate and relative humidity.

The time at which the burst is finished is calculated by adding $2\Delta t$ (the length of the burst) to the time at which the burst begins (when V is within 10% of V_{crit}) The vapor concentration value is kept constant during the burst as all of the available chemical source is added to the particles. After a burst has been predicted and calculated, the analytical growth calculation from Equation (4.62) is applied, using the appropriate timestep, until another burst is predicted.

II. Evaluation of the nucleation scheme in the absence of particles

This method of nucleating and growing particles has been tested over a wide range of vapor source rates and for relative humidities between 50% and 90%. Figure 5.4 shows that it predicts the number of particles nucleated during a burst with less than 10% error for the relative humidity and source rate ranges of interest.

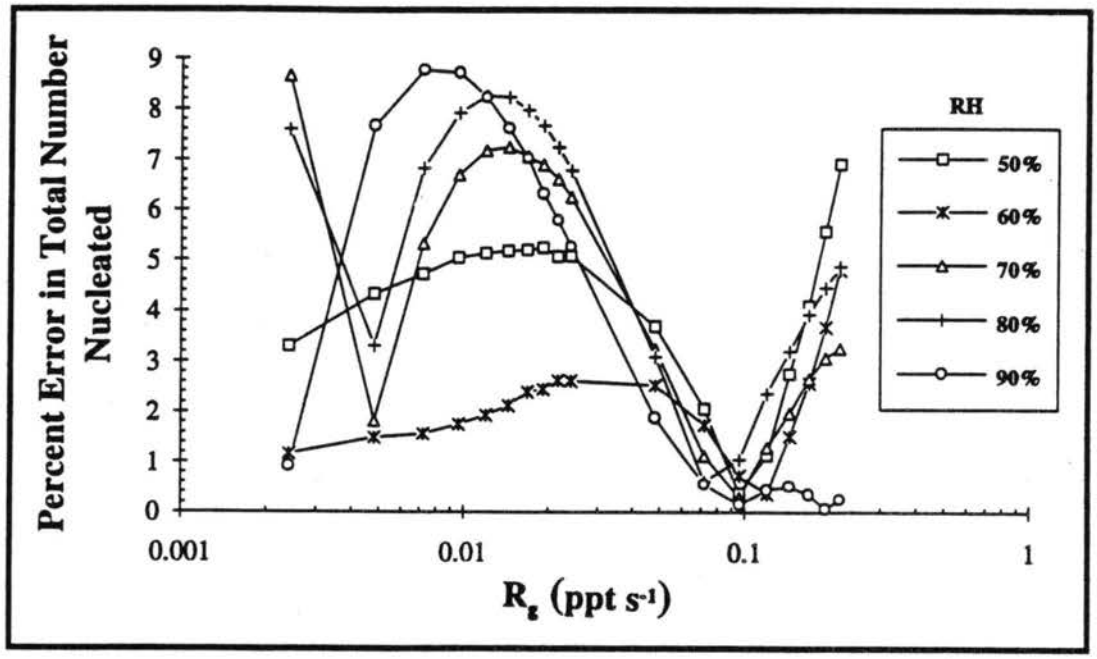

Figure 5.4. Percent error in number of particles nucleated, using the mechanism described in the text.

Example 1

Figure 5.5 is a specific example of how this procedure compares with a BIMODAM I simulation. The situation modeled is a nucleation burst in the absence of seed particles. Initial vapor and aerosol concentration values were zero. The source rate used was 0.024 ppt s^{-1}, and the relative humidity was 80%. The simulation was done for 6 hours, but only the first 1.5 hours, when the nucleation burst occurs, is shown in Figure 5.5. In the first figure (5.5a), total aerosol number concentration versus time, it is evident that the nucleation mechanism developed here produces the correct number of particles nucleated during the burst. The vapor concentration is kept constant during the burst under the assumption that all of the vapor produced over the length of the burst is scavenged by the nucleated particles (Figure 5.5b). The resulting aerosol mass

concentration and diameter are shown in Figures 5.5c and 5.5d. The mass resulting from the burst is slightly underpredicted, which results in a slightly underpredicted diameter.

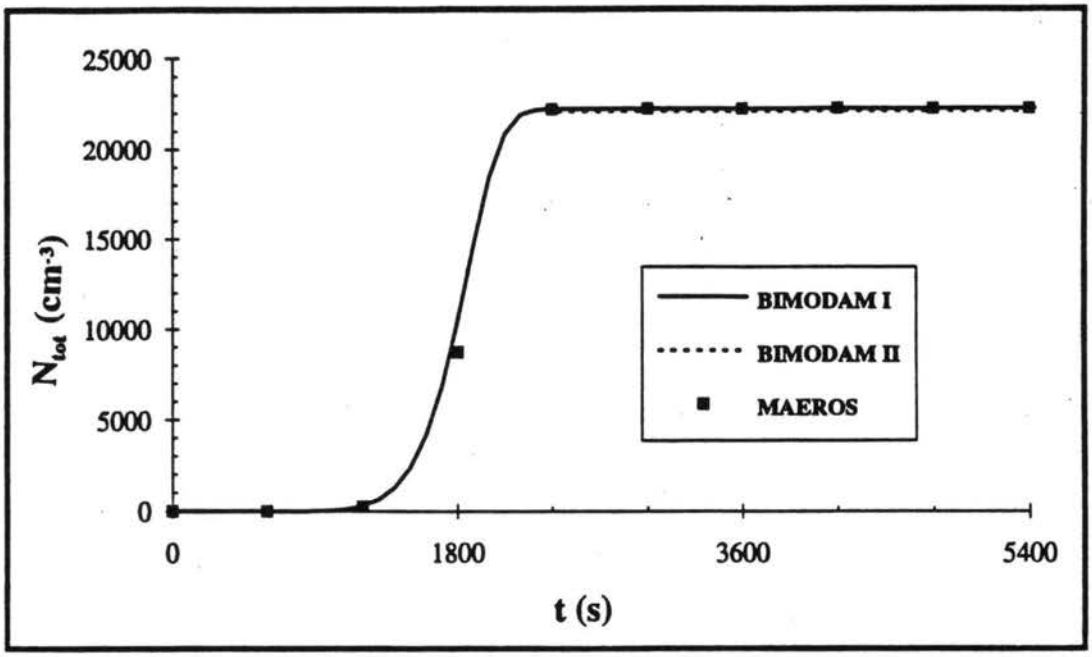

Figure 5.5a. Total aerosol number concentration, N_{tot}, predicted using the nucleation mechanism.

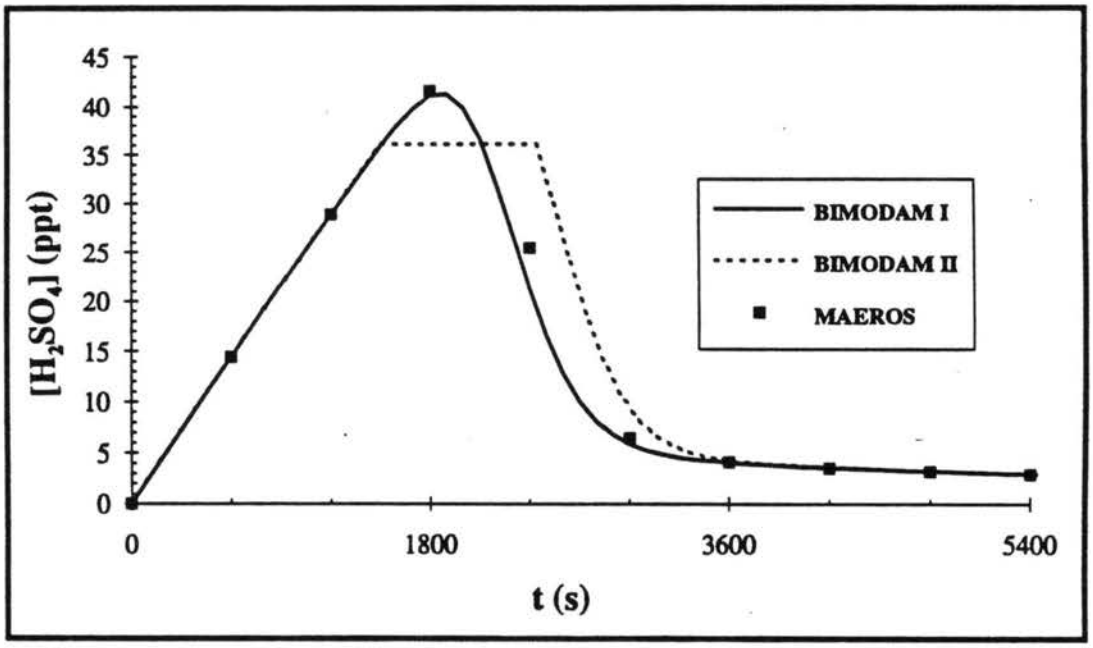

Figure 5.5b. Sulfuric acid vapor concentration, $[H_2SO_4]$, predicted using the nucleation mechanism.

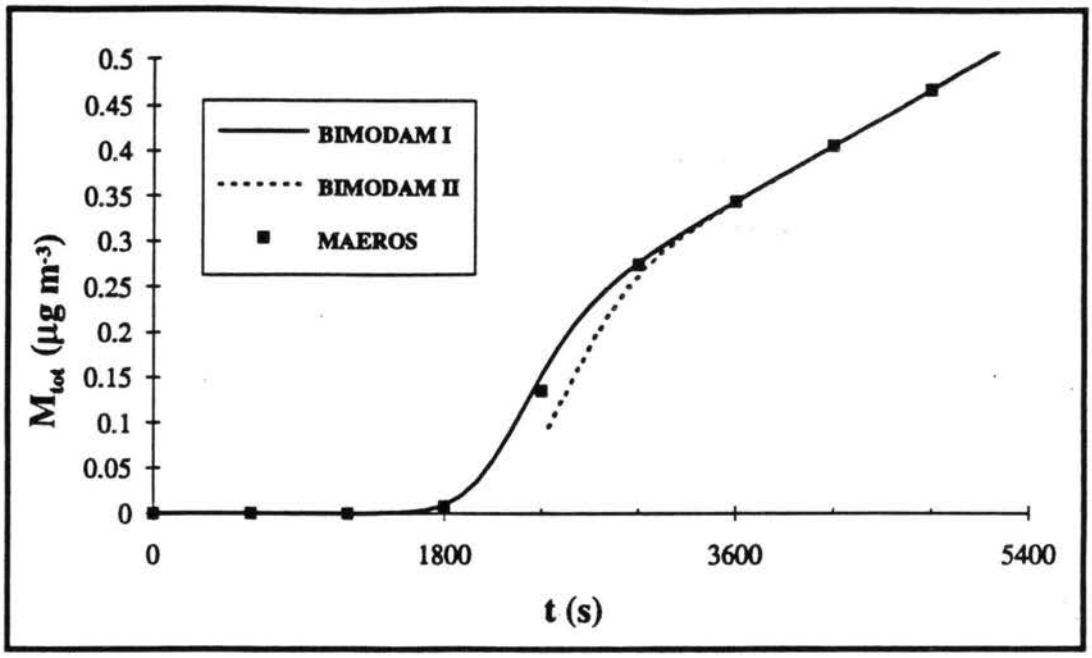

Figure 5.5c. Total aerosol mass concentration, M_{tot}, predicted using the nucleation mechanism.

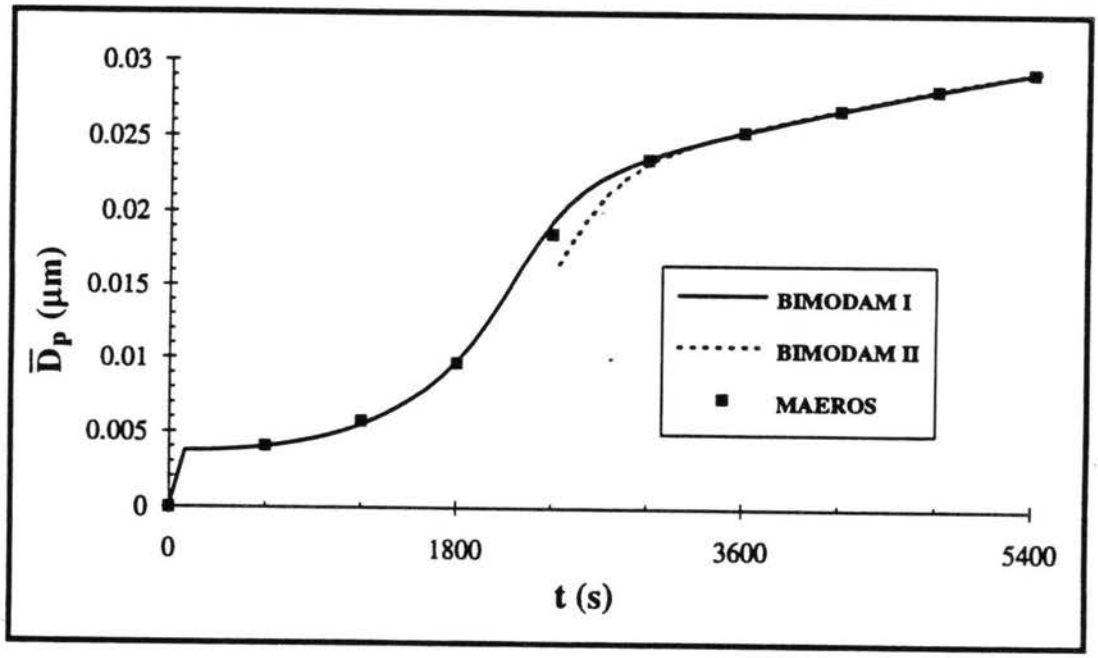

Figure 5.5d. Mass mean diameter, $\overline{D}_p$, predicted using the nucleation mechanism.

Weaknesses

The main weakness associated with this method is that the correlations are limited to relative humidities between 50 and 90% and for source rates between 0.0024 and 0.216 ppt/s. These ranges could be easily extended by analyzing further BIMODAM I simulations and extending the correlations.

Another limitation is the timestep. If the timestep used is too large, the nucleation burst could be missed because of overshooting the value of V which is within 10% of V_{crit}. In the absence of particles, the equation which is used to calculate the amount of material in the vapor phase is:

$$V(t+\Delta t) = V(t) + R_g \Delta t. \qquad (5.7)$$

As a specific example, consider a case such that V_{crit} is 24 ppt and R_g is 0.024 ppt s-1. Figure 5.6 shows the V values from Equation (5.7), based on the indicated timestep. The solid horizontal lines represent the range of values for V which are within 10% of V_{crit}. It can be seen that timesteps of 100 and 255 seconds have output times which correspond to values of V which are within this range. However, using a timestep of 570 seconds, indicated by the large solid squares, the nucleation burst would be missed.

In practice, a variable timestep could be selected by computation of characteristic times (chapter 4) and selection of the shortest characteristic time as the appropriate model timestep. For the simulations presented in this work, a time step of 100s was used.

III. Nucleation in the presence of particles

Explanation of the problems involved

Adapting the nucleation scheme to work in the presence of preexisting particles is necessary in order to quantify the condensation/nucleation competition problem. When there are other particles present, the vapor concentration requires a longer time to build up before a nucleation burst can occur because the preexisting particles scavenge some of the vapor. Figure 5.7 is an example of how, for the same vapor source rate, the vapor concentration before, during and after the burst changes when there are preexisting particles. The curves are flat during the nucleation burst when it is assumed that all of the vapor produced during the timestep is scavenged by the new and preexisting particles, as shown in Figure 5.5b. During the nucleation burst, it is not a good assumption for all of the vapor produced during the timestep to go onto the new particles, because that would mean assuming that the preexisting particles do not grow during the burst. Figure 5.8 is an example using BIMODAM I which shows that mode 2 does indeed gain mass while mode 1 experiences a nucleation burst.

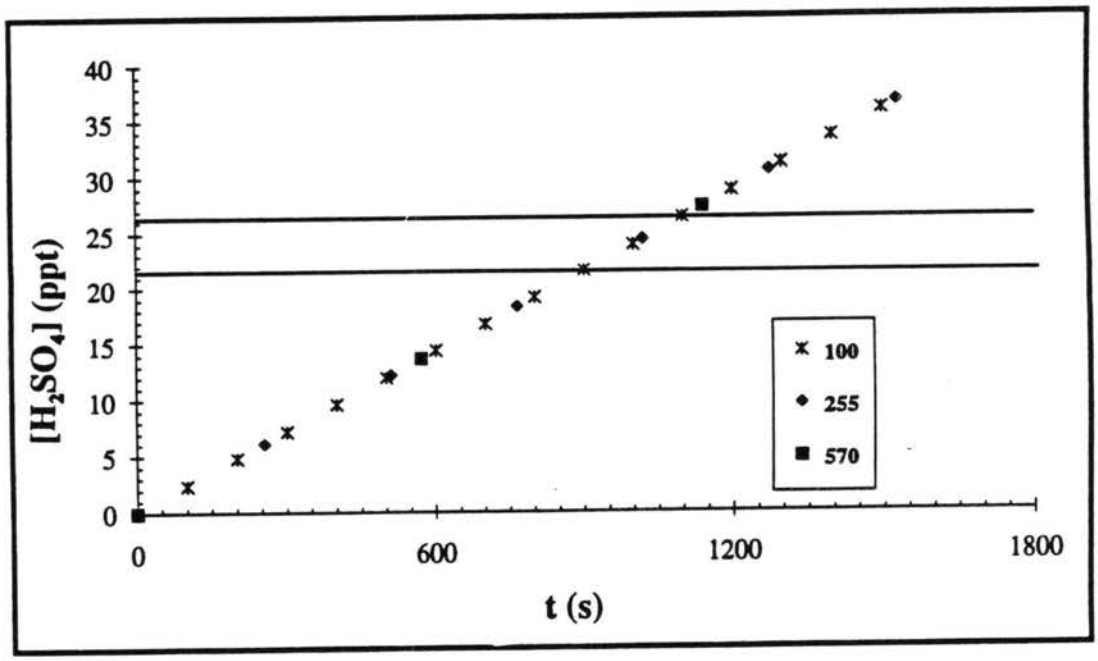

Figure 5.6. An example of the effect of timestep on Equation (5.7).

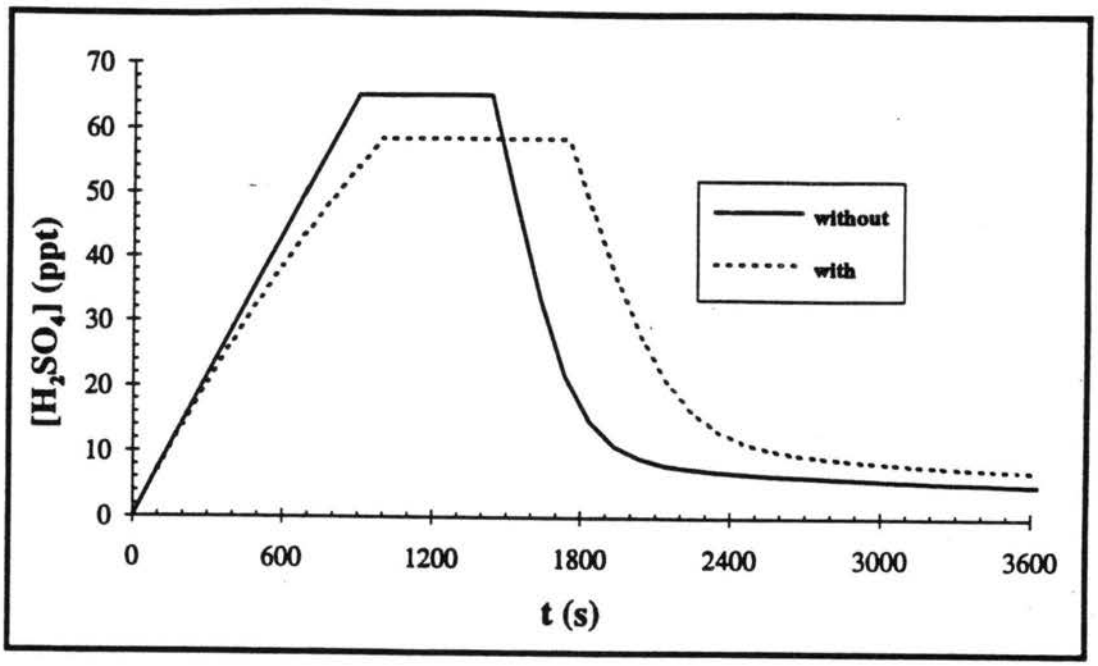

Figure 5.7. Sulfuric acid vapor concentration, $[H_2SO_4]$ with and without preexisting particles.

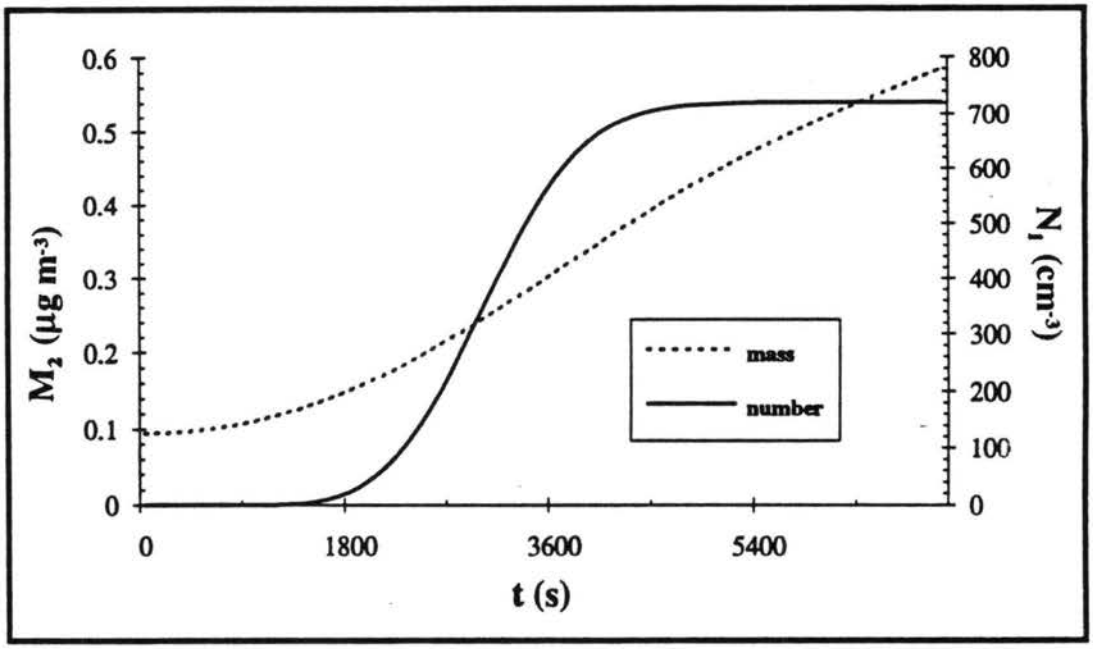

Figure 5.8. An example showing that mode 2 does gain mass during a nucleation burst.

The method

The method used to determine whether or not a nucleation burst will occur is to check whether the critical saturation ratio has been reached. For simulations done without preexisting particles, this check is based on the total chemical source rate, since all available vapor goes to the new particles. Because it is not a good assumption to apply the total chemical source rate to the new particles when there are preexisting particles, a method is needed to identify the effective source rate for nucleation. To do this, the vapor loss rate due to condensation onto the preexisting aerosol is subtracted from the chemical source rate to obtain an 'effective' vapor source rate at every timestep:

$$\hat{R}_g = R_g - R_{c2}. \tag{5.8}$$

Using $\hat{R}_g$, a value for V_{crit} is calculated with the correlations. By following V_{crit} based on $\hat{R}_g$, a check is made to see if the vapor phase is saturated with respect to instantaneous conditions. The same procedure is then followed as when there are no preexisting particles. The current value of V is compared with V_{crit}. If V is within 10% of V_{crit} a nucleation burst is predicted according to equations, using the effective source rate.

IV. Evaluation of nucleation scheme in the presence of seed particles

Conditions tested

A variety of initial conditions were used to test the effectiveness of this scheme in the presence of preexisting particles. The number and initial diameter of particles in mode 2 play distinct role in determining whether or not a nucleation event will occur. The other contributing factors are relative humidity and source rate strength.

2 play distinct role in determining whether or not a nucleation event will occur. The other contributing factors are relative humidity and source rate strength.

A special input file was created which contained 36 sets of initial conditions in which D_{p2} ranged from 0.001 to 100.0 microns, and N_2 ranged from 1 to 100,000 per cubic centimeter. The values that were scanned are shown in Table 5.1; for each initial D_{p2} value in column 1, each of the initial N_2 values in column 2 were used to calculate the initial mass. In order to cover the large range of source rates and relative humidities, 9 simulations were completed with this input file, for a total of 9 x 36 test cases (324). For each simulation, the set of 9 initial conditions shown in Table 5.2 were used. The relative humidities and source rates were chosen to represent the low, medium, and high values of each.

BIMODAM I and BIMODAM II were executed for six hour simulations. Total number nucleated by each model was compared. The two criteria used for testing accuracy were whether BIMODAM II predicted the occurrence of a burst, and if BIMODAM II calculated the correct number of particles resulting from the burst.

Initial D_{p2} (μm)	*Initial N_2 (cm^{-3})*
0.001	1
0.01	10
0.1	100
1.0	1000
10.0	10000
100.0	100000

Table 5.1. Initial conditions scanned for mode 2.

Simulation #	*Relative Humidity*	*Source Rate*
1	50%	0.005 ppt s^{-1}
2	70%	0.005 ppt s^{-1}
3	90%	0.005 ppt s^{-1}
4	50%	0.024 ppt s^{-1}
5	70%	0.024 ppt s^{-1}
6	90%	0.024 ppt/ s^{-1}
7	50%	0.193 ppt s^{-1}
8	70%	0.193 ppt s^{-1}
9	90%	0.193 ppt s^{-1}

Table 5.2. Initial conditions for simulations of a nucleation event in the presence of preexisting particles.

Results

In these nine simulations, 128 parcels experienced a nucleation event in BIMODAM I. A nucleation event was defined by nucleating more than 1 particle cm^{-3} during an entire nucleation event. BIMODAM II predicted that 118 of the parcels experienced a nucleation event, or about 92% effectiveness in predicting that a nucleation event will occur. Of the 118 parcels predicted to experience a nucleation event, 93 parcels predicted total number nucleated with less than 30% error, which amounts to 78% accuracy in predicting a nucleation event in the presence of preexisting particles.

Table 5.3 shows the parcels in which BIMODAM I predicted a nucleation event, but BIMODAM II did not predict. Shown in this table are the relative humidity, source rate, and initial diameter and number of particles in mode 2. The last column shows the number of particles which BIMODAM I nucleated during the event. For all of the

less than 10% of the number of preexisting particles. Therefore, it is questionable whether or not these cases can be defined as nucleation bursts.

By eliminating the parcels which contained very small or very large particles (0.001 and 100.0 microns), and a very large number (100,000 cm^{-3}) of preexisting particles, the precision increases to 97% and the accuracy increases to 80%. Under these conditions, BIMODAM I predicts 83 parcels to experience a nucleation event; BIMODAM II predicts 81 parcels. Of the 81 parcels predicted by BIMODAM II, 65 have less than 30% error in total number nucleated. If these cases are eliminated, then only one case remains for which BIMODAM II did not predict a burst which it should have. For this case, the number nucleated is less than 0.1% of the particles preexisting in mode 2.

RH	R_g (ppt s^{-1})	D_{n2} (μ m)	N_2 (# cm^{-3})	N_1 (# cm^{-3})
50	0.193	0.001	10,000	486
50	0.193	0.001	100,000	2.55
50	0.193	0.01	100,000	29.6
70	0.193	0.001	100,000	9440
70	0.193	0.01	100,000	4.2
90	0.0024	0.001	10,000	1
90	0.024	0.001	100,000	78.4
90	0.024	0.01	10,000	5.51
90	0.193	0.01	100,000	69.2

Table 5.3. The conditions associated with parcels which experienced a nucleation event in BIMODAM I, but was not predicted by BIMODAM II.

The results of the cases in which a nucleation burst was predicted in both BIMODAM I and BIMODAM II are shown in Figure 5.9, for the 70% (open symbols)

and 90% (closed symbols) relative humidity cases. The number of initial particles residing in mode 2 is indicated on the plot legend. The dashed lines indicate 30% error based on:

$$(5.9) \quad \%error = \frac{(N_{BI} - N_{BII})}{N_{BI}} * 100,$$

where N_{BI} is the number nucleated by BIMODAM I, and N_{BII} is the number predicted to nucleate by BIMODAM II. It can be seen that when there are a very small number of particles in mode 2, the nucleated number is accurately predicted by BIMODAM II. However, as the number of particles in mode 2 increases, the error increases. This is true for all source rates. By comparing the three figures, it can be seen that the error decreases as source rate increases.

Example 1

A time history comparison of number concentration in mode 1 and vapor concentration is shown in Figure 5.10. The conditions modeled correspond to simulation #5 with 100 preexisting particles cm^{-3}, with a diameter of 0.01 μm. It can be seen that the number of particles nucleated is predicted well by BIMODAM II. The vapor concentration is also predicted accurately. Aerosol mass in mode 2 is a key issue because during the nucleation burst, the condensation rate in mode 2 is kept constant. Figure 5.10c shows that that assumption results in approximately 11.5 % error in aerosol mass in mode 2.

Weaknesses

One weakness of this method is that it does not predict a nucleation event for some conditions for which new particles are predicted when Equations (2.34)-(2.38) are

integrated. Another weakness, mentioned earlier, is that the correlations are valid for source rates down to 0.0024 ppt s^{-1}, simply because that was the lower limit that was chosen. As explained earlier, the correlations could be extended.

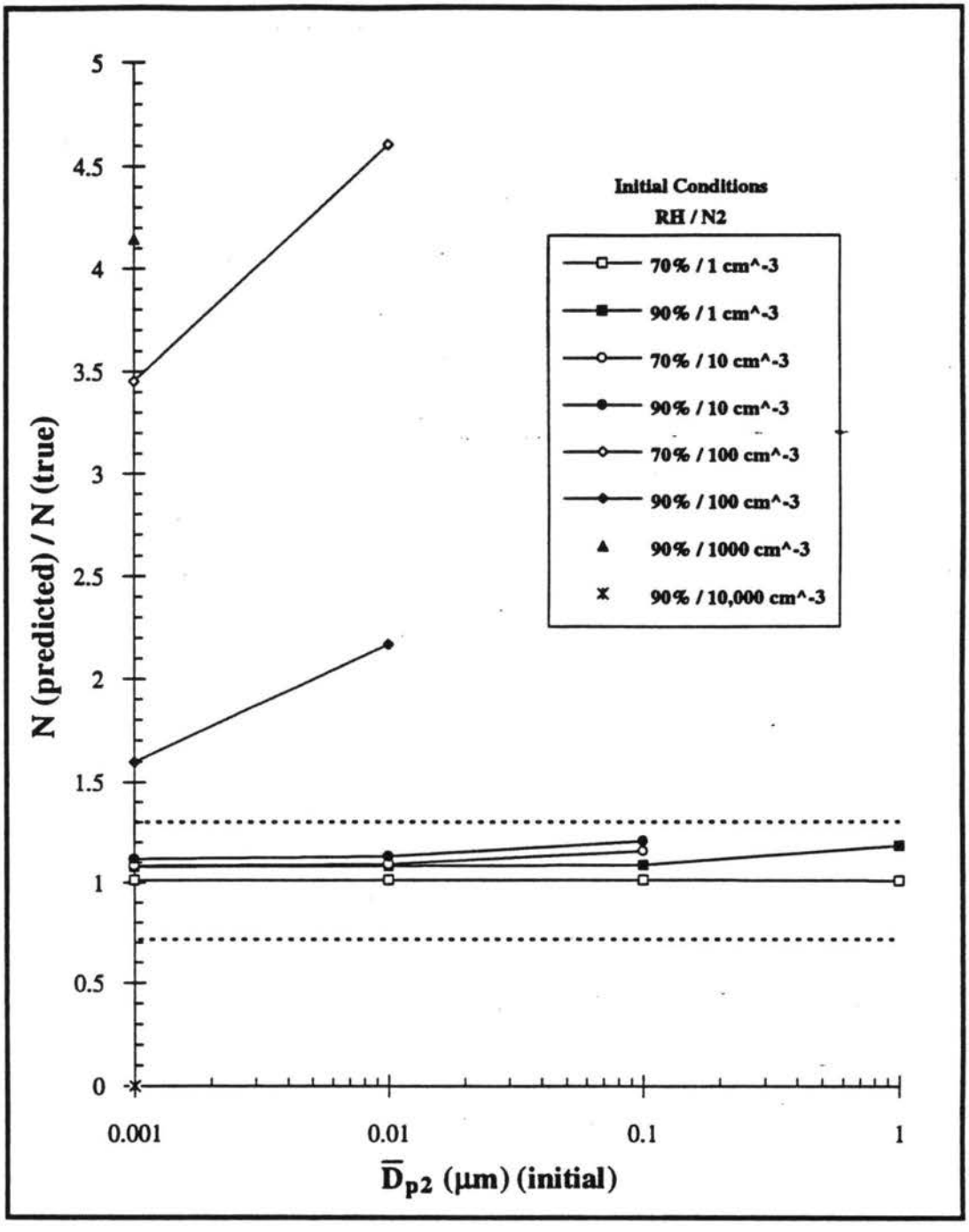

Figure 5.9a. Analysis of the number predicted to nucleate by each code, BIMODAM I and BIMODAM II. The source rate is 0.0024 ppt s^{-1}.

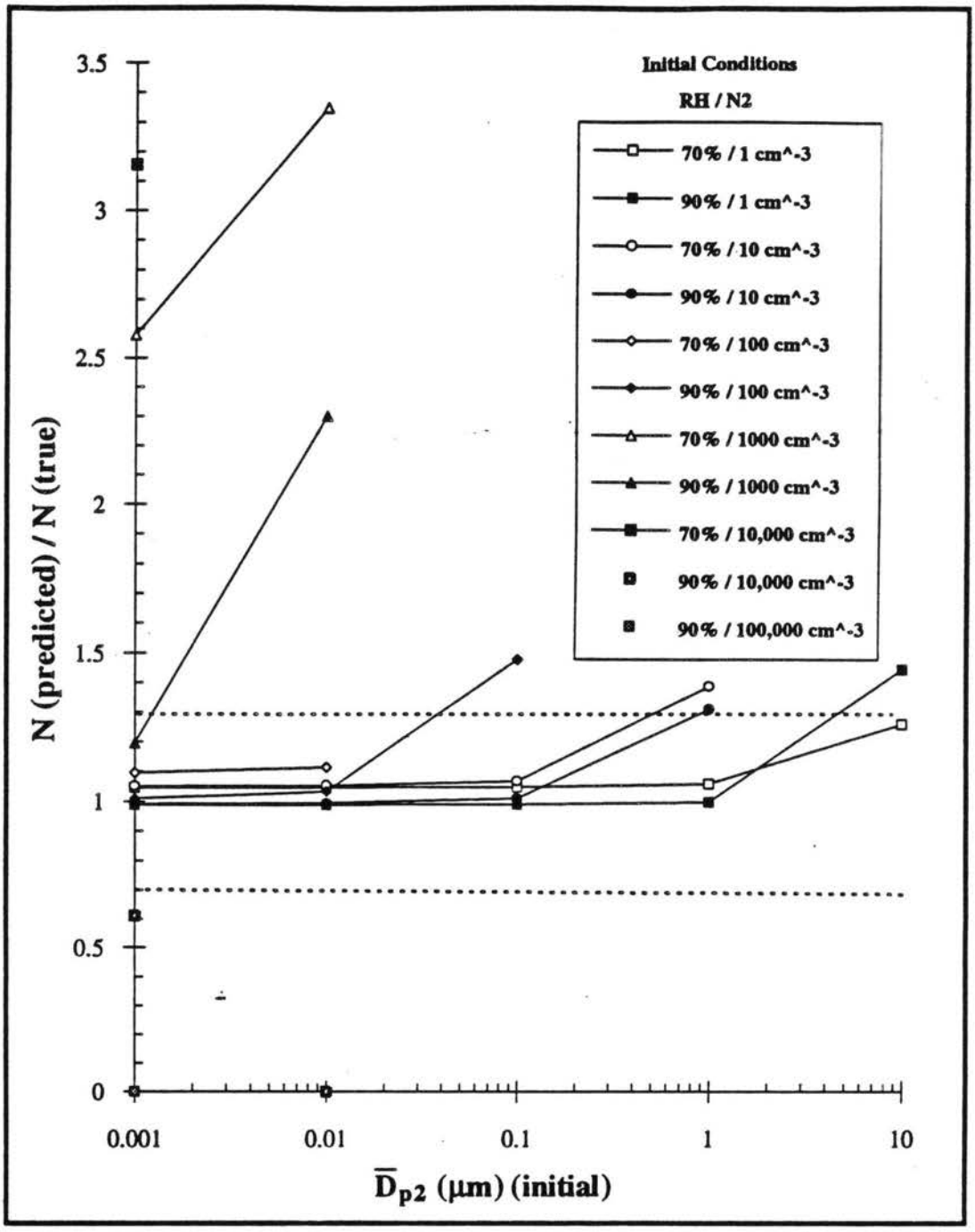

Figure 5.9b. Analysis of the number predicted to nucleate by each code, BIMODAM I and BIMODAM II. The source rate is 0.024 ppt s^{-1}.

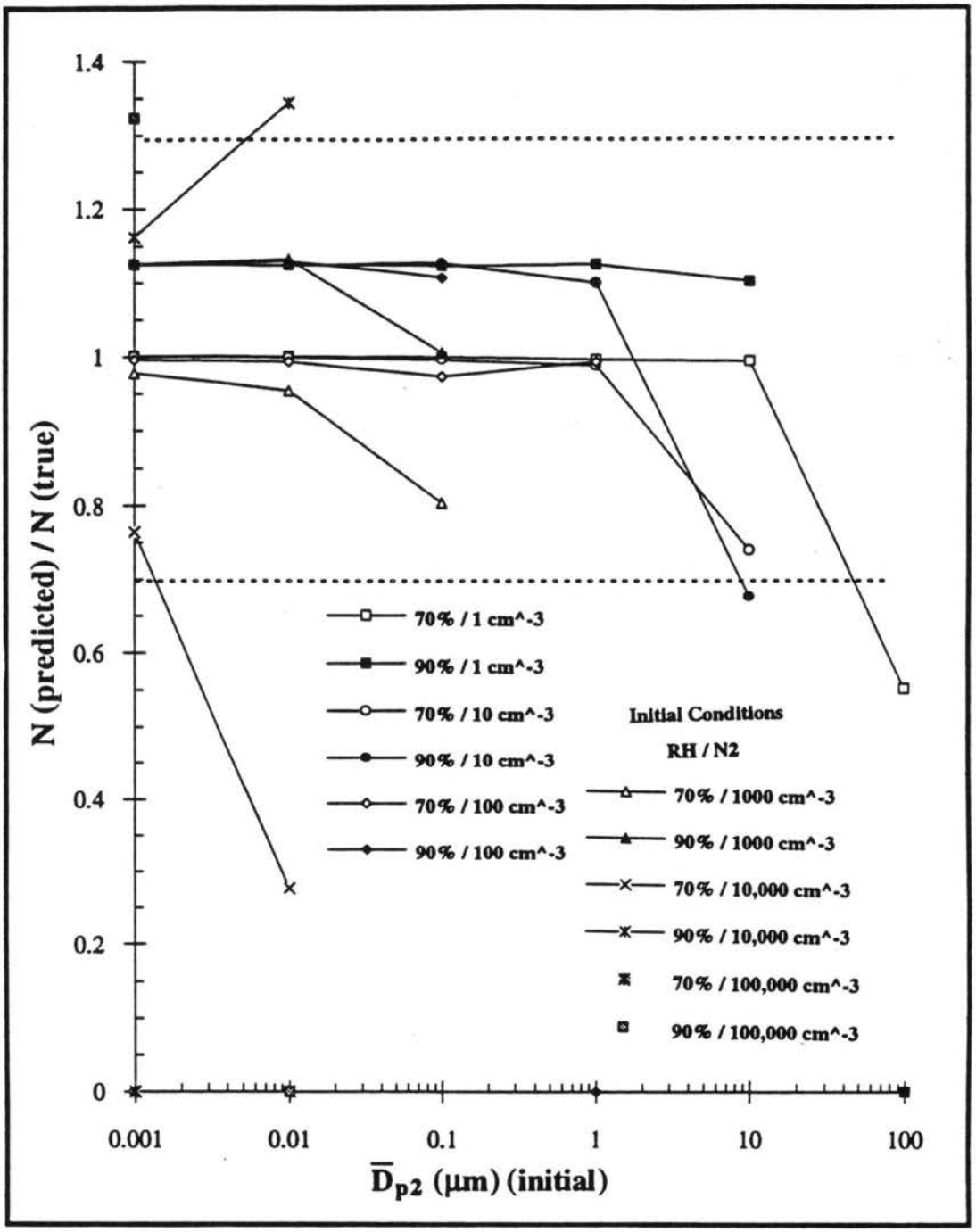

Figure 5.9c. Analysis of the number predicted to nucleate by each code, BIMODAM I and BIMODAM II. The source rate is 0.193 ppt s^{-1}.

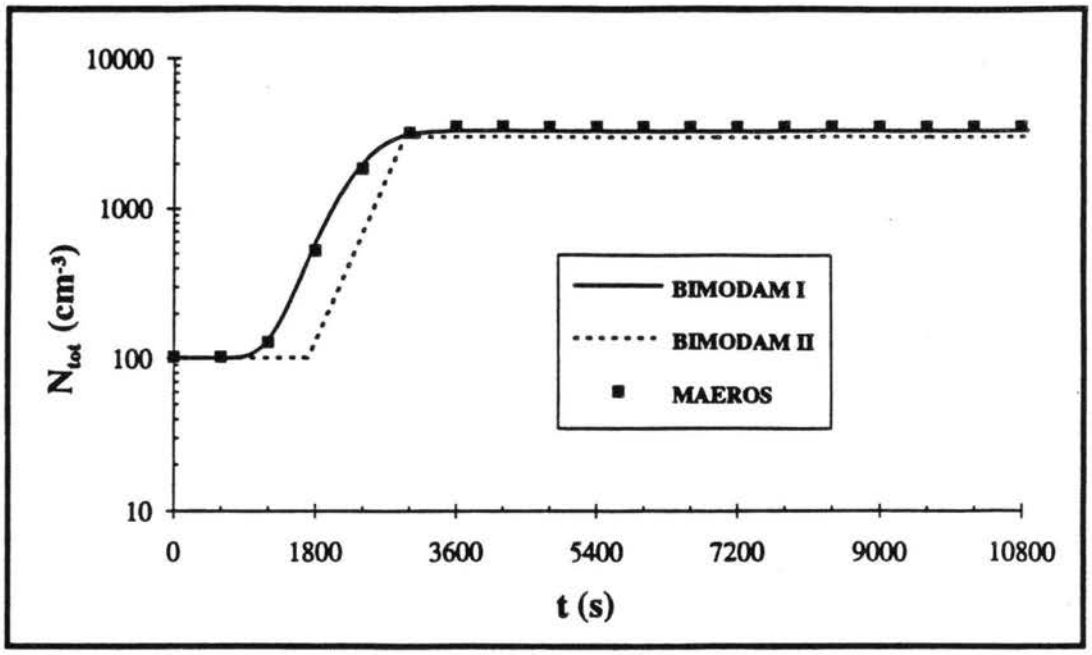

Figure 5.10a. Total aerosol number concentration, N_{tot}, resulting from a nucleation burst in the presence of preexisting particles.

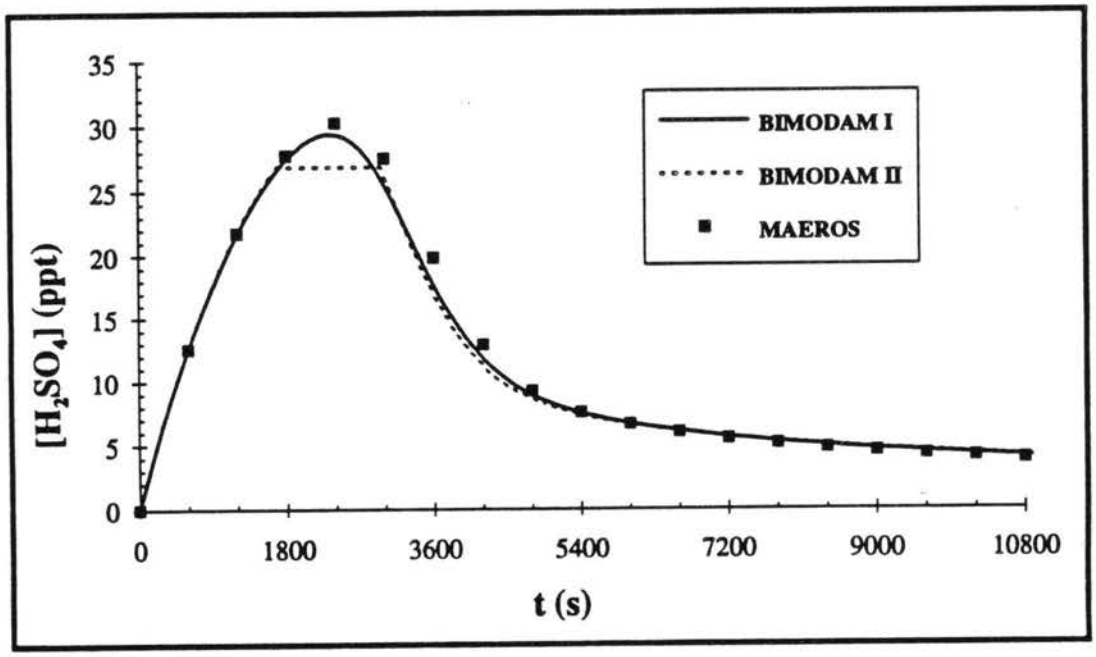

Figure 5.10b. Sulfuric acid vapor concentration, $[H_2SO_4]$, resulting from a nucleation burst in the presence of preexisting particles.

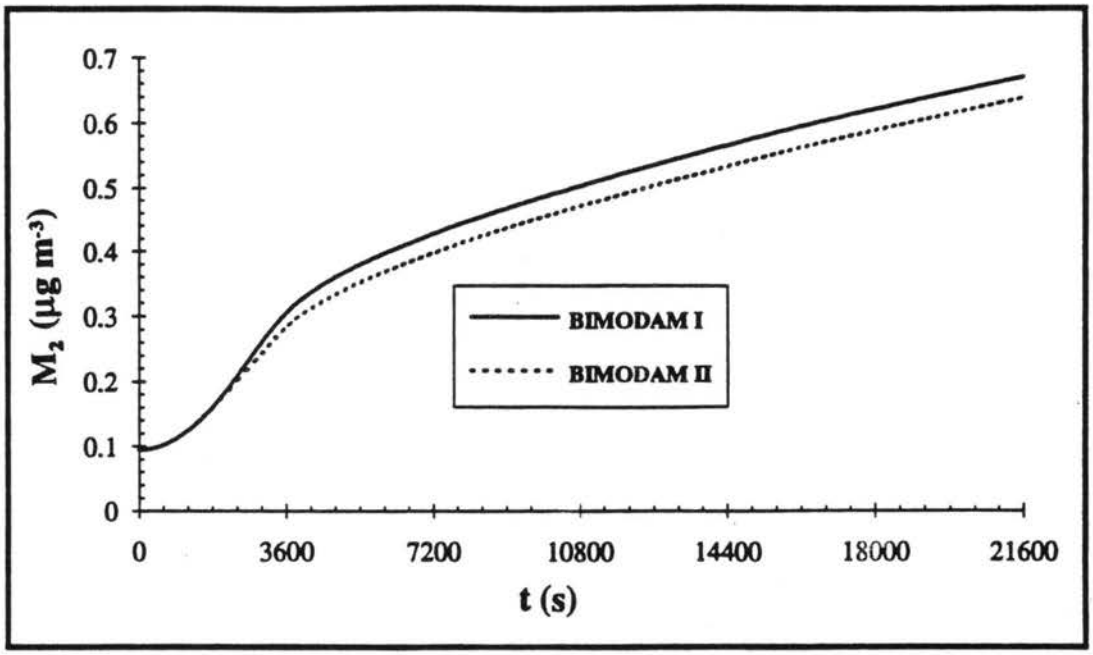

Figure 5.10c. Aerosol mass concentration in mode 2, M_2, resulting from a nucleation burst in the presence of preexisting particles.

CHAPTER 6 AN ANALYSIS OF THE COMPLETE BIMODAM II FORMULATION

6.A INTRODUCTION

Although each component of BIMODAM II has been separately tested against MAEROS and against the original aerosol model, BIMODAM I, intercomparison studies which combine all components to simulate a realistic atmospheric situation, and which can be used to compare accuracy and total computational costs between models, were also performed. For these simulations, all simplifications and parameterizations discussed in chapter 5 are used in BIMODAM II, except where noted.

6.B. SHORT TERM SIMULATIONS

The first set of simulations involves short term simulations of 6 hours in length.

I. 6-hour simulation with no seed particles

Initial Conditions

This simulation was done for a relative humidity of 65%, and a source rate of 0.02 ppt s^{-1}. The corresponding α for the newly formed particles is 0.7273. The merging process was not utilized in the BIMODAM simulations. The vapor was assumed to deplete during the simulation, while the source rate was held constant.

Results

The results are shown in Figure 6.1. For this simulation, the length of the burst in BIMODAM II was 1584 seconds, which is slightly longer than the burst in BIMODAM I. This can be seen in the figure of $[H_2SO_4]$ vs time (Figure 6.1a), as the vapor concentration is kept constant during the BIMODAM II burst. The end of the burst is indicated on the aerosol mass and number plots (6.1b and 6.1c) at the point where the BIMODAM II curve begins.

Figure 6.1c shows the most important result: prediction of total aerosol number concentration. It can be seen that BIMODAM II overpredicts by 6% the number of particles produced during the burst, which is indicated by the maximum number of particles. By examining the slope of N after the burst, it can be seen that BIMODAM I and BIMODAM II lose number at approximately the same rate, which indicates that the analytical solutions to the differential equations for coagulation and deposition perform well. Because of the overprediction of aerosol number, and the near-exact prediction of aerosol mass, BIMODAM II slightly underpredicts the diameter of the resulting particles.

Timing

The timing results are shown in Table 6.1. The column labeled EDIT indicates the frequency of output requested for each simulation. Significant CPU time is saved with BIMODAM II over both BIMODAM I and MAEROS, with very little accuracy lost.

CODE	*EDIT (s)*	*CPU (s)*
MAEROS	600	18.52
BIMODAM I	100	6.35
BIMODAM II	100	0.29

Table 6.1 Comparison of CPU time required to run the different codes for a 6 hour simulation with no seed particles.

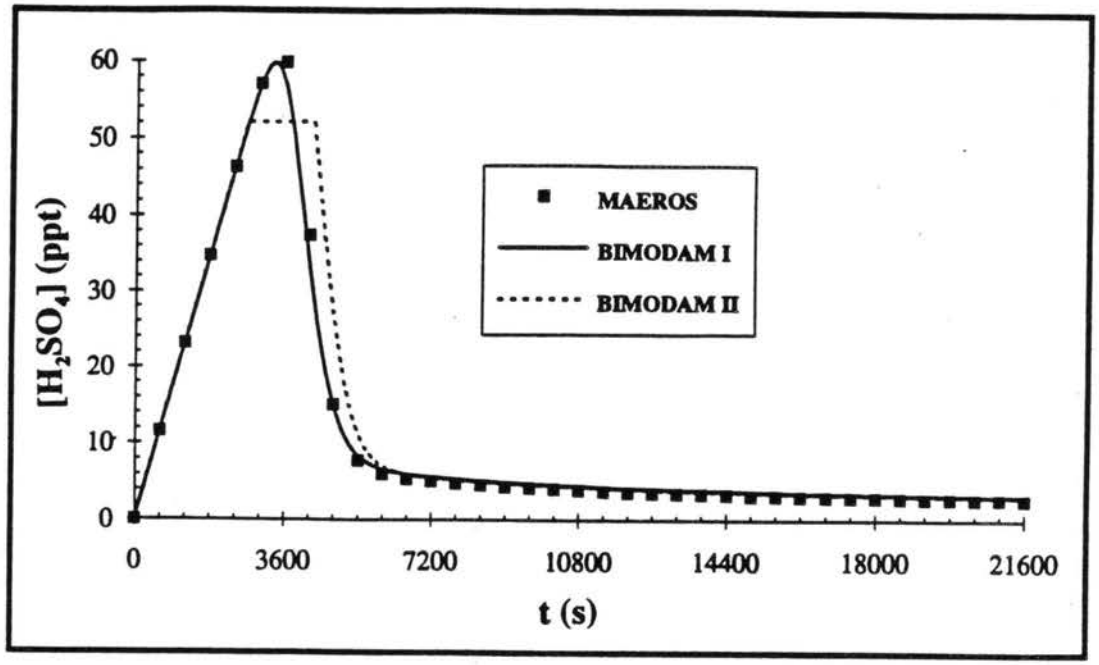

Figure 6.1a. Sulfuric acid vapor concentration, $[H_2SO_4]$, resulting from a six hour simulation with no seed particles, for a source rate of 0.02 ppt s^{-1} and a relative humidity of 65%.

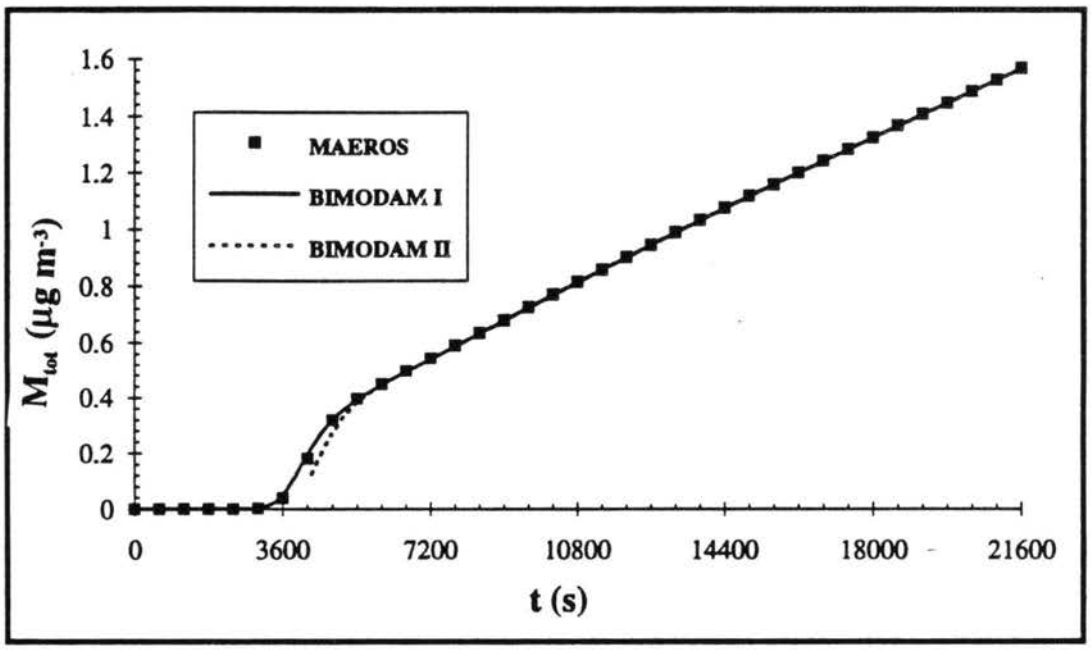

Figure 6.1b. Total aerosol mass concentration, M_{tot}, resulting from a six hour simulation with no seed particles, for a source rate of 0.02 ppt s^{-1} and a relative humidity of 65%.

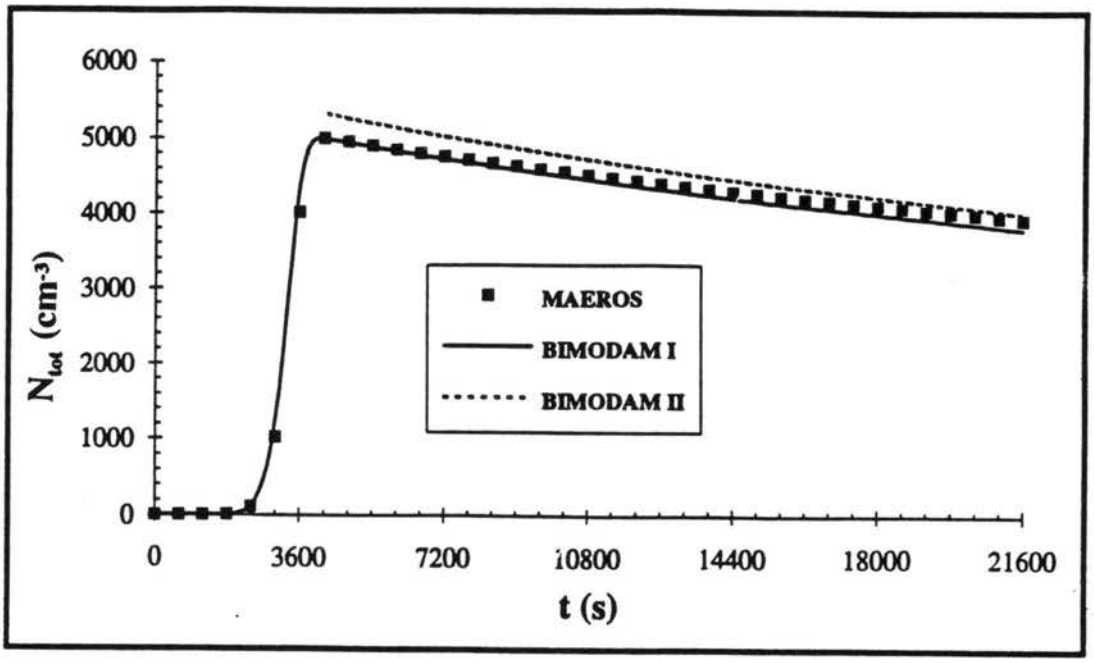

Figure 6.1c. Total aerosol number concentration, N_{tot}, resulting from a six hour simulation with no seed particles, for a source rate of 0.02 ppt s^{-1} and a relative humidity of 65%.

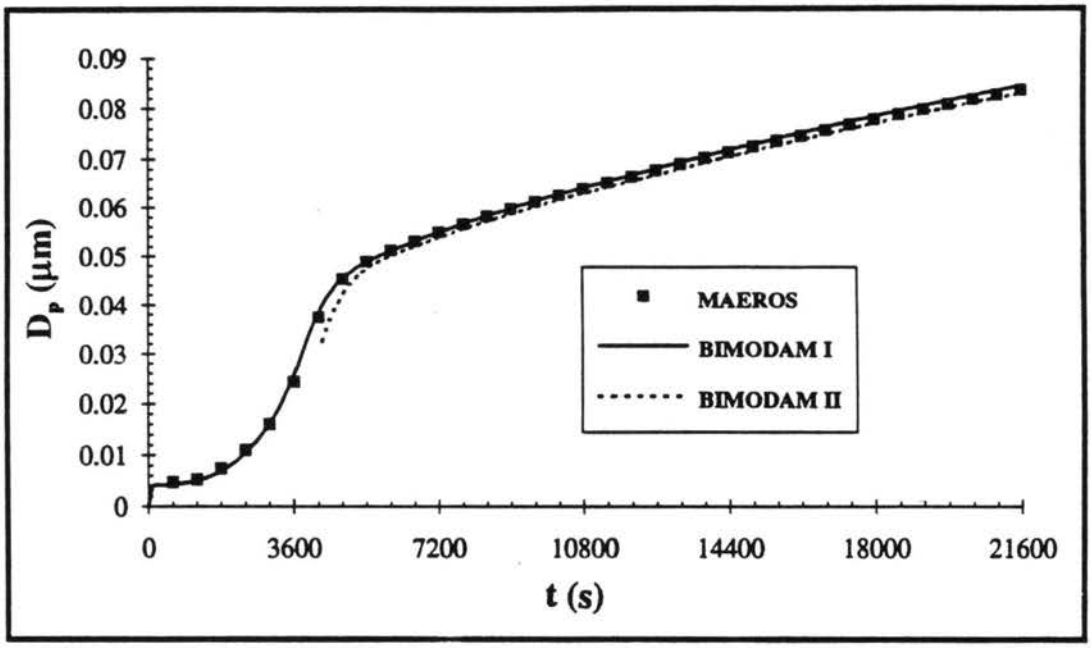

Figure 6.1d. Mass mean diameter, $\overline{D}_p$, of particles resulting from a six hour simulation with no seed particles, for a source rate of 0.02 ppt s^{-1} and a relative humidity of 65%.

I. 6-hour simulation with seed particles

Initial Conditions

This simulation was done with 1000 cm^{-3} preexisting particles with a mass mean diameter of 0.1 μm. The vapor source rate was 0.144 ppt s^{-1}, relative humidity was 80%, and merging was turned on using a χ value of 0.97. These conditions were chosen in order to simulate a case where the number of nucleated particles is on the same order as the number of preexisting particles.

Results

The results are shown in Figure 6.2. Total mass and number concentrations are compared between all three simulations, and the single modes are compared between BIMODAM I and II. No merging occurs in BIMODAM because the number concentration and size of the preexisting particles prohibit any new particles from growing rapidly enough to reach the diameter of the preexisting particles.

The nucleation burst was approximately 600 seconds in length; the rapidity of the burst is due to the high source rate and relative humidity. The vapor concentration (Figure 6.2a) follows the same trend as in the case without preexisting particles, except that the maximum value is significantly lower for this case with preexisting particles. The preexisting particles and the nucleated particles rapidly condense any available vapor. Total aerosol mass (Figure 6.2b) increases significantly as both modes consume the vapor.

The figure of total aerosol number concentration (6.2c) shows that the nucleation burst is on the same order as the number of preexisting particles. The competition between condensation and nucleation is, therefore, strong. This is a good test of the capability of BIMODAM II to resolve this competition and it can be seen that BIMODAM II more closely follows the MAEROS output, but that the slope is the same

as BIMODAM I, indicating that the analytical solutions for the coagulation and deposition processes behave well.

By looking at the individual modes in BIMODAM II (Figures 6.2d-6.2i), it can be seen that no merging occurs. Mode 2 condenses mass faster than it loses mass to deposition (Figure 6.2g), while the number of particles in mode 2 (Figure 6.2h) slowly declines as particles coagulate and deposit. The mass mean diameter of particles in mode 2 (Figure 6.2i) increases because mass is added, while number is lost. The nucleation burst is evident in the mode 1 results (Figure 6.2d-6.2f). The particles are formed in the first 600 s of the simulation and are slowly lost to coagulation and deposition.

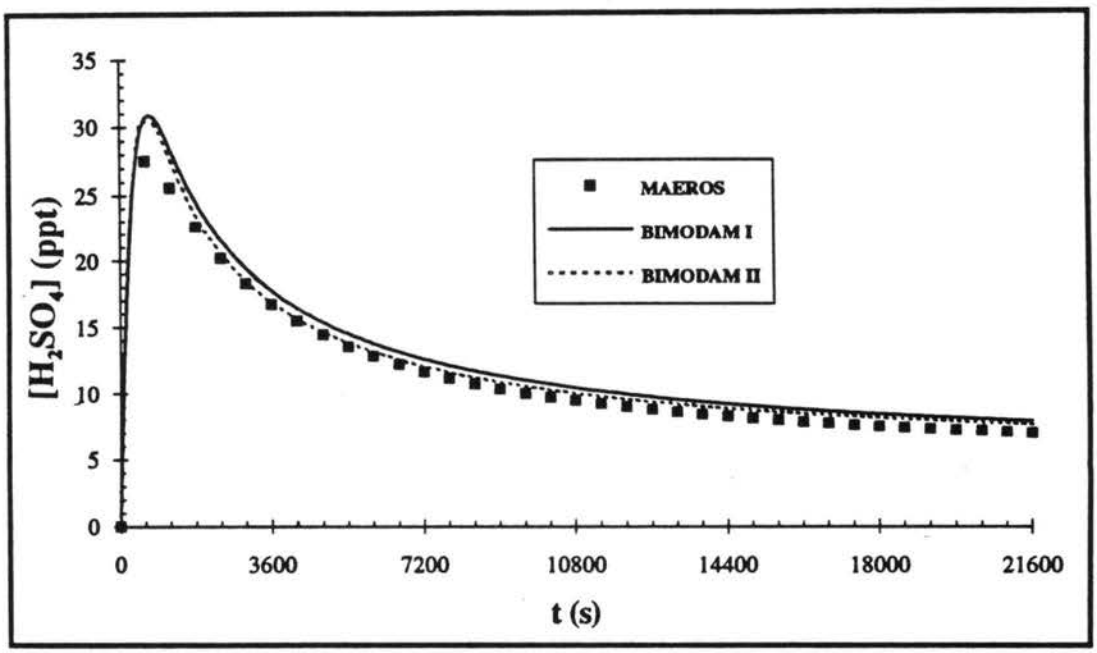

Figure 6.2a. Sulfuric acid vapor concentration, $[H_2SO_4]$, resulting from a 6-hour simulation with 1000 cm^{-3} particles initially residing in mode 2.

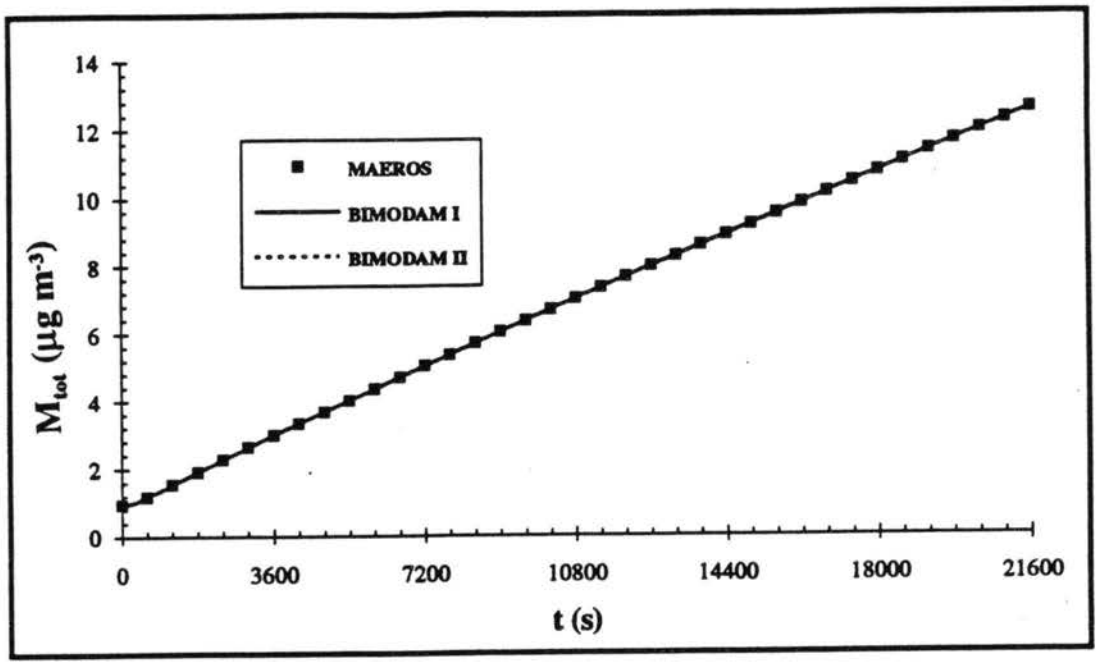

Figure 6.2b. Total aerosol mass concentration, M_{tot}, resulting from a 6-hour simulation with 1000 cm^{-3} particles initially residing in mode 2.

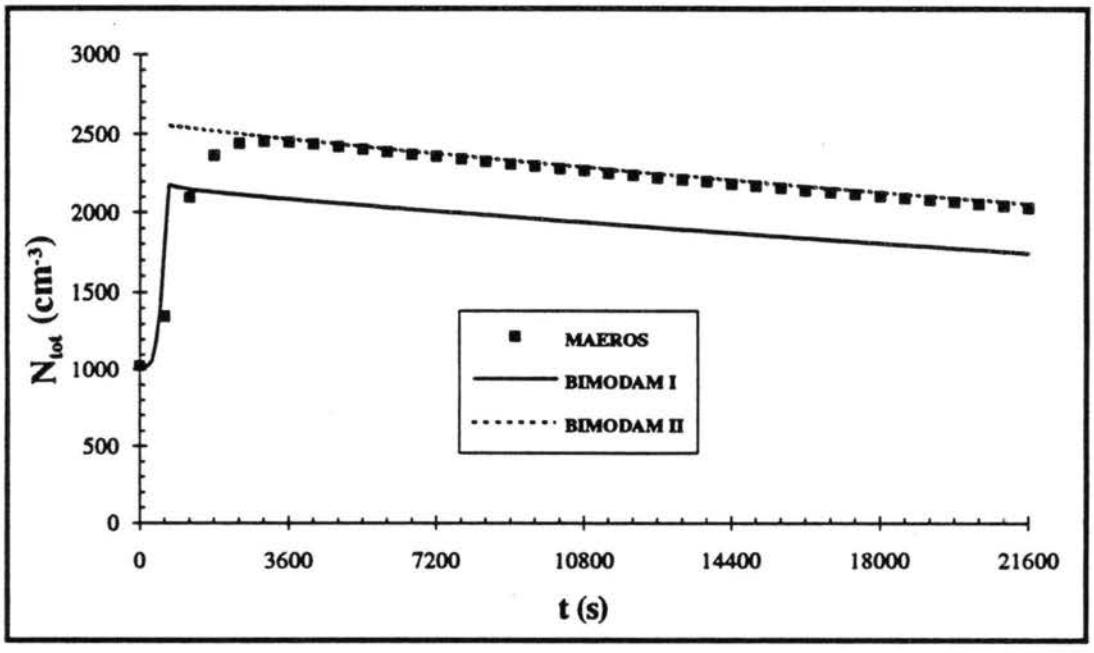

Figure 6.2c. Total aerosol number concentration, N_{tot}, resulting from a 6-hour simulation with 1000 cm^{-3} particles initially residing in mode 2.

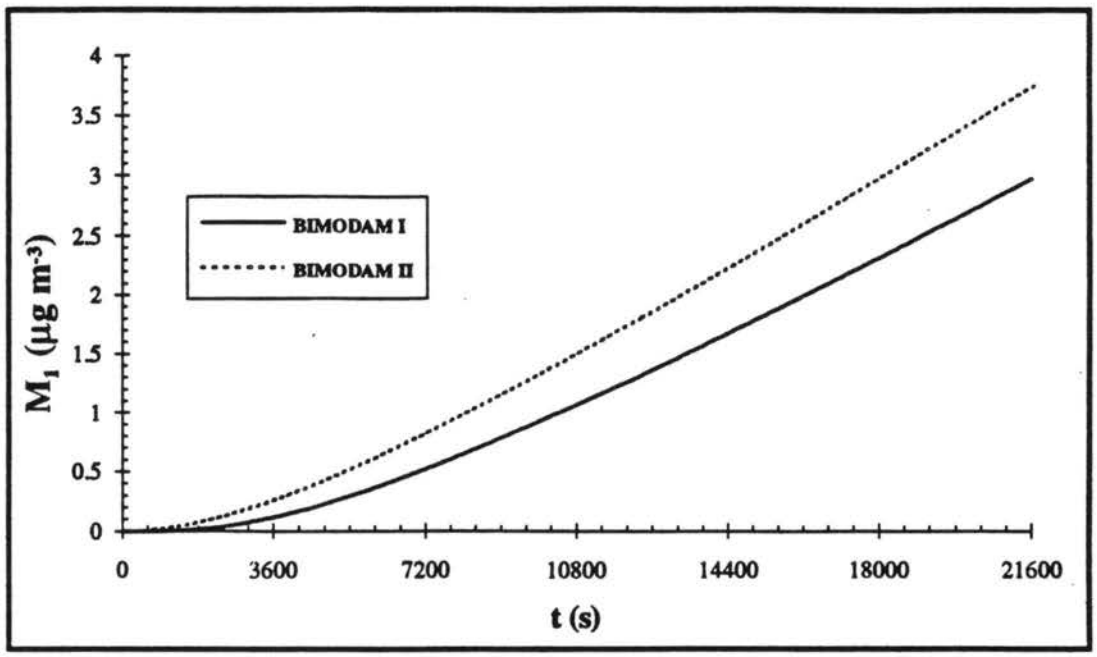

Figure 6.2d. Aerosol mass concentration in mode 1, M_1, resulting from a 6-hour simulation with 1000 cm^{-3} particles initially residing in mode 2.

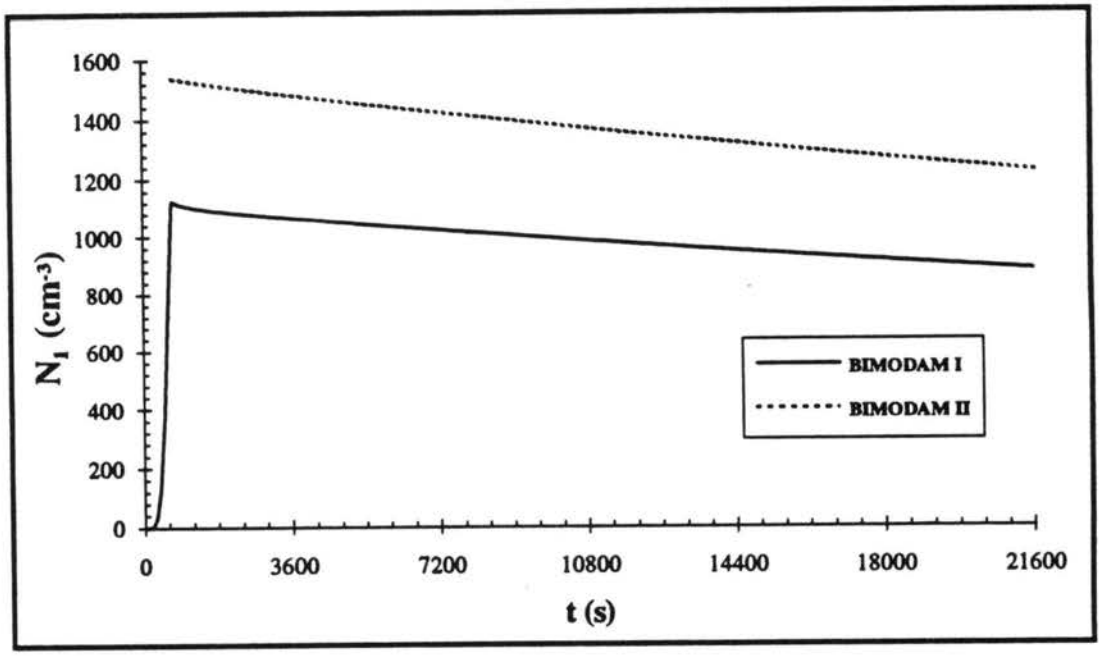

Figure 6.2e. Aerosol number concentration in mode 1, N_1, resulting from a 6-hour simulation with 1000 cm^{-3} particles initially residing in mode 2.

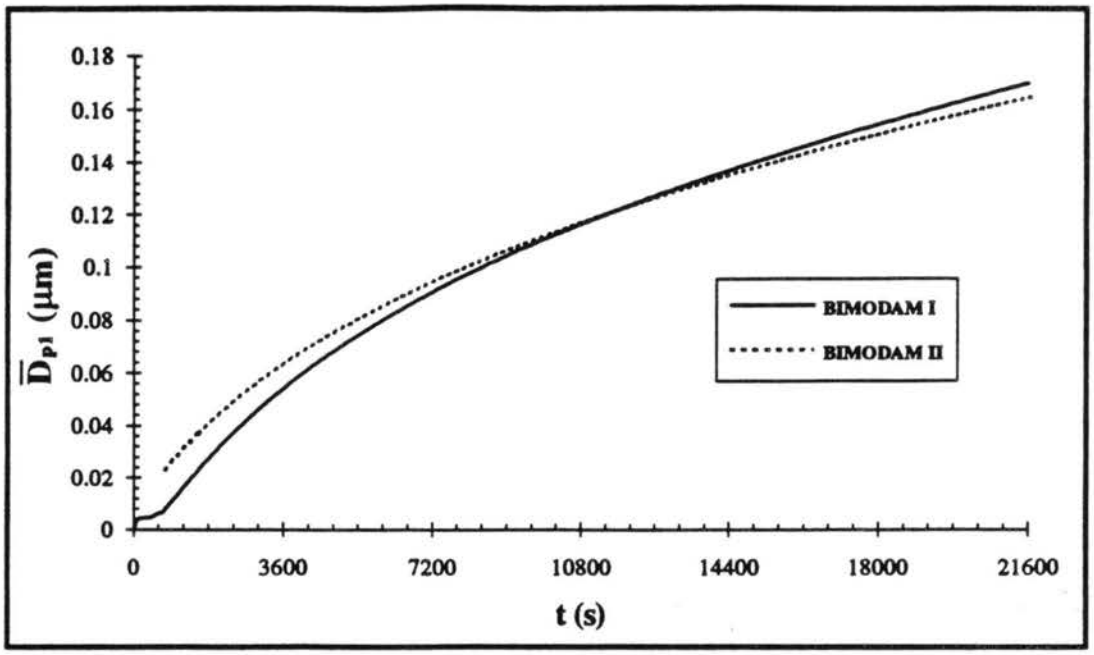

Figure 6.2f. Mass mean diameter of particles in mode 1, $\overline{D}_{p1}$, resulting from a 6-hour simulation with 1000 cm^{-3} particles initially residing in mode 2.

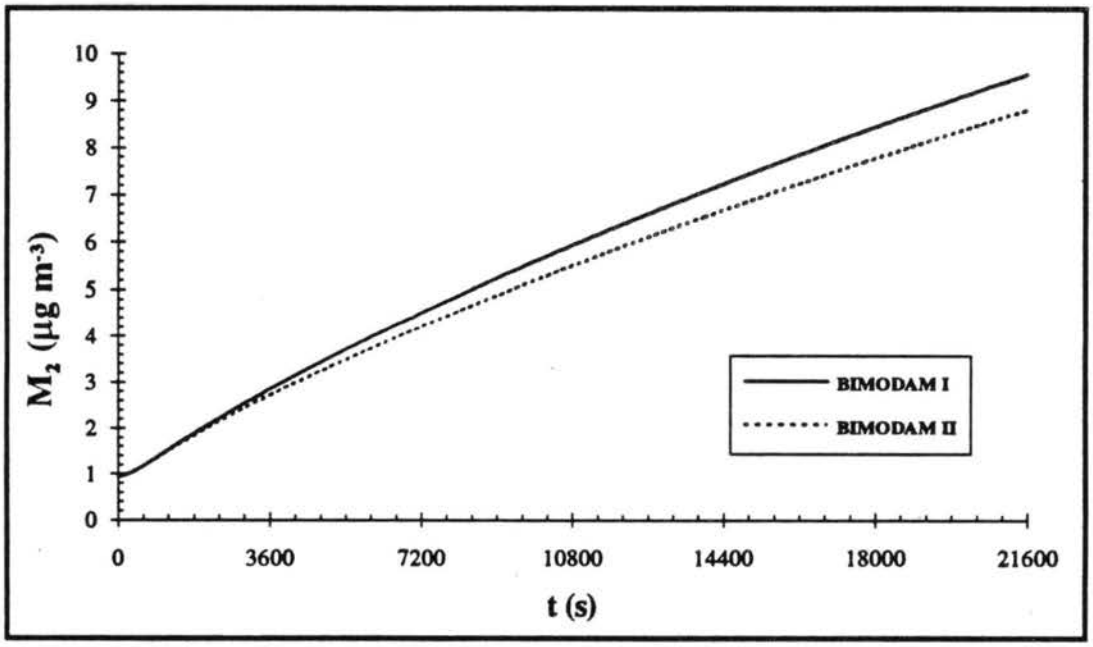

Figure 6.2g. Aerosol mass concentration in mode 2, M_2, resulting from a 6-hour simulation with 1000 cm^{-3} particles initially residing in mode 2.

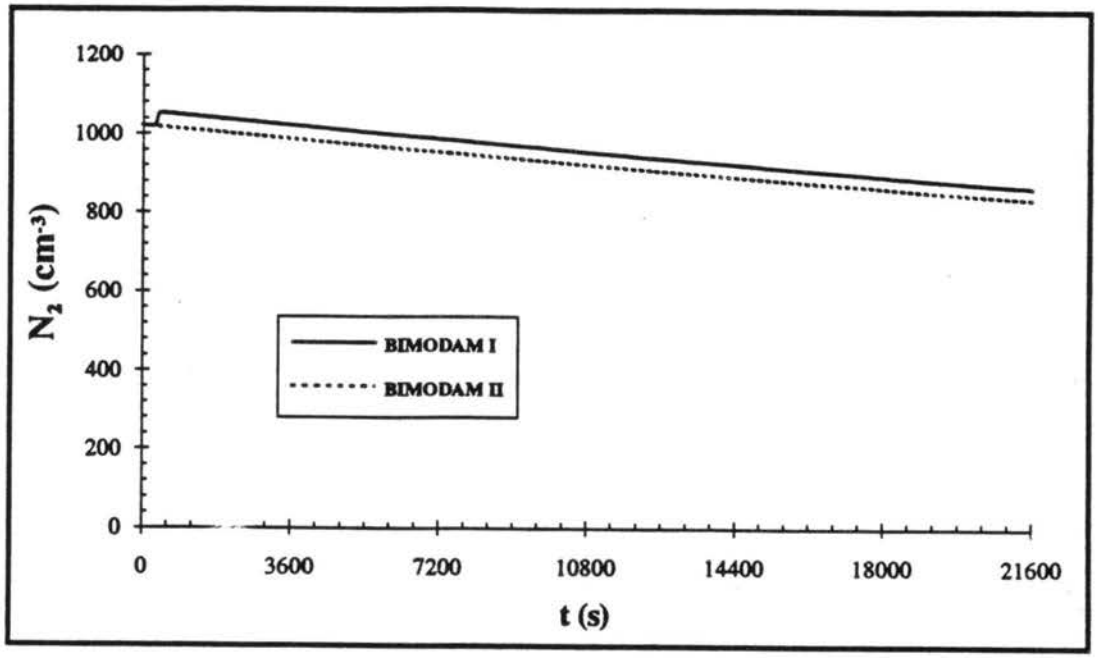

Figure 6.2h. Number concentration of particles in mode 2, N_2, resulting from a 6-hour simulation with 1000 cm^{-3} particles initially residing in mode 2.

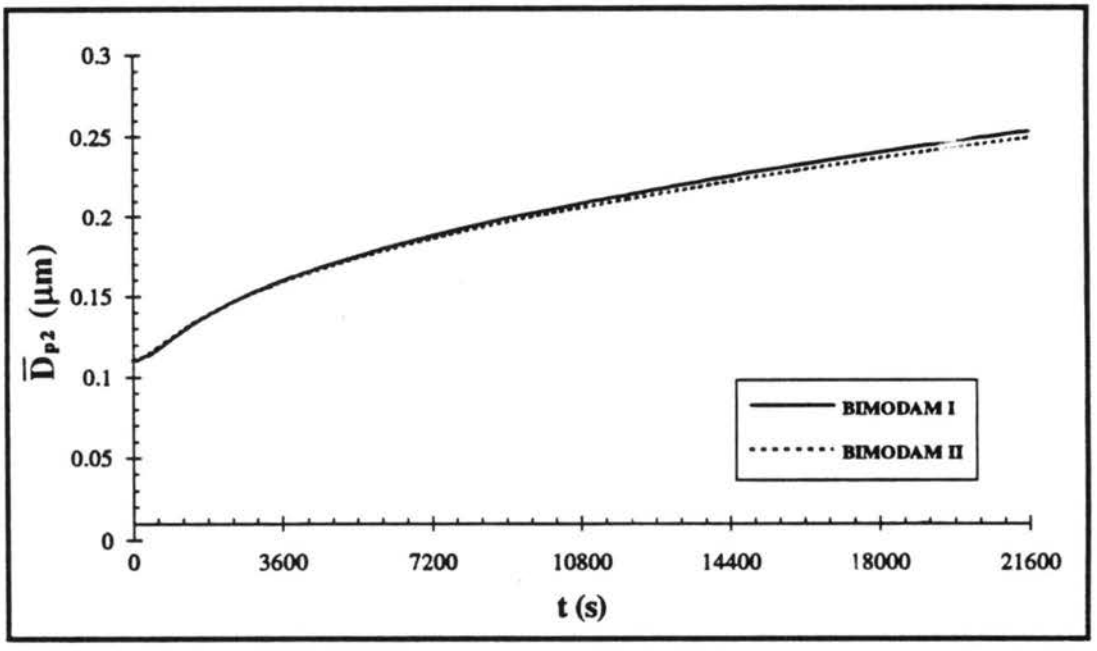

Figure 6.2i. Mass mean diameter of particles in mode 2, $\overline{D}_{p2}$, resulting from a 6-hour simulation with 1000 cm^{-3} particles initially residing in mode 2.

Timing

The timing results are shown in Table 6.2. BIMODAM II requires 1% and 4% of the CPU time that MAEROS and BIMODAM I, respectively, require to run this simulation, with very little accuracy lost. The uncertainty in these times is on the order of 0.1 seconds.

CODE	*EDIT (s)*	*CPU (s)*
MAEROS	600	25.3
BIMODAM I	100	6.56
BIMODAM II	100	0.25

Table 6.2. Comparison of CPU time required to run the different codes for a 6 hour simulation with seed particles.

6.C. STEADY STATE SIMULATIONS

The steady state simulations were done to examine how BIMODAM II performs over long time scales. One important question is whether or not the α value derived for the initial nucleation burst can be carried for times longer than the original run from which it was derived.

I. 15-day simulation with no seed particles

Initial Conditions

The initial conditions are exactly the same as in the 6-hour simulation without seed particles. The merging criterion was set to 0.97.

Results

The results are shown in Figures 6.3. Neither MAEROS, nor BIMODAM I or II maintained a bimodal distribution; for simplicity, the BIMODAM simulations show only the total values of the parameters.

The vapor concentration shows a steep increase in the very beginning of the simulation, followed by a steep decrease as the initial burst of particles condenses much of the vapor (Figure 6.3a). After the initial burst, the vapor concentration rises slowly until it reaches a steady value of approximately 20 ppt. All three codes show the same trends. BIMODAM I and II underpredict the steady state vapor concentration, relative to MAEROS, by approximately 1%. Total aerosol mass concentration (Figure 6.3b) rises steadily until a steady value is reached whereby mass production exactly balances loss due to deposition. This behavior is typical of the steady state simulations that were studied.

BIMODAM II predicts the initial nucleation burst very well, and follows the BIMODAM I results almost exactly (Figure 6.3c). They both reach steady state at approximately the same time; the MAEROS simulation requires two extra days. Compared with MAEROS, BIMODAM I and II underpredict total aerosol number by a factor of 2. MAEROS has about 23 particles per cubic centimeter at steady state, while BIMODAM I and II have 14 and 15 particles, respectively. This factor of two difference in aerosol number produces the errors seen in particle diameter. At 15 days, BIMODAM II exhibits about 20% error in comparison with MAEROS, but very little error in comparison with BIMODAM I.

Timing

The timing results are shown in Table 6.3. BIMODAM II requires only 3% of the CPU time that MAEROS requires for this steady state simulation.

CODE	*EDIT*	*CPU*
MAEROS	1 day	3 min 9 s
BIMODAM I	3600	26.06 s
BIMODAM II	100	5.97 s

Table 6.3. Comparison of CPU time required to run the different codes for a 15 day simulation with no seed particles.

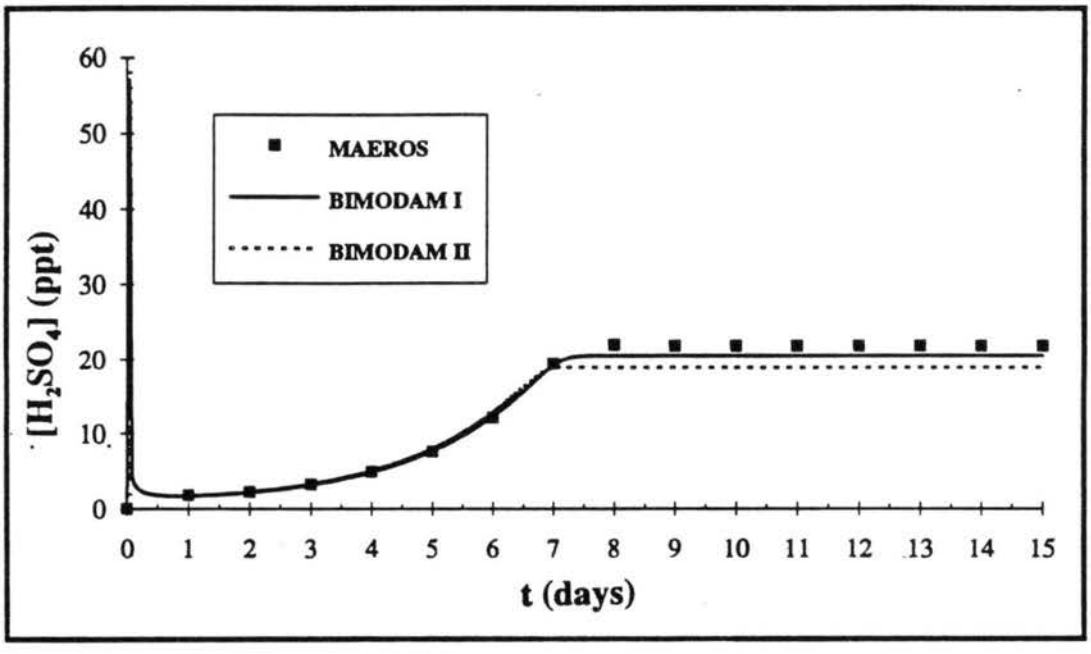

Figure 6.3a. Sulfuric acid vapor concentration, $[H_2SO_4]$, resulting from a 15-day simulation with no seed particles.

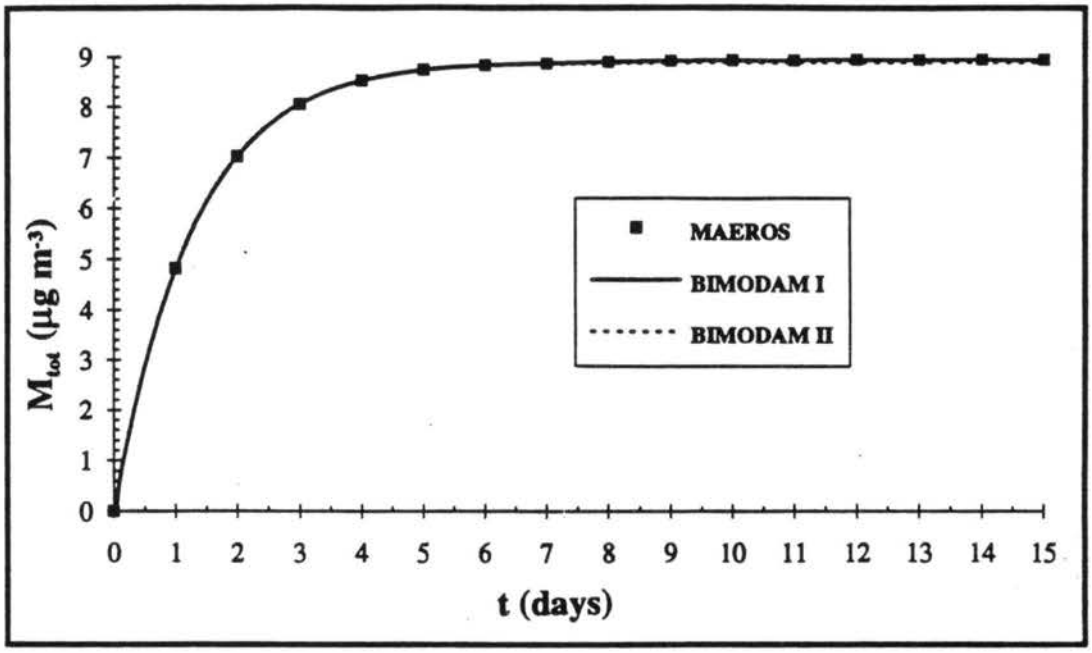

Figure 6.3b. Total aerosol mass concentration, M_{tot}, resulting from a 15-day simulation with no seed particles.

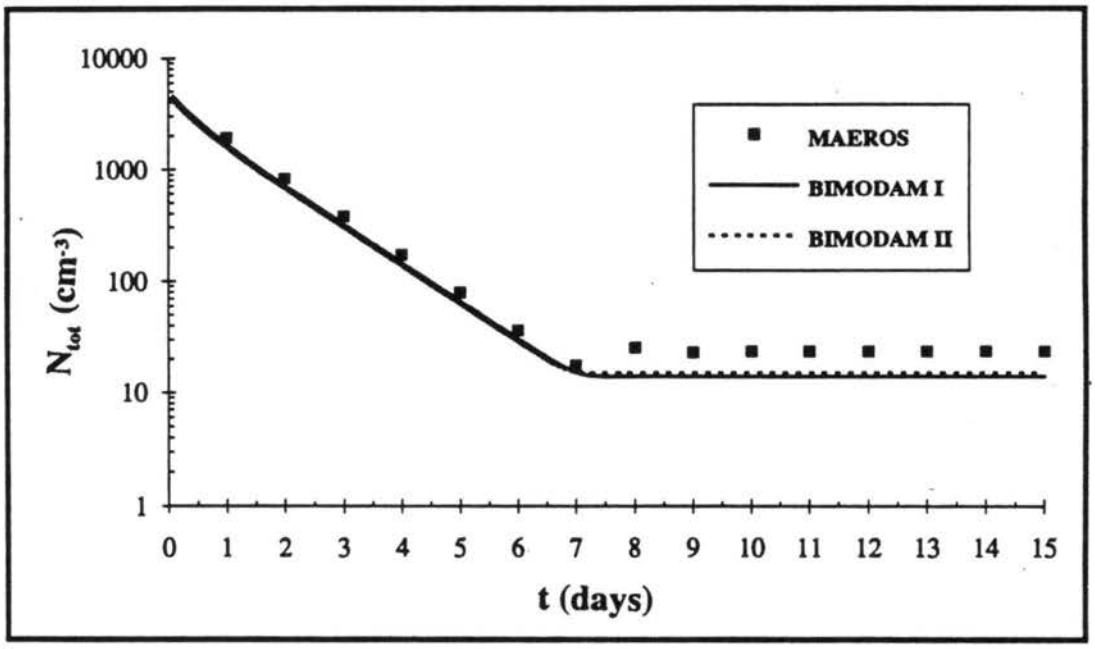

Figure 6.3c. Total aerosol number concentration, N_{tot}, resulting from a 15-day simulation with no seed particles.

I. 15-day simulation with seed particles

Initial Conditions

The initial conditions are identical to those of the 15-day simulation without seed particles, but with 10 cm^{-3} preexisting in mode 2. The longer simulation is used to examine steady state behavior.

Results

The results are shown in Figures 6.4. The very small values of M_1 and N_1 which are predicted by BIMODAM I (Figures 6.4d and 6.4e) are the result of a merge in the first 6-hours of the simulation. Merging continuously empties mode 1, so that most of the aerosol mass and number concentrations is contained in mode 2. BIMODAM II shows no particles in mode 1 until the last half of the simulation, because the initial burst is immediately transferred into mode 2.

The results of the comparison between models are almost identical to the case without preexisting particles. Both cases, with and without preexisting particles, reach the same steady state.

Timing

The timing results are shown in Table 6.4. BIMODAM II requires 80% less CPU time than BIMODAM I. A 97% decrease of CPU time is seen over MAEROS for BIMODAM II.

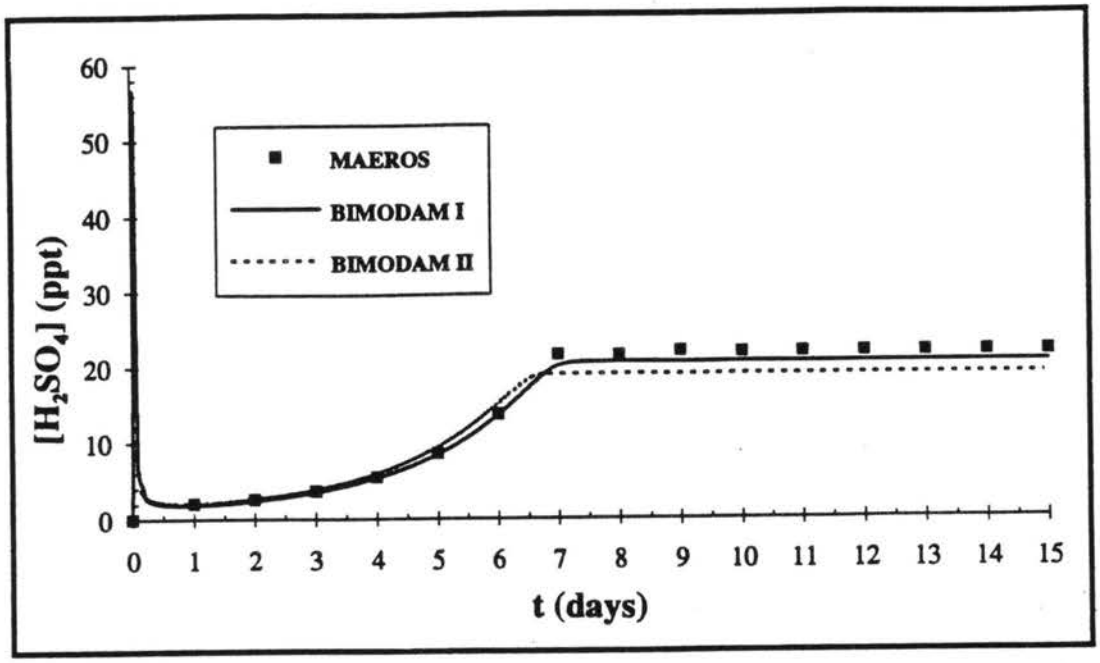

Figure 6.4a. Sulfuric acid vapor concentration, $[H_2SO_4]$, resulting from a 15-day simulation with 10 cm^{-3} particles initially residing in mode 2.

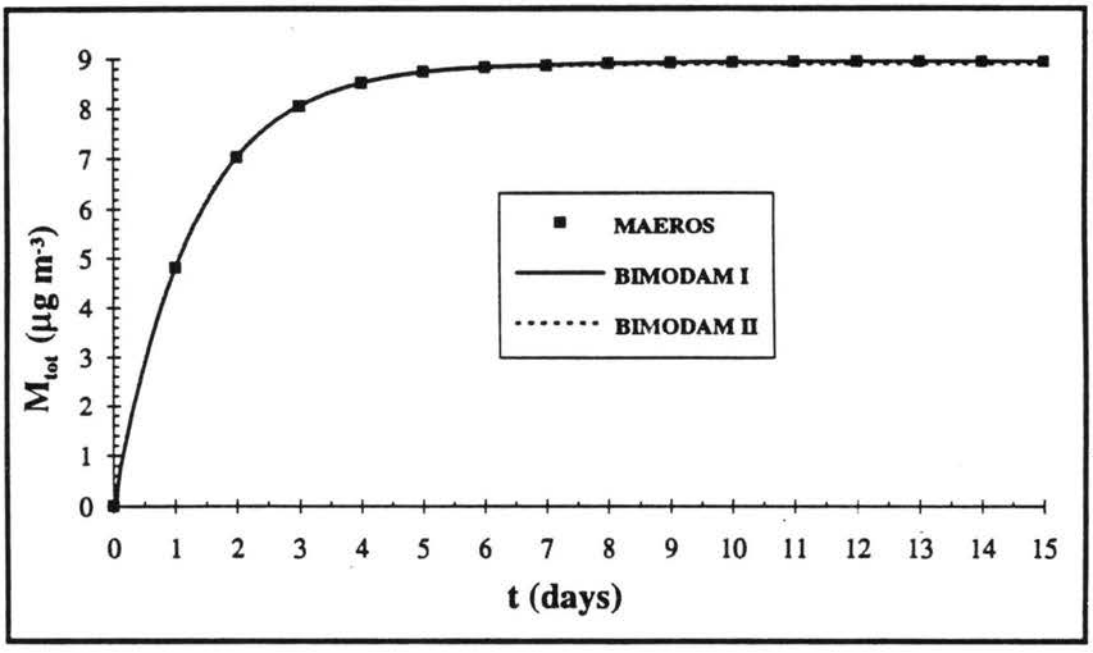

Figure 6.4b. Total aerosol mass concentration, M_{tot}, resulting from a 15-day simulation with 10 cm^{-3} particles initially residing in mode 2.

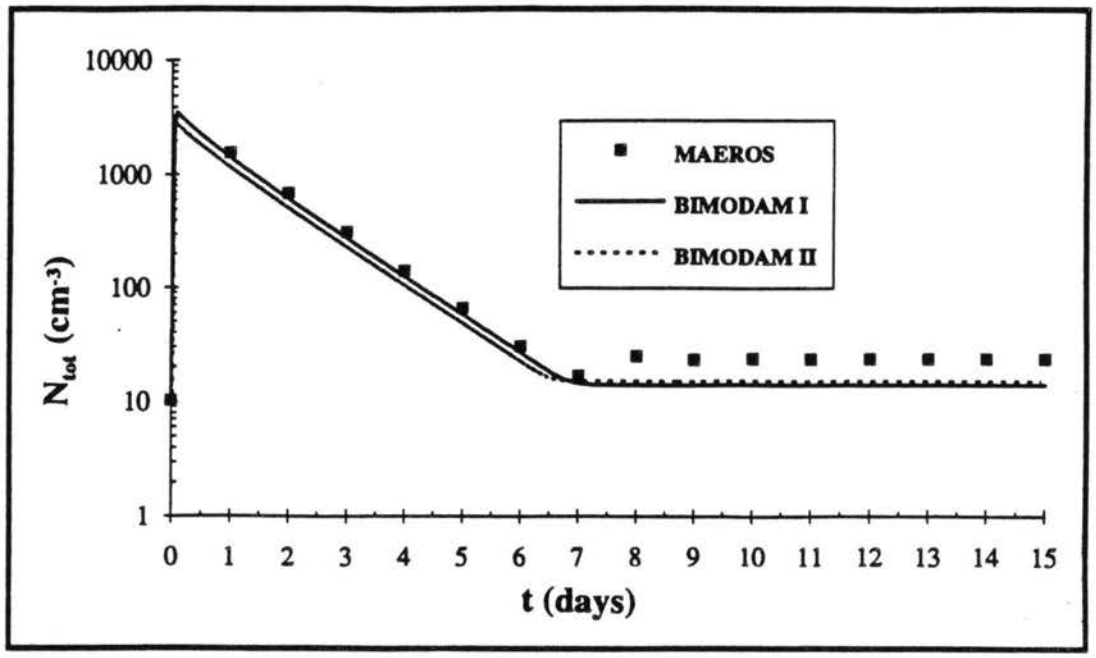

Figure 6.4c. Total aerosol number concentration, N_{tot}, resulting from a 15-day simulation with 10 cm^{-3} particles initially residing in mode 2.

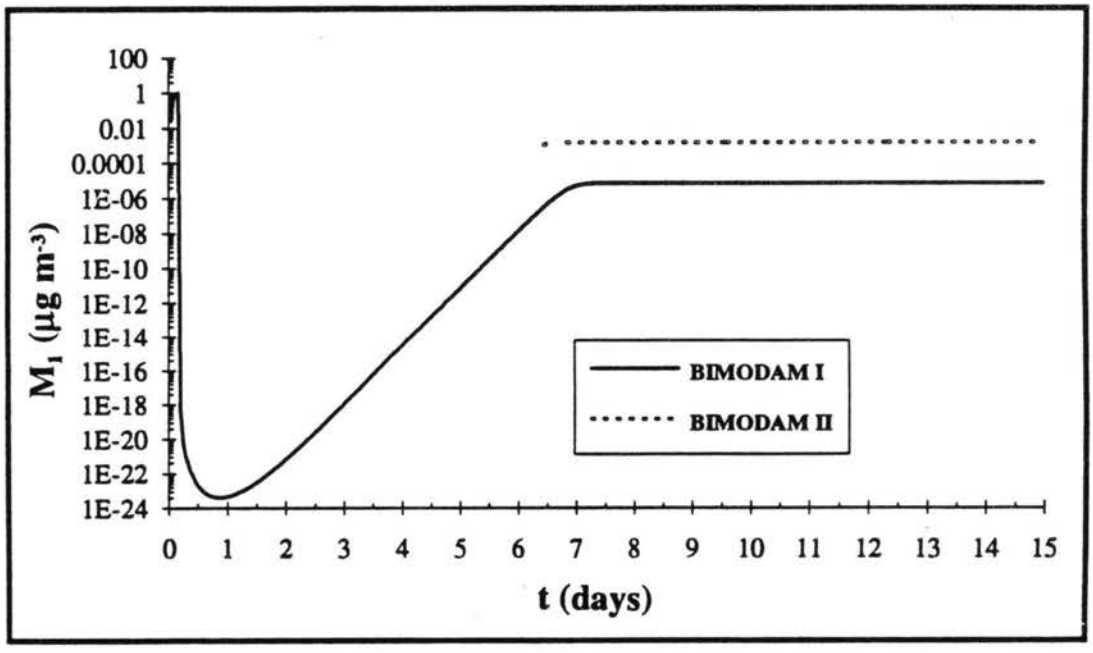

Figure 6.4d. Aerosol mass concentration in mode 1, M_1, resulting from a 15-day simulation with 10 cm^{-3} particles initially residing in mode 2.

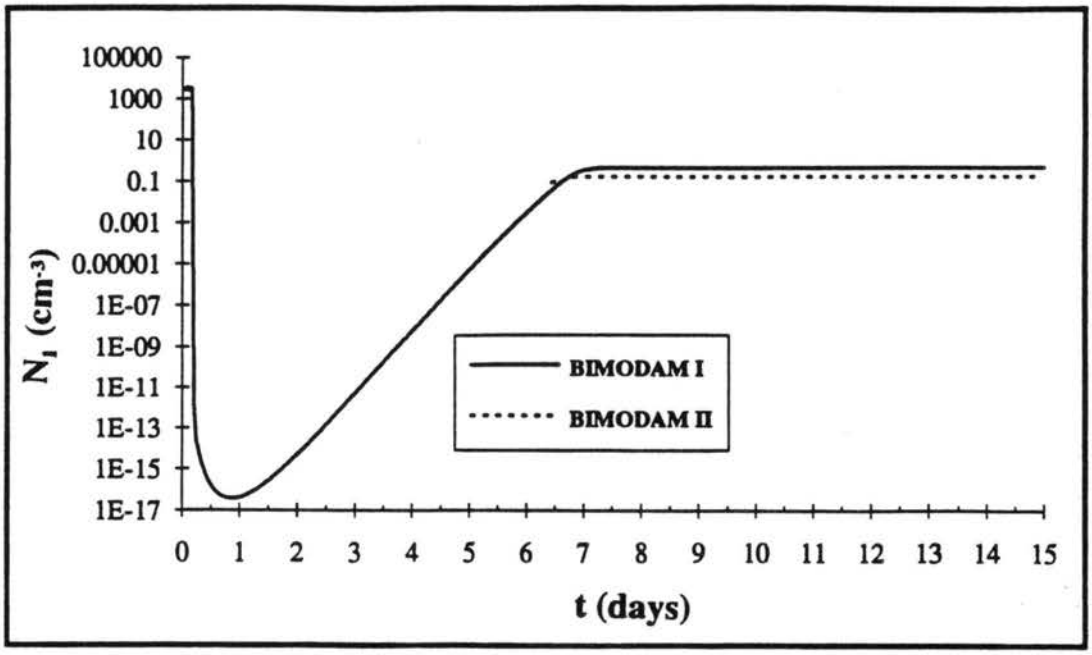

Figure 6.4e. Aerosol number concentration in mode 1, N_1, resulting from a 15-day simulation with 10 cm^{-3} particles initially residing in mode 2.

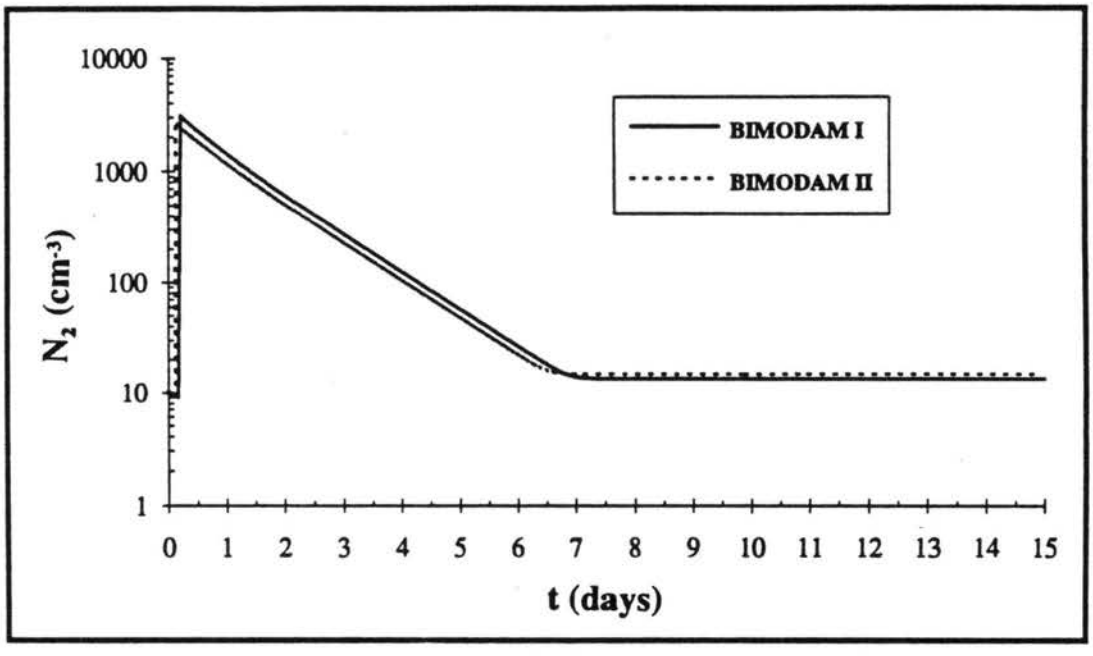

Figure 6.4f. Aerosol number concentration in mode 2, M_2, resulting from a 15-day simulation with 10 cm^{-3} particles initially residing in mode 2.

CODE	*EDIT*	*CPU*
MAEROS	1 day	2 min 52 s
BIMODAM I	3600	26.11 s
BIMODAM II	100	5.40 s

Table 6.4. Comparison of CPU time required to run the different codes for a 15 day simulation with seed particles.

6.D. SUCCESSIVE 6-HOUR SIMULATIONS

The previous case studies were all done at the same relative humidity and source rate to identify the trends in the output from BIMODAM II when all processes are simulated. A more stringent test of the code is to simulate conditions in which the relative humidity and source rate are changing. This is the purpose of the successive six hour simulations.

A six hour cycle of relative humidity and source rates was simulated for one day. The relative humidities and source rates at each 6 hour interval are shown in Table 6.5. The output at the end of each six hour simulation was used as input for the next six hour simulation.

Time (s)	*Relative Humidity*	*Source Rate (ppt)*
0	70	0.0024
21600	80	0.013
43200	85	0.055
64800	90	0.204

Table 6.5. Conditions used for successive 6-hour simulations.

Results

The response of the vapor concentration to the changes in the relative humidity and source rate is shown in Figure 6.5a. An increase is seen at the beginning of each six hour section of time as the source rate increases. The trends in BIMODAM II follow those of BIMODAM I, with relatively small errors in the maximum concentration of H_2SO_4 resulting from each source rate change. It appears that the errors which exist at the end of the prior six-hour simulation are the cause of the errors in the next six-hour simulation.

BIMODAM I does a very good job of following MAEROS output for the entire 24 hours, while BIMODAM II does a very good job of following BIMODAM I output for the first 18 hours. In the last six-hour simulation BIMODAM II does not predict a nucleation burst because of the stipulation that mode 1 be empty before a burst can occur. At the beginning of the last simulation, there are a significant number of particles in mode 1. By the time the merge occurs (~ 66,000 s; indicated by the drop in [H2SO4]), the vapor concentration has fallen too low to support a nucleation burst. The timing results are shown in Table 6.6.

In order to improve BIMODAM II for this case a nucleation burst should be allowed to occur at any time. To do this requires that the merging calculations be used to identify how to incur the least amount of error by either merging the new particles with mode 1 particles, or merging mode 1 particles with mode 2 particles.

CODE \ SEGMENT	1	2	3	43	TOTAL CPU
MAEROS	19.28	14.75	15.30	22.08	71.41 s
BIMODAM I	5.38	5.56	5.91	6.32	23.17 s
BIMODAM II	0.25	0.23	0.28	0.30	1.06 s

Table 6.6. Comparison of CPU time required to run the different codes for the successive 6-hour simulations.

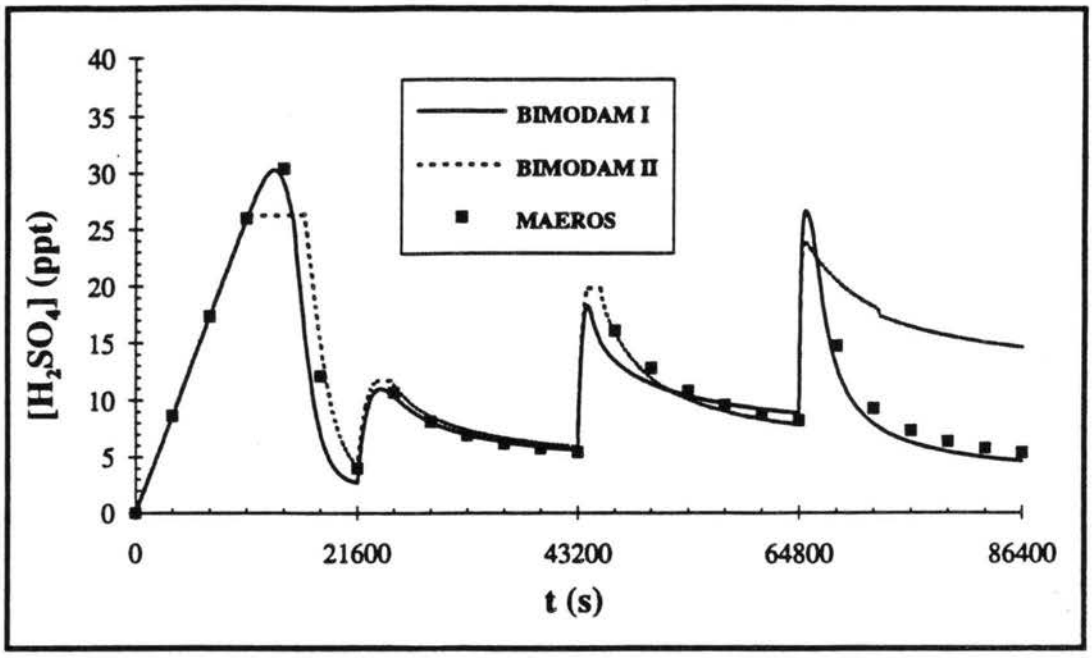

Figure 6.5a. Sulfuric acid vapor concentration, $[H_2SO_4]$, resulting from four successive 6 hour simulations in which the vapor source rate and relative humidity were changed according to Table 6.6.

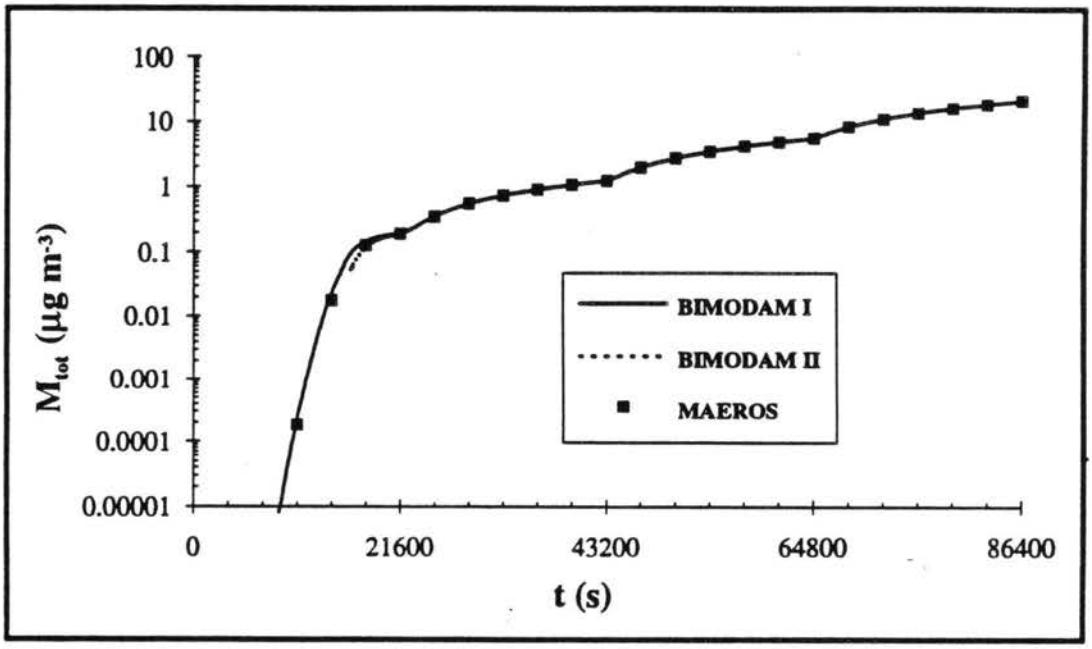

Figure 6.5b. Total aerosol mass concentration, M_{tot}, resulting from four successive 6 hour simulations in which the vapor source rate and relative humidity were changed according to Table 6.6.

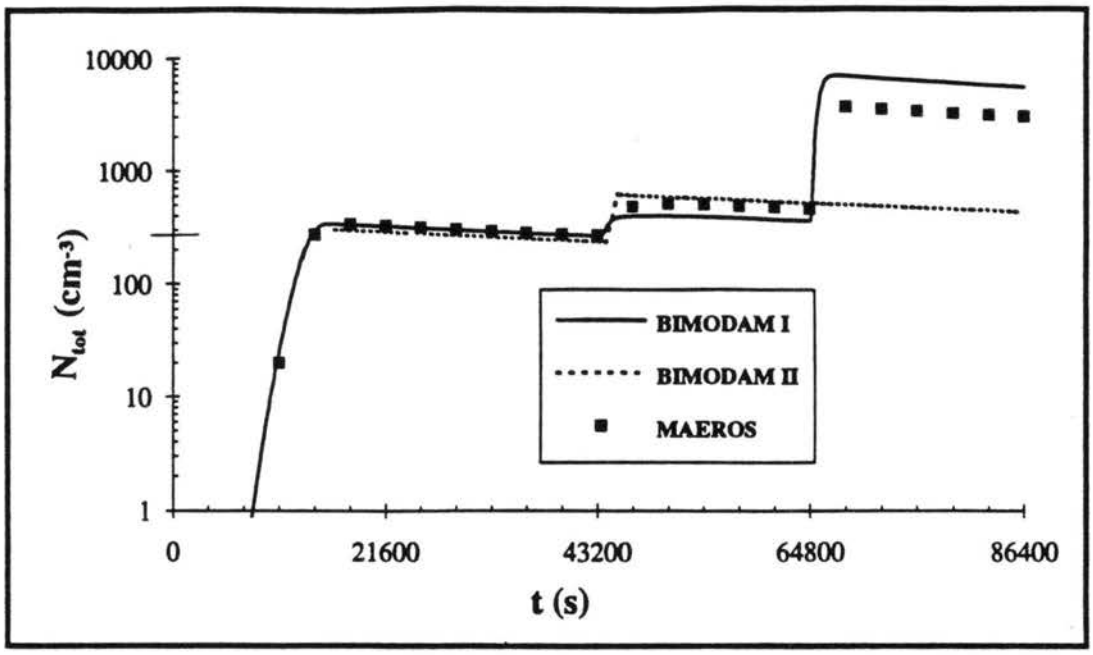

Figure 6.5c. Total aerosol number concentration, N_{tot}, resulting from four successive 6 hour simulations in which the vapor source rate and relative humidity were changed according to Table 6.6.

CHAPTER 7 CONCLUSIONS

7.A. RESTATEMENT OF PROBLEM

I. BIMODAM I objectives

BIMODAM I is an integral model which follows the evolution of two monodisperse aerosol modes. There are five prognostic variables which describe the system. The variables are aerosol mass and number in each mode, and vapor mass concentration. The two modes experience particle inception, growth, coagulation, and deposition.

This integral model was lacking two key parameters: a condensation rate factor and a merging criterion.

The condensation rate factor is necessary due to the assumption of a monodisperse size distribution for each mode. The condensation rate onto a monodisperse particle exceeds that onto a particle size distribution. Therefore, the condensation rates onto these monodisperse modes will be overpredicted relative to an evolving polydisperse distribution. The condensation rate factor, α, is a number less than one which lowers the condensation rate to simulate polydispersity.

A merging mechanism was needed to allow for transfer of mass and number between the two modes. The only other mechanism for transfer between modes is coagulation between the two modes, and this mechanism only transfers mass, and not number, from mode 1 to mode 2. A means was needed to combine the two modes when appropriate, so that new mode 1 trajectories could be initiated.

II. BIMODAM II objectives

Despite the parameters developed for BIMODAM I, its simplicity, it is still not efficient for use in global models. In order to make it suitable for such purposes, the differential equation solver should be eliminated because it is not vectorizable and it chooses computationally expensive time steps during the most rapidly changing processes in the simulation.

In order to eliminate the solver, the differential equations must be solved analytically. This involves approximations for some equations, but exact solutions can be found for other equations. Simplification of the nucleation process is also necessary because during nucleation, the system changes rapidly, therefore, the differential equation solver must take very small steps.

7.B. SUMMARY OF BIMODAM I WORK

I. Condensation rate factor

Condensation rate factors have been derived in this work for the explicit purpose of correctly predicting the number of particles resulting from a burst. The value of α significantly affects the nucleation burst because if the condensation rate is overpredicted, the number of particles will be underpredicted, as too much vapor mass goes towards condensation, leaving too little to nucleate the correct number of particles.

The methodology used was as follows. MAEROS simulations were completed for the length of a burst, using a constant vapor source rate and allowing depletion of the vapor concentration during the simulation. Total number nucleated was compared with that predicted from a BIMODAM I simulation which assumed a monodisperse distribution (α=1). Subsequent BIMODAM I simulations were completed with lower values of α until the number predicted from each nucleation burst in MAEROS and BIMODAM I agreed to within 0.01%.

The resulting α values were plotted for each relative humidity as a function of source rate. It was shown that for a given source rate in the range between 0.0024 and 0.216

ppt s^{-1}, α increases with relative humidity. This is a result of the rapid and strong bursts which occurs at higher relative humidities. The rapid bursts leave little opportunity for the distribution to broaden. For the same reason, for a given relative humidity, as source rate increases, α increases.

The values of α derived here were tested and have been shown to perform well for predicting the number and mass of particles resulting from a nucleation burst, when the vapor concentration depletes, and the vapor source rate is held constant.

II. Merging mechanism

A method for merging two modes such that the total condensation rate is not substantially affected by the merge has been developed. This method is based on taking the ratio of the sum of the condensation rates onto the individual modes to the condensation rate onto the lumped mode. The ratio is based on condensation rates because the error associated with merging inappropriately lies in the condensation rate, as the condensation rate is overpredicted for a monodisperse aerosol.

An appropriate value of the merging criterion was derived from studies of nucleation in the presence of preexisting particles. A value for the merging criterion of 0.97 was used throughout the rest of the work, except where noted, and was shown to perform well for the cases studied.

7.C. SUMMARY OF BIMODAM II WORK

The main outcome of this work is an extension of BIMODAM I which is suitable for inclusion in large scale models.

I. Nucleation parameterization

A parameterization for nucleating aerosol particles has been developed. The parameterization involves approximating the time-dependent nucleation rate as a

triangular function. Correlations for two parameters were developed which allow for quick and accurate calculation of the number concentration of particles predicted to nucleate during a burst. The correlations have been shown to behave well in the range of chemical source rates and relative humidities studied.

The nucleation parameterization was tested over a wide range of relative humidities and chemical source rates, and has been shown to predict total number nucleated to within 10% error, when there are no preexisting particles.

The parameterization was extended to include nucleation bursts in the presence of preexisting particles. By utilizing an effective source rate, obtained by subtracting the condensation rate onto the preexisting particles from the total source rate, the same correlations as were used without preexisting particles can be used.

The mechanism was tested over a range of size and number of particles preexisting in mode 2 and was shown to perform well in at least 80% of the cases tested. When this mechanism failed, either by missing a nucleation event, or predicting an event, but with large errors in number of particles nucleated, it was when there were a significant number of small particles in mode 2. For many of these failed cases, the number nucleated by BIMODAM I was less than 10% of the preexisting.

II. Simplified growth

The differential equation for vapor conservation was solved assuming that the diameters of the individual modes do not change during a time step. The resulting solution for $V(t)$ is subtracted from the vapor produced over the time step, yielding the amount of mass added to the aerosol phase. This equation was shown to be sensitive to the time step over which the diameters could be considered constant. The fractional condensation rates are used to divide the mass added to the aerosol phase between the modes. This method of growing particles is used when a nucleation burst is not occurring.

For growth of particles during a nucleation burst in which there are no seed particles, it is assumed that all of the vapor mass generated during the burst length goes into the newly formed particles. For growth during a nucleation burst in which there are seed particles, the condensation rate onto mode 2 is subtracted from the total vapor source rate, yielding an effective source rate for nucleation. During the burst, it is assumed that the condensation rate onto the seed particles remains constant during the burst, therefore, that the effective source rate for nucleation is also constant.

III. Analytical solutions to differential equations

Analytical solutions were derived for the differential equations for coagulation and deposition assuming the coefficients are constant. The performance of the analytical solutions closely follows that of the time-integrated equations in BIMODAM I.

IV. Results from short and long-term simulations

Simulations were done with all simplifications and parameterizations in place in BIMODAM II for short and long time scales. All four cases presented were shown to behave well when compared with the BIMODAM I formulation, as well as when compared with the more detailed sectional model, MAEROS.

It was shown, however, that if the vapor concentration, resulting from a nucleation burst which occurs with a given source rate, is incorrectly predicted, the remainder of the simulation will be in error, if the source rate is changed. This subject warrants further study.

BIMODAM II has been shown to be a computationally feasible model suitable for inclusion in large scale models. The errors associated with this monodisperse approach have been limited, and therefore, the results predicted from BIMODAM II agree well

with more detailed approximations of the size distribution. The time saved over more detailed approximations of the size distribution is quite significant.

7.D SUGGESTIONS FOR FUTURE RESEARCH

Although BIMODAM II has been shown to be an effective model for predicting aerosol size and number concentration resulting from a variety of conditions, further work would be useful.

The mechanism for calculating α used in this work is applicable for situations when the preexisting mode of particles is represented as a monodisperse mode in MAEROS: all of the preexisting mass is put into one section. A new method is needed, however, to calculate α if the preexisting aerosol mass is log-normally distributed in MAEROS. This would entail further simulations of both MAEROS and BIMODAM I. Once the new method for calculating α has been developed in BIMODAM I, it would be applied the same way in BIMODAM II.

The nucleation and condensation parameterizations developed for BIMODAM II were developed under the assumption that the sticking coefficient for both modes is always 1. Although values of the sticking coefficient are not well known, there is a possibility that the value is less than 1. For these cases, the nucleation parameterization should be modified to account for values of the sticking coefficient less than 1. When the sticking coefficient is less than 1, there is more vapor available for nucleation, therefore, the source rate for nucleation is higher. Modifying the nucleation parameterization would entail deriving parameters which account for this effect.

BIMODAM I and BIMODAM II are both capable of simulating a particle source rate. Particles can be added to both modes. Simulations should be done using the particle source rate to test the sensitivity of both models. The smaller mode particle source rate could represent particles which are generated in the upper troposphere/lower stratosphere via homogeneous nucleation and 'fed' into the lower troposphere. The

larger mode particle source rate might be used to represent sea salt particles for oceanic simulations or dust particles for land simulations.

One weakness of BIMODAM II is that mode 1 must be empty in order for a nucleation event to occur. There are cases when a nucleation burst should occur, but cannot because of this limitation. In order to remove this limitation, a third mode could be added. This third mode would be the nucleation mode which would accept the particles resulting from a nucleation burst and would keep them there until they have grown large enough to be incorporated into the next largest mode. It is possible, however, that even with a third mode there will be cases where all three modes are full. In that instance, tests should be done to determine which would create the largest error: ignoring the nucleation burst, or merging 2 of the 3 modes.

The final test of BIMODAM II is to incorporate into a model of the global sulfur cycle, such as GRANTOUR, which is currently in operation at Lawrence Livermore National Laboratory.

REFERENCES

Andreae, M. O., Barnard, W. R., and Ammons, J. M. (1983) The biological production of dimethylsulfide in the ocean and its role in the global atmospheric sulfur budget. *Ecol. Bull.* **35:** 167-177.

Andreae, M. O. (1986) The ocean as a source of atmospheric sulfur compounds. In *The Role of Air-Sea Exchange in Geochemical Cycling* (edited by P. Buat-Menard) Reidel, Hingham, MA.

Andreae, Meinrat O. (1992) The global biogeochemical sulfur cycle: A review. In *Trace Gases and the Biosphere* (edited by Berrien Moore III and David Schimel) UCAR, Boulder, CO.

Barrett, J. C., and Clement, C. F. (1991) Aerosol concentrations from a burst of nucleation. *J. Aerosol Science* **22(3):** 327-335.

Bates. T. S., Johnson, J. E., Quinn, P. K., Goldan, P. D., Kuster, W. C., Covert, D. C., and Hahn, D. J. (1990) The biogeochemical sulfur cycle in the marine boundary layer over the northeast pacific ocean. *J. Atmospheric Chemistry* **10:** 58-81.

Brown, Peter N., Byrne, George D., and Hindmarsh, Alan C. (1989) VODE: A variable coefficient ODE solver. *SIAM J of Sci Stat Comput.* **10(5):** 1038-1051.

Charlson, R. J., Langner, J., Rodhe, H., Leovy, C. B., and Warren, S. G. (1991) Perturbation of the northern hemisphere radiative balance by backscattering from anthropogenic sulfate aerosols. *Tellus* **43AB:** 152-163.

Cline, J. D. and Bates, T. S. (1983) Dimethyl sulfide in the equatorial Pacific Ocean: a natural source of sulfur to the atmosphere. *Chem. Phys. Lett.* **130:** 463-466.

Dahneke, B. (1983) Theory of Dispersed Multiphase Flow (edited by Meyer, R. E.) Academic press, New York.

Erickson, David J. III, Walton, John J., Ghan, Steven J., and Penner, Joyce E. (1991) Three-dimensional modeling of the global atmospheric sulfur cycle: a first step. *Atmospheric Environment* **25A(11):** 2513-2520.

Fehlberg, E. (1970) Low-order classical Runge-Kutta-Fehlberg (4,5) formulas with stepsize control. *Computing* **6:** 61-71.

Fitzgerald, James W. (1991) Marine Aerosol: A Review. *Atmospheric Environment* **25A:** 533-545.

Friedlander, S. K. (1977) Smoke, Dust, and Haze. John Wiley and Sons, New York.

Gelbard, Fred, and Seinfeld, John H. (1980) Simulation of multicomponent aerosol dynamics. *J Colloid and Interface Science* **78(2):** 485-501.

Gras, J. L. and Ayers, G. P. (1983) Marine aerosol at southern mid-latitudes. *Journal of Geophysical Research* **88:** 10,661-10,666.

Jaecker-Voirol, A., and Mirabel, P. (1988) Nucleation rate in a binary mixture of sulfuric acid and water vapor. *J. Physical Chemistry* **92:** 3518-3521.

Kiehl, J. T., and Briegleb, B. P. (1993) The relative roles of sulfate aerosols and greenhouse gases in climate forcing *Science* **260:**311-314.

Kreidenweis, Sonya M., and Seinfeld, John H. (1988) Nucleation of sulfuric acid-water and methanesulfonic acid-water solution particles: implications for the atmospheric chemistry of organosulfur species. *Atmospheric Environment* **22(2):** 283-296.

Kreidenweis, Sonia M., Yin, Fangdong, Wang, Shih-Chen, Grosjean, Daniel, Flagan, Richard C., and Seinfeld, John H. (1991) Aerosol formation during photooxidation of organosulfur species *Atmospheric Environment* **25A(11)** 2491-2500.

Kreidenweis, S. M., Penner, J. E., and Yin, F. and Seinfeld, J. H. (1991) The effects of dimethylsulfide upon marine aerosol concentrations. *Atmospheric Environment* **25A(11):** 2501-2511.

Landgrebe, James D., and Pratsinis, Sotiris E. (1989) Gas-phase manufacture of particulates: interplay of chemical reaction and aerosol coagulation in the free-molecular regime. *Ind. Eng. Chem. Res.* **28(10):** 1474-1481.

Langner, J., and Rodhe, H. (1991) A global three-dimensional model of the tropospheric sulfur cycle. *J. Atmospheric Chemistry* **13:** 225-263.

McMurry, P. H., and Friedlander, K. (1979) New particle formation in the presence of an aerosol. *Atmospheric Environment* **13:** 1635-1651.

Meszaros, A., and Vissy, K. (1974) Concentration, size distribution and chemical nature of atmospheric aerosol particles in remote ocean areas. *Journal of Aerosol Science* **5:** 101-109.

Okuyama, Kikuo, Kousaka, Yasuo, Kreidenweis, Sonia, Flagan, Richard C., and Seinfeld, John H. (1988) Studies in binary nucleation: The dibutylphthalate/dioctylphthalate system *J Chemical Physics* **89:** 6442-6453.

Pratsinis, Sotiris, E. (1988) Simultaneous nucleation, condensation, and coagulation in aerosol reactors. *J. Colloid and Interface Science* **124(2):** 416-427.

Seigneur, Christian, Hudischewskyj, A. Belle, Seinfeld, John H, Brock, Whitby, Kenneth T., Whitby, Evan R., Brock, James R., and Barnes, Harold M. (1986) Simulation of aerosol dynamics: A comparitive review of mathematical models. *Aerosol Science and Technology* **5:** 205-222.

Seinfeld, J. H. (1986) *Atmospheric Chemistry and Physics of Air Pollution.* John Wiley & Sons, New York.

Shaw, Glenn E. (1989) Production of condensation nuclei in clean air by nucleation of H_2SO_4. *Atmospheric Environment* **23(12):** 2841-2846.

Shampine, L. F., Watts, H. A., Davenport, S. (1976) Solving non-stiff ordinary differential equations-the state of the art. *SIAM Review* **18:** 376-411.

Twomey, S. (1977) Atmospheric Aerosols. Elsevier, Amsterdam.

Twomey, S. (1991) Aerosols, clouds, and radiation *Atmospheric Environment* **25A(11):** 2435-2442.

Warren, Dale R., and Seinfeld, John H. (1984) Nucleation and growth of aerosol from a continuously reinforced vapor. *Aerosol Science and Technology* **3:** 135-153.

---- (1985) Simulation of aerosol size distributions evolution in systems with simultaneous nucleation, condensation, and coagulation. *Aerosol Science and Technology* **4:** 31-43.

---- (1985) Prediction of aerosol concentrations resulting from a burst of nucleation. *J. of Colloid and Interface Science* **105(1):** 136-142.

Whitby, Evan R., McMurry, Peter H., Shankar, Uma, and Binkowski, Francis S. (1991) Modal aerosol dynamics modeling. PhD dissertation.

892002E